Nuclear structure of neutron-deficient nuclei in the mass region A≈180

Inaugural-Dissertation

zur
Erlangung des Doktorgrades
der Mathematisch-Naturwissenschaftlichen Fakultät
der Universität zu Köln

vorgelegt von

Claus Müller-Gatermann
aus Koblenz

Köln 2020

Abstract

To describe the nuclear structure of one or a group of nuclei several observables should be consulted. The excitation energies of states with given spin and parity is often known and gives a good first impression. Nevertheless transition strengths of excited states are a much better probe, since they depend quadratically on the wavefunction. These can be determined in a model-independend way from the corresponding level lifetime.

Within this work a total of four experiments were performed to measure the lifetime of excited states in ^{180}Pt and ^{178}Hg. In the neutron-deficient mass region close to the shell closure at lead (Z=82) interesting phenomena such as shape coexistence and shape transitions are observed. The most prominent example is ^{186}Pb, which exhibits three different shapes. The ground state as well as two excited 0^+ states together with the corresponding rotational bands are associated to multiparticle-multihole excitations resulting in the different shapes. A similar situation is established for the Hg isotopes near the neutron N=104 midshell, where the lightest isotope for which transition strengths are known is ^{180}Hg. Going further away from the shell closure the ^{176,178,180}Os isotopes are good candidates for the X(5) symmetry, i.e. the transition from spherical to axially deformed. Two questions arise: How can the Pt isotopes just between Os and Hg be described and what is the evolution of shape coexistence in the Hg isotopes leaving neutron midshell?

Both questions are addressed within this thesis. ^{180}Pt shows no remains of a X(5) like shape transition and multiparticle-multihole excitations are evident. This structure reaches the ground state and a new so-called island of inversion is found. This simultaneously answers the longlasting question whether configuration mixing is needed to describe the Pt isotopes or not. From the excitation energies ^{178}Hg is expected to be at the edge of the shape-coexistence region. The measured transition strengths confirm the shift of the structure with different shape to higher-lying states, but also a new phenomenon of intermediate deformation (between normal and superdeformation) shows up with decreasing neutron number. The interpretation is given by comparison to several existing calculations as well as particular calculations using geometrical models and the interacting boson model.

The experiments were carried out at different accelerator facilities employing the recoil distance Doppler-shift (RDDS) method, except one experiment when electronic-timing techniques were used to measure long lifetimes. Further a dedicated plunger apparatus was commissioned during one experiment. The GALILEO γ-ray spectrometer is the successor of GASP, which necessitated a completely new mechanical design of the plunger. This fragile device newly allows the combination with charged-particle detectors, e.g. EUCLIDES.

Zusammenfassung

Um die Kernstruktur eines oder mehrerer Kerne zu beschreiben, sollten mehrere Observablen herangezogen werden. Die Anregungsenergien von Zuständen mit gegebenem Spin und Parität sind oft bekannt und liefern einen guten ersten Eindruck. Übergangsstärken von angeregten Zuständen liefern eine bessere Aussage, da sie quadratisch von der Wellenfunktion abhängen. Diese können modellunabhängig aus korrespondierenden Zustandslebensdauern bestimmt werden.

Innerhalb dieser Arbeit wurden insgesamt vier Experimente durchgeführt, um die Lebensdauer von angeregten Zuständen in ^{180}Pt und ^{178}Hg zu messen. Im neutronenarmen Massenbereich am Schalenverschluss bei Blei (Z = 82) werden interessante Phänomene wie Formkoexistenz und Formübergänge beobachtet. Das prominenteste Beispiel ist ^{186}Pb, das drei verschiedene Formen aufweist. Der Grundzustand sowie zwei angeregte 0^+-Zustände zusammen mit den entsprechenden Rotationsbanden können Teilchen-Loch-Anregungen zugeordnet werden, die zu den verschiedenen Formen führen. Eine ähnliche Situation ergibt sich für die Hg-Isotope in der Nähe der Schalenmitte für Neutronen bei N = 104, das leichteste Isotop, für das Übergangsstärken bekannt sind, ist ^{180}Hg. Entfernt man sich vom Schalenabschluss, sind die ^{176,178,180}Os-Isotope gute Kandidaten für die X(5)-Symmetrie, bzw. dem Übergang von sphärisch zu axial deformierten Kernen. Es stellen sich zwei Fragen: Wie können die Pt-Isotope zwischen Os und Hg beschrieben werden und wie ist die Entwicklung der Formkoexistenz in den Hg-Isotopen jenseits der Schalenmitte?

Beide Fragen werden in dieser Arbeit diskutiert. ^{180}Pt zeigt keine Eigenschaften eines X(5)-ähnlichen Formübergangs und Teilchen-Loch-Anregungen spielen eine entscheidende Rolle. Diese Struktur erreicht den Grundzustand und eine neue sogenannte "island of inversion" wurde gefunden. Dies beantwortet gleichzeitig die langjährige Frage, ob es erforderlich ist veschiedene Konfigurationen zu mischen, um die Pt-Isotope zu beschreiben oder nicht. Aus den Anregungsenergien in ^{178}Hg liegt der Kern voraussichtlich am Rande der Form-Koexistenz-Region. Die gemessenen Übergangsstärken bestätigen, dass sich die Struktur mit unterschiedlicher Form zu höher liegenden Zuständen verschiebt. Es tritt jedoch mit abnehmender Neutronenzahl ein neues Phänomen auf, es bildet sich eine mittlere Deformation (zwischen normaler und Superdeformation) aus. Die Interpretation erfolgt durch den Vergleich mit mehreren vorhandenen Rechnungen sowie eigenen Berechnungen unter Verwendung geometrischer Modelle und des Interacting Boson Modells.

Die Experimente wurden an verschiedenen Beschleunigeranlagen mittels der Recoil Distance Doppler-Shift Methode (RDDS) durchgeführt, lediglich bei einem Experiment zur Messung von langen Lebensdauern wurde elektronisches Timing zur Messung verwendet. Ferner wurde während eines Experiments ein dedizierter Plunger getestet und in Betrieb genommen. Das GALILEO-Spektrometer ist der Nachfolger von GASP und erforderte ein völlig neues mechanisches Design des Plungers. Die fragile Konstruktion ermöglicht erstmalig die Kombination mit Teilchendetektoren wie z.B. EUCLIDES.

Contents

Introduction

1.1 Determination of nuclear level lifetimes

The experimental observables are the lifetimes of excited states, alongside with excitation energies, branching ratios, conversion coefficients and multipole mixing ratios. This work is restricted to E2 transitions in the yrast band of exotic nuclei, therefore the formulas in the following are valid for this case. For the comparison to the predictions of nuclear models the transition strength between two states is a good probe as it is very sensitive to the composition of the wavefunction. The B(E2) value in units of $e^2 b^2$ is calculated from the lifetime τ of a state in ps with initial spin $J_i = J$ and the γ-ray transition to a state $J_f = J - 2$ via

$$B(E2; J_i \rightarrow J_f) = 8.197 \cdot 10^{-2} \frac{b_{ij}}{1 + \alpha_{ic}(E_\gamma)} E_\gamma^{-5} \tau^{-1},$$
(1.1)

where E_γ is the transition energy in MeV, α_{ic} the conversion coefficient and b_{ij} the branching ratio [1]. Using the rotor model one can further calculate a transition quadrupole moment Q_t and a quadrupole deformation β

$$Q_t = \sqrt{\frac{16\pi}{5} \frac{B(E2; J \rightarrow J - 2)2(2J - 1)(2J + 1)}{3J(J - 1)}}$$
(1.2)

$$\beta = 0.625(-5a + \frac{\sqrt{25a^2 + 16aQ_t}}{a})$$

$$a = \frac{3}{\sqrt{5\pi}ZR_0^2}$$
(1.3)

with Z the nuclear charge and R_0 the nuclear radius [2]. The latter is of course only meaningful if the transition happens between two states of an unperturbed rotational band. The B(E2) value on the contrary is model independent and directly connected to the lifetime. The nuclear level lifetimes measured within this work range from few to hundreds ps employing the recoil distance Doppler-shift (RDDS) and electronic-timing methods, which are described in the next two sections.

1.1.1 Recoil distance Doppler-shift method and analysis

The RDDS method is suitable to measure lifetimes between approximately 1 ps to 1 ns. At the limits stopping effects (for short lifetimes) and geometric effects using collimated detectors or nuclear deorientation (for long lifetimes) has to be taken into account. None of that was necessary in the analysis of this data, because the electronic-timing experiment was performed for a long lifetime. The RDDS method relies on the Doppler shift of γ rays with respect to the velocity of a moving source. A plunger device is needed for the application of this method and is depicted in Fig. 1. A plunger for the GALILEO spectrometer [3, 4] in Legnaro, Italy was build within this work and tested successfully. In this design every optional component is resigned and the setup consists only of a piezo motor
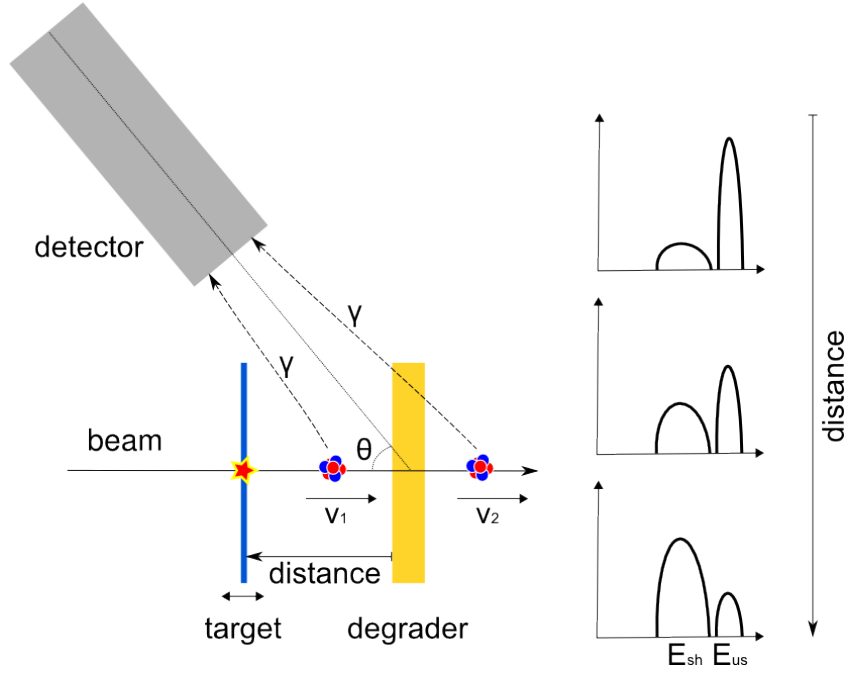
Figure 1: Schematic picture of a plunger device.

and two stretched foils for the sake of maximal transparency of γ rays and evaporated partciles. In the plunger the incident beam produces recoils of interest in the target. These excited recoils leave the target with velocity v_1 and after the flight through vacuum with a set distance pass through the degrader foil where they are slowed down to a velocity $v_2 < v_1$. Excited recoils can therefore radiate γ rays while at a velocity v_1, referred to as shifted (E_{sh}), or while travelling at v_2, referred to as unshifted (E_{us}). The shifted and unshifted γ rays can be differentiated when they are detected in the laboratory as they undergo different Doppler shifts. If the velocity v_2 is unequal zero, a Doppler correction is applied. The lifetime of an excited state can be derived from the ratio of intensites of shifted and unshifted component with respect to the distance between target and degrader. In the following only fusion-evaporation reactions are discussed, although the method is independent of reaction/excitation mechanism. Especially in these kind of reactions the nuclei are highly excited and one observes a cascade of transitions. The decay curve of the state of interest l_i includes not only the lifetime information of l_i, but all the feeding transitions l_h with their branching ratios b_{hi} between states l_h and l_i have to be taken into account. From the decay law and the superposition of all participation levels one gets the basic differential equation

$$\dot{n}_i(t) = -\lambda_i n_i(t) + \sum_h b_{hi} \lambda_h n_h(t) \tag{1.4}$$

where $n_h(t)$ denotes the population of level l_h at the time t and $\lambda_h = 1/\tau_h$ is the decay probability of level l_h with the lifetime τ_h. The solution of the set of differential equations are the well-known Bateman equations [5]. Nowadays mathematical programs e.g. Mathematica [6] can be used to determine the function of the decay curve for the explicit case. This was done in the analysis of

^{178}Hg using the γ-singles data after recoil-decay tagging (RDT) [7]. Two problems remain in this method, first one needs to know the absolute distances between target and degrader and second but even more important is the exact knowledge of feeding. The first problem is easy to overcome by extrapolation of the capacitance between the two stretched foils [8] or even better by the use of the Differential decay-curve method (DDCM) [9]. The DDCM only needs relative target to degrader distances, which are usually known with a precision below 1 μm from an inductive transducer or the position signal of the motor, which moves the target. In the case of ^{178}Hg the advantage of the DDCM disappeared, because only four distances were measured and the feeding of many states had to be taken into account. The DDCM is even stronger, if the statistics are sufficient to analyse $\gamma\gamma$-coincidences. A coincidence condition is set on a decay branch and eliminates possibly different feeding times from other branches if set on a feeding transition. In the case of a direct feeder the lifetime can be directly calculated for each distance using normalized intensities of shifted (I_{sh}) and unshifted (I_{us}) component and given recoil velocity v via

$$\tau(x) = \frac{I_{us}(x)}{v \frac{d}{dx} I_{sh}(x)} \tag{1.5}$$

if the condition is set only on the shifted component of the feeder [9]. In the case of an indirect gate or including the unshifted component, the coincident unshifted component of the direct feeder has to be subtracted from unshifted component of the decay after efficiency correction. The plunger experiments on ^{180}Pt were analyzed using $\gamma\gamma$-coincidences. The recoil-decay tagging used in the analysis of ^{178}Hg is of course also a coincidence condition, but without any influence on the feeding history. This gate cleans the γ-ray spectra just from the contaminations of all other γ-decaying nuclei. Here the recoils are not stopped in the degrader and further transported through a recoil separator. The recoil separator makes use of magnetic and/or electric fields to separate the primary beam from the nuclei of interest and can be operated either in vacuum or in a gas-filled mode. Here the gas-filled recoil ion transport unit (RITU) [10, 11] was used to enable the lifetime measurement of excited states in ^{178}Hg which is produced with only around 20 μb. Ritu consists of a dipole magnet which is filled with He gas, that the ensemble of recoils is forced to a mean charge state and can be transported to the focal plane without much losses. In the focal plane the Gamma Recoil Electron Alpha Tagging (GREAT) Spectrometer [12] is mounted. The detector system starts with a multiwire proportional counter (MWPC) which measures an energy loss and the time of flight (ToF) with respect to the following implantation detector. The radioactive nuclei are finally implanted in a double-sided silicon strip detector (DSSSD), which measures also the energy of the α decays. With energy and ToF of the MWPC the recoils can be distinguished from the decay products and the spacial coincidence in the DSSSD between implantation and decay in a time window given by the half life of the mother nucleus reduces the background significantly. Ancillary detectors of the GREAT spectromter, which were not used shall not be discussed here further. Two additional methods were implemented in the sorting code of GRAIN [13] to increase the statistics and to reduce the background. There is a non-negligible probability that the α particle leaves the DSSSD without depositing all of its energy, mostly in the cases when the α particle decays towards the entrance of the DSSSD. If the daughter

nucleus shows a significant α-decay branch a second time window can be opened corresponding to the half life of the daughter nucleus after a decay event is detected within the time window for the mother nucleus and a smaller energy deposition. This can be continued of course for subsequent decays if an α particle is emitted. In the case of ^{178}Hg only the successive decay of ^{174}Pt was used and increased the statistics by 25 %. Further a random subtraction was implemented which made use of the timestamps of events registered by the Germanium detector array for the prompt γ emission and the MWPC. Below the prompt peak in the timespectrum a plateau of random events is present, which can be subtracted taking events next to the peak since they are randomly distributed. This was a crucial point, because the energy of $4_1^+ \rightarrow 2_1^+$ transition in ^{178}Hg and the $2_1^+ \rightarrow 0_1^+$ transition in ^{78}Kr are separated by only 0.5 keV. ^{78}Kr was used as the beam and introduced a lot of random Coulomb excitation events in the γ spectrum before the subtraction.

1.1.2 Electronic timing and analysis

The electronic-timing, fast-timing or delayed-coincidence technique is capable to measure lifetimes longer than 10 ps. It does not rely on Doppler shifts and can therefore be used in experiments with light projectiles. The principle is to measure the time difference between two time-correlated events [14, 15]. There are several possibilities to measure the time difference, e.g. using timestamps of the data acquisition system (DAQ) or time to amplitude converters (TAC) and it is independent of the type of event, e.g. a beam pulse or decay (α, β, γ, conversion electron). The following description is restricted to the methods used in the electronic-timing experiment on ^{180}Pt. $LaBr_3(Ce)$ detectors [16] detect γ rays with high efficiency and good energy resolution (compared to other scintillators). The timing properties are comparable to fast plastic scintillators enabling the operation as start and stop detectors for the time-difference measurement between the γ rays with good resolution. The energy resolution is crucial for a high peak to background ratio as the background has a different timing behaviour. Each detector signal is fed into two branches, the energy and the time branch, taking the signals from the dynode (energy) and the anode (time) from the photomultiplier of each detector. The energy signal is connected directly to the DAQ to measure the pulse height. The time signal is processed first in a constant-fraction discriminator (CFD) and the time difference of signals converted to an amplitude with a TAC connected to the DAQ. To reduce the needed amount of analogue electronics (especially TACs) one uses a multiplexed start and multiplexed stop signal for the time branch [17]. The disadvantage is that the correlation between the time and energy is lost and only events with multiplicity two in the LaBr detectors can be used. The sorting code has to be adopted that every detector combination is counted only once, if this combination is connected to several TACs. Taking triple conicidences an additional energy gate can be set in a HPGe detector to clean the LaBr spectra from unwanted contaminations by other reactions utilizing the high energy resolution of the germanium detector [18]. The statistics of several energy gates (for different transitions in the cacscade) in the germanium detectors can be added up to increase the overall statistics, but it has to be taken care that in this case only single events in the germanium detectors are used. Otherwise certain events can be counted more than once. After setting the energy gates in the LaBr

detectors of the fast-timing matrix and possibly a gate in the germanium detector two time spectra are generated, since both the start and stop detectors see the same γ rays. The so-called delayed time distribution corresponds to the case when the start detector counted the feeding transition and the stop detector observed the decay. The anti-delayed distribution is generated for the opposite case. For a short lifetime the time distributions have a gaussian shape and the lifetime can be extracted according to the generalized centroid-difference method (GCD) [19]. The mean lifetime equals half of the difference between the centroids of the two distributions after correction for the response function of the detector system including the analogue electronics. A prompt response difference (PRD) calibration is performed measuring the $\gamma - \gamma$ time-walk characteristics (with respect to the energy) mostly stemming from the CFD. This takes adavantage of the known lifetimes of a γ-ray source. For both the calibration and the analysis the formula

$$\Delta C = PRD + 2\tau \tag{1.6}$$

is used, where ΔC is the centroid difference, PRD the prompt response difference and τ the lifetime. A typical calibration curve of a PRD with respect to the γ energy is shown in Fig. 2. If the lifetime
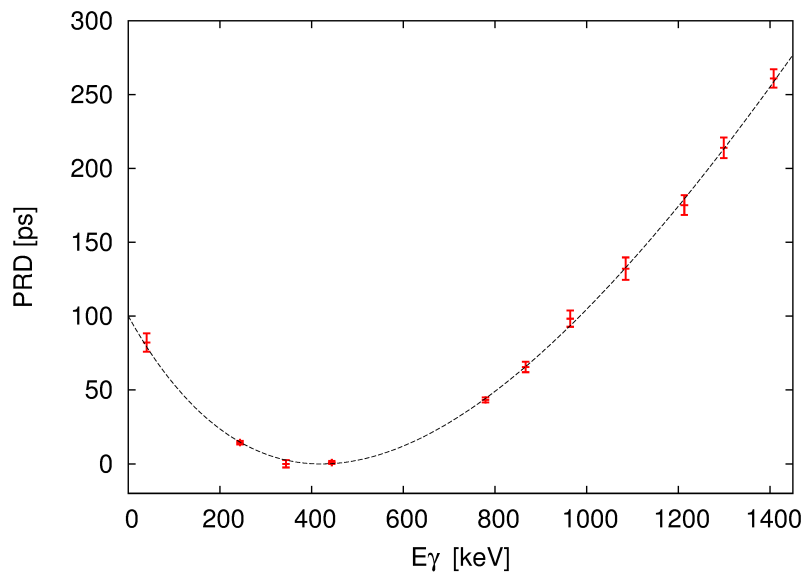

Figure 2: A typical PRD curve with respect to the γ energy. The γ decays of a ^{152}Eu source and the X-rays after the electron capture were used.

is long compared to the prompt peak, the time distribution assumes a shape of a convolution of the prompt peak and an exponential function according to the decay law. In this case one fits the exponential decay outside of the prompt peak and directly obtains the lifetime. If the statistics are low beyond a reasonable distance to the prompt peak one can also fit the convolution, like it is done in the case of the $2_1^+ \rightarrow 0_1^+$ transition in ^{180}Pt. A common problem in all methods is the treatment of the background. If a germanium gate is applied it is reasonable to assume, that the background below a peak in the energy spectrum stems from the a Compton event with higher total γ energy in the same nucleus. Since it concerns a different state with a different lifetime, the timing behaviour

of the background will be different and should be accounted for in the analysis. This was done as described in the publication on [180]Pt when employing the GCD method. There was no sign, that any correction is needed in the fit of the convolution. According to the gates only very short-lived decays from high-lying states in [180]Pt can generate the background and should all lie within the prompt peak.

1.2 Nuclear structure of the neutron-deficient mass region around lead

Before this work it was known that the neutron-midshell lead isotopes as well as their even-even neighbors can be interpreted in terms of shape coexistence [20]. Deformed intruder states coexist with nearly spherical normal states, where in this context intruder states means a multiparticle-multihole excitation of protons across the shell gap at Z=82 [21, 22]. Excited 0^+ states as band heads of rotational bands are linked to these excitations of different numbers of particles. Since the energy spacing between states within one band is different from another band with a different deformation, the yrast states may change their membership with increasing excitation energy. Additionally mixing sets in for states with the same spin when close in energy. The deformation of the ground state, and if existing isomeric states, has been measured via the isotope shifts. A very pronounced staggering of the charge radius between odd and even Hg isotopes was found at neutron midshell with this method [23]. This was indeed the first hint of shape coexistence in this region and the experimental data points have recently been extended to more neutron-deficient Hg nuclei [24]. The deformation of (nonisomeric) excited states has been determined on the basis of Coulomb excitation and lifetime experiments [25–27], with [180]Hg being the most neutron-deficient Hg isotope. Predictions from theoretical calculations on the influence of the intruding structure at the limits where the parabola of deformed states crosses the weakly deformed ground-state band go back to Ref. [28] in 1993. Fig. 3 shows the level energy systematics of the even-even mercury isotopes and the intruding parabola of deformed states. Just from these systematics one would expect that the shape existence phenomenon is at least shifted to higher-lying states for even more neutron-deficient isotopes. The heavier Hg nuclei outside the neutron-midshell region exhibit at minimum an 12^+ isomer, which hinders Doppler-shift experiments using fusion-evaporation reactions. Neglecting these shell effects one would expect a change from spherical to deformed rotorlike nuclei when moving away from a shell closure for one type of nucleons. This is quantified with the valence space in a $N_\pi N_\nu$ scheme, called the P-factor [2]. The leading term is $N_\pi \cdot N_\nu$ being the valence-nucleon numbers for protons and neutrons respectively. In the context of the neutron-midshell lead region very good candidates for the transition from spherical to axially-deformed nuclei are found to be [176,178,180]Os [29]. They fulfill all the criteria of the critical-point symmetry X(5) proposed by Iachello [30], unfortunately no absolute transition strengths are known so far for non-yrast states. The platinum isotopes are located just in between the chains of Os and Hg. Before this work it was unclear how the midshell platinums can be described. [182]Pt seems to show B(E2) ratios compatible with the X(5) symmetry [31], but this relies strongly on the 2_1^+ lifetime which was measured with low Doppler shift. In [180]Pt contradicting lifetimes were measured [32, 33] even showing a $B_{4/2} = B(E2; 4_1^+ \rightarrow 2_1^+)/B(E2; 2_1^+ \rightarrow 0_1^+)$ ratio
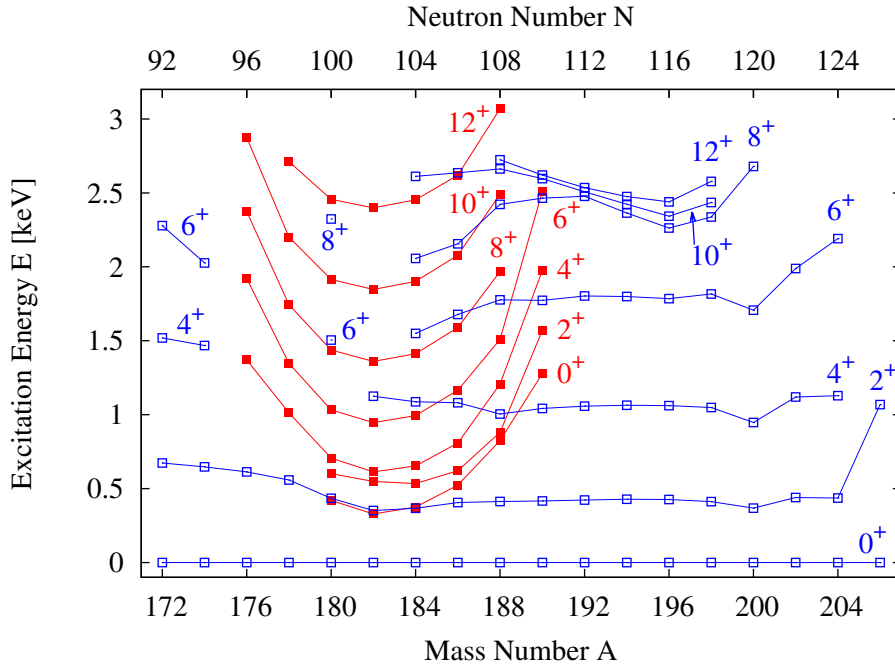
Figure 3: Level energy systematics of the even-mass mercury isotopes. Red filled squares refer to the assumed intruder states while blue open squares refer to the assumed oblate states. The figure is adopted from Ref. [27].

below unity. This cannot be described with collective models and is expected only for magic nuclei, where seniority is a good quantum number. For more neutron-deficient Pt isotopes there existed some data stemming from RDDS experiments using γ singles, but no conclusive picture could be drawn. It was also a longlasting question if multiparticle-multihole excitations are needed to describe the spectroscopic properties [34].

1.3 Nuclear models

Three different models have been applied within this thesis and shall be described very briefly in the following. In the publications also other model predictions are cited, but since only the output is compared to the experimental observables these are not described here.

Rigid rotor model

The first model is a geometric model, which assumes the mass and charge to be equally distributed in a form of the nuclear volume. This implies an intrinsic electric quadrupole moment Q_0 for a deformed nucleus, which is a measure of the deviation of sphericity. A parametrization of the form can be written via an expansion of spherical harmonics and in the case of a quadrupole deformation is given

by

$$R = R_0[1 + \sum_{\mu=-2}^{2} \alpha_{2\mu} Y_{2\mu}^*(\theta, \phi)] \tag{1.7}$$

where R_0 is the radius of a sphere with the same volume. Introducing the Hill-Wheeler-coordinates β and γ, one can describe the nucleus as an triaxial deformed ellipsoid with the parametrisation of semiaxes

$$\alpha_{20} = \beta cos\gamma, \quad \alpha_{22} = \alpha_{2-2} = \frac{1}{\sqrt{2}}\beta sin\gamma, \quad \alpha_{21} = \alpha_{2-1} = 0$$

$$R_k = R_0[1 + \sqrt{\frac{5}{4\pi}}\beta cos(\gamma - \frac{2\pi}{3}k)], \quad (k = 1, 2, 3) \tag{1.8}$$

To keep the form of the nucleus well defined, one has to restrict β to positive values and γ within the interval $0° \leq \gamma \leq 60°$. In this representation one can quantify the magnitude of deformation with β and γ would correspond to the characterization of the form. A spherical nucleus has therefore $\beta = 0$, fixing the value of γ to $0°(60°)$ describes a prolate(oblate) form other values of γ depict triaxial deformations.

The rigid rotor model is restricted to axially-symmetric deformations which are fixed in the ground state. Rotations occur along an axis perpendicular to the symmetry axis and vibrations enter independendly of the rotation at higher energies. In the ground-state band the whole angular momentum is determined by the rotation (K=0, K being the projection of an intrinsic excitation with spin $\vec{j}$ on the symmetry axis). The excitation energies of the rotational band can be calculated the by

$$E_{rot} = \frac{\hbar^2(I(I+1))}{2\mathfrak{J}} \tag{1.9}$$

with I the angular momentum and $\mathfrak{J}$ the moment of inertia. In this simplified picture of a rigid rotor the intrinsic quadrupole moment is constant within a rotational band. Closer to reality one defines a transitional quadrupole moment Q_t via the reduced transiton probabilty of each γ transition. The relation is given in formula 1.2 in which the variables Q_0 and Q_t can be substituted [35].

General collective model

The general collective model (GCM) [36] is a phenomenological model, which is restricted to quadrupole deformation but allows vibrational excitations and the coupling of them to rotations. It assumes the nucleus to behave like an incompressible liquid drop and does not distinguish between protons and neutrons. Therefore it is again a geometrical model without including single-particle excitations. The Hamiltionian consists of the sum of kinetic energy $\hat{T}$ and collective potential $V(\beta, \gamma)$. The kinetic energy contains the two lowest order terms proportional to the square of the momenta.

$$\hat{T} = \frac{1}{2B_2}[\hat{\pi} \times \hat{\pi}]^{[0]} + \frac{P_3}{3}\{[[\hat{\pi} \times \alpha]^{[2]} \times \hat{\pi}]^{[0]}\}, \tag{1.10}$$

14

where {...} means the sum over all even permutations of α and the conjugated momenta $\hat{\pi}$, while B_2 is the common mass parameter and P_3 accounts for the deformation-dependent inertial functions. The potential is described with a polynomial expansion of deformation variables up to the sixth order.

$$V(\beta,\gamma) = C_2 \frac{1}{\sqrt{5}}\beta^2 + C_4 \frac{1}{5}\beta^4 + D_6 \frac{1}{5\sqrt{5}}\beta^6 - C_3\sqrt{\frac{2}{35}}\beta^3 cos3\gamma - C_5\sqrt{\frac{2}{175}}\beta^5 cos3\gamma + C_6 \frac{2}{35}\beta^6 cos^2 3\gamma$$
(1.11)

The parameters in the collective potential can be divided in three groups, one for the γ-independend part (C_2, C_4, D_6), one describing the prolate-oblate energy differences (C_3, C_5) and the part symmetric to $\gamma = 30°$ (C_6) which describes the asymmetry of the nuclear shape. It is very convenient that one gets immediately the potential energy surface (PES) with respect to the intrinsic variables β and γ. Not only that one reads directly the deformation, but sees as well the softness of β or γ. The model is also capable of dealing with shape coexistence, which was one main question to be solved in the platinum isotopes. Double minima or saddle points in the PES would indicate such phenomena. One disadvantage is that one needs to fit eight parameters to the experimental observables, but often only few of them determine already the basic structure of the nucleus (e.g. bandhead energies, two rotational energies and few intra- and interband transition strengths).

Interacting boson model

The interacting boson model (IBM) [37] has an algebraic approach and the main idea is to reduce the shell-model space that also far away from closed shells collective states can be described. In the simplest case (IBM-1) only even-even nuclei can be examined. Valence particles (holes) are merged in pairs to bosons for protons and neutrons individually and then treated equally. This approximation is based on the assumptions that contributions of nucleons in low-lying closed shells are neglectable for collective excitations, the pairing force facilitates to unite protons and neutrons to bosons and the nuclear properties are determined by the interaction of these bosons. In the IBM-1 the bosons are allowed only in two states with angular momentum L=0 (s-boson) or L=2 (d-boson). There are several extensions to include also states with higher and odd angular momentum or the coupling with unpaired nucleons, which will not be discussed here. The Hamiltonian with the least number of variables (in the Extended Consistent Q-formalism (ECQF)[38]) is then

$$H(\zeta,\chi) = c\left[(1-\zeta)\hat{n}_d - \frac{\zeta}{4N_B}\hat{Q}^\chi \cdot \hat{Q}^\chi\right]$$
(1.12)

$$\hat{n}_d = d^\dagger \cdot \tilde{d}, \hat{Q}^\chi = [s^\dagger \tilde{d} + d^\dagger s]^{(2)} + \chi[d^\dagger \tilde{d}]^{(2)}, \hat{T}(E2) = e_B\hat{Q}^\chi$$

with N_B being the boson number, $\hat{n}_d$ the d-boson number operator, $\hat{Q}^\chi$ the quadrupole operator, $s^\dagger$, s, $d^\dagger$, $\tilde{d}$ the creation- and annihilation-operators for s- and d-bosons, c a scaling parameter for the energies, $\hat{T}(E2)$ the E2 transition operator and e_B the effective boson charge. e_B is again a scaling parameter, but since one is often interested in ratios of B(E2) values there is no need to know this value exactly. The fitting parameters ζ, χ in this formalism can be directly used for the classification within the Casten triangle [2] corresponding to the space spanned by this Hamiltonian (c.f. Fig.

4). The corners of the Casten triangle are associated with the three dynamical symmetries U(5),
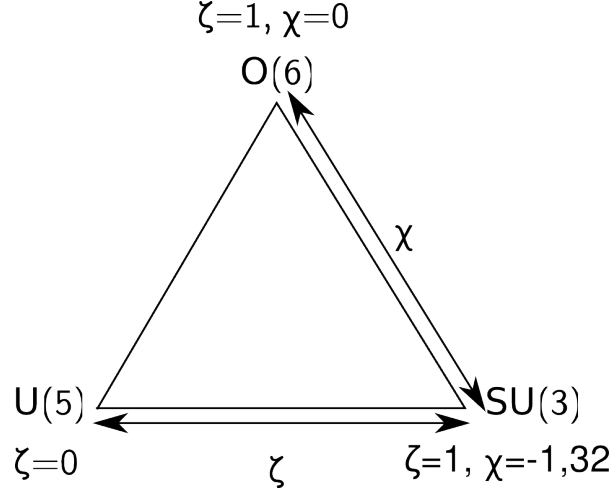

Figure 4: The Casten triangle.

SU(3) and O(6), which can be interpreted geometrically in the limit of an infinite boson number as a spherical vibrator, an axially-symmetric rigid rotor and a γ-soft rotor respectively. Also for the case of finite boson number one can find analytical expressions to calculate B(E2) values for each of the symmetries [2, 35, 37]. The excitation pattern of U(5) and O(6) are very similar, but they differ by the selection rules for the transitions. Therefore B(E2) values are more practical and are as follows for the ground-state band

$$
\begin{aligned}
U(5) : & B(E2; J+2 \rightarrow J) = e_b^2 \frac{1}{4}(J+2)(2N-J) \\
SU(3) : & B(E2; J+2 \rightarrow J) = e_b^2 \frac{3}{4} \frac{(J+2)(J+1)}{(2J+3)(2J+5)}(2N-J)(2N+J+3) \\
O(6) : & B(E2; J+2 \rightarrow J) = e_b^2 \frac{1}{8} \frac{J+2}{J+5}(2N-J)(2N+J+8)
\end{aligned}
\tag{1.13}
$$

with e_B the effective boson charge, N the boson number and J the angular momentum. It is very convenient to describe also transitions between these extreme cases with this model, but though every point in the Casten triangle can be associated with a nuclear structure this statement is not reversible. Additional terms in the Hamiltonian, e.g. operators for pairing, angular momentum or higher multipoles than the quadrupole, may be needed to describe the properties of a given nucleus properly. Another extension would lead to configuration mixing, when a sum of Hamiltonians for different boson numbers plus an interaction term between the configurations is used. This was explicitly not used to show that the neutron-deficient platinum isotopes are dominantly consisting of one configuration.

Two band mixing

When two rotational bands come close in energy for the individual states, the states with the same spin will start to mix with each other. The altered wavefunctions of the perturbed states especially the overlap between them will have an influence on the transition rates. Also the excitation energy of the perturbed state will shift with respect to the unperturbed state, this will not be discussed further because the explanation for the shape coexistence in ^{178}Hg is solely based on transition probabilities. The spectroscopic information about ^{178}Hg is so sparse that a quantitative calculation is not feasible anyhow, e.g. only one mixed state per spin is known. The following is based on the notations in Ref. [2]. One starts with a simple level scheme of two unperturbed rotational bands (band I and II) with spin sequence $0^+_{I,II}$, $2^+_{I,II}$, $4^+_{I,II}$... The corresponding perturbed states are labeled $0^+_{1,2}$, $2^+_{1,2}$, $4^+_{1,2}$ and only E2 transitions are taken into account. Usually interband transitions are forbidden for the unperturbed states, so the transition strength stems from the mixing. A perturbed state has then the composition

$$|J_1^+\rangle = \alpha_J|J_I^+\rangle + \beta_J|J_{II}^+\rangle, \quad |J_2^+\rangle = \alpha_J|J_{II}^+\rangle - \beta_J|J_I^+\rangle \tag{1.14}$$

where $\alpha_J^2 + \beta_J^2 = 1$ has to be fulfilled. The relation of the reduced transition strength $B(E2; J_i \rightarrow J_f)$ for a transition from a state with spin J_i to a state with spin J_f to the reduced matrix element $\langle J_i||E2||J_f\rangle$ is given by

$$B(E2; J_i \rightarrow J_f) = \frac{1}{2J_i + 1}|\langle J_i||E2||J_f\rangle|^2 \tag{1.15}$$

The Wigner-Eckart theorem connects the matrix elements and the reduced matrix elements by Clebsch-Gordan coefficients, which contain the dependency of the projection quantum number. Assuming now that the unperturbed interband transition strength is zero and that the intraband matrix elements have the same sign for both bands, one can derive

$$\begin{aligned}
\langle 4_2^+|E2|2_1^+\rangle =& \langle \alpha_4 4_{II}^+ - \beta_4 4_I^+|E2|\alpha_2 2_I^+ + \beta_2 2_{II}^+\rangle \\
=& \alpha_4\alpha_2\langle 4_{II}^+|E2|2_I^+\rangle + \alpha_4\beta_2\langle 4_{II}^+|E2|2_{II}^+\rangle - \alpha_2\beta_4\langle 4_I^+|E2|2_I^+\rangle - \beta_2\beta_4\langle 4_I^+|E2|2_{II}^+\rangle \\
=& \alpha_4\beta_2\langle 4_{II}^+|E2|2_{II}^+\rangle - \alpha_2\beta_4\langle 4_I^+|E2|2_I^+\rangle
\end{aligned} \tag{1.16}$$

for the example of a 4^+ state decaying to the 2^+ of the other band, like it is the case in ^{178}Hg. The last step uses $\langle 4_I^+|E2|2_{II}^+\rangle = \langle 4_{II}^+|E2|2_I^+\rangle = 0$, because interband transitions were assumed to be forbidden. The other perturbed matrix elements may be calculated accordingly. By comparison with the experimental B(E2) values and assuming a rotational band with almost constant (transition) quadrupole moment one can calculate the portion of the two wavefunctions participating to this state. One uncertainty arises in calculating the B(E2) values connected to the quadratic proportionality. The sign of the quadrupole moments needs to be known to correctly calculate the binomic formula. In Tab. 1.1 a sample calculation sticking to the case described above is presented, to show how large the discrepancy can be if a wrong sign is assumed. The J dependance is neglected, because always the same states are compared. Only the deviation of the values (given by the "mixed terms") is essential assuming different or the same signs of the quadrupole moments $Q_0^{I/II}$. The problem is

symmetric and it is sufficient to change only one sign. The square of the amplitudes α_2 and α_4 is given to directly accentuate the portion of structure I and II respectively in the corresponding state. The "mixed term" given in the table is the part of the B(E2) values stemming from the mixed term in the binomic formula.

One notices that the percentage error can get large very fast, if a wrong sign is assumed relative to

Q_0^I [eb]	Q_0^{II} [eb]	α_2^2 [%]	α_4^2 [%]	$\propto B(E2)$ [e^2b^2]	mixed term [e^2b^2]	comment
3	8	100	0	9.0	0	no mixing
3	8	0	100	64.0	0	no mixing
3	8	10	90	50.0	-2.1	small mixing
-3	-8	10	90	50.0	-2.1	changing both signs
3	-8	10	90	54.1	2.1	changing only one sign
3	-8	20	80	45.2	3.8	larger mixing
3	-8	1	90	57.7	0.7	very small mixing of one state
3	-8	1	70	45.5	1.1	more mixing of the second state
3	-8	70	1	7.5	1.1	dependance of the Q_0
4	4	10	90	11.7	-1.4	same Q_0
3	8	50	50	12.3	-6	large mixing

Table 1.1: sample-mixing calculations of B(E2) values depending on the sign of the quadrupole moments

the other one. But there are also cases in which one can even neglect the term with both quadrupole moments in the binomic formula, e.g. small perturbation of the band with much smaller quadrupole moment. Most interesting is the case, where the difference ("mixed term") can be used to determine the relative signs of quadrupole moments. Sometimes the quadrupole moments are known, e.g. from other unperturbed transitions in the corresponding band. The B(E2) values for the same or opposite sign differ by twice the "mixed term" and in special cases one is sensitive to the relative sign for the region of mixing. For example in the last row of Tab. 1.1 the B(E2) value would be twice as high for one opposite sign.

Publication I:
Low-lying electromagnetic transition strengths in ^{180}Pt

Low-lying electromagnetic transition strengths in ^{180}Pt

C. Müller-Gatermann,[1,*] A. Dewald,[1] C. Fransen,[1] T. Braunroth,[1] J. Jolie,[1] J. Litzinger,[1] J. M. Régis,[1] F. von Spee,[1] N. Warr,[1]
K. O. Zell,[1] T. Grahn,[2] P. T. Greenlees,[2] K. Hauschild,[2] U. Jakobsson,[2] R. Julin,[2] S. Juutinen,[2] S. Ketelhut,[2] P. Nieminen,[2]
M. Nyman,[2] P. Peura,[2] P. Rahkila,[2] P. Ruotsalainen,[2] M. Sandzelius,[2] J. Sarén,[2] C. Scholey,[2] J. Sorri,[2]
S. Stolze,[2] J. Uusitalo,[2] and P. Petkov[3]

[1]*Institut für Kernphysik der Universität zu Köln, Zülpicher Strasse 77, D-50937 Köln, Germany*
[2]*University of Jyvaskyla, Department of Physics, P.O. Box 35, FI-40014, University of Jyvaskyla, Finland*
[3]*"Horia Hulubei" National Institute for Physics and Nuclear Engineering, R-76900, Bucharest-Magurele, Romania*

Lifetime measurements have been performed using the ^{98}Mo(^{86}Kr,4n)^{180}Pt reaction at a beam energy of 380 MeV, and the recoil distance Doppler-shift method. In a second experiment the ^{168}Yb(^{16}O,4n)^{180}Pt reaction at a beam energy of 88 MeV using the Ge-gated γ-γ fast timing technique was used to determine lifetimes. Lifetimes of the four lowest yrast states of ^{180}Pt have been determined. The experimental data are compared to calculations within the framework of the interacting boson model and the general collective model. Both models predict a deformed ground state and are consistent with all the remaining experimental results.

I. INTRODUCTION

Even-even nuclei close to shell closures are a subject of numerous experimental and theoretical studies [1,2]. One of the challenges is to understand the shape evolution in the chains of nuclei when one type of nucleon approaches magicity. In the case of the platinum isotopic chain the proton number is close to the shell closure at $Z = 82$. Phenomena such as shape coexistence [2] and shape transitions [3] are observed in this region near the neutron $N = 104$ midshell. The mean lifetime τ of excited states is an experimental observable from which one can extract model-independent transition probabilities that can be compared to theoretical approaches. In this context the model-dependent quadrupole deformation parameter β can also be derived.

A simple correlation for the description of the $B(E2,0_1^+ \to 2_1^+)$ values in even-even nuclei was proposed by Casten [4]. It is a function of the valence neutrons N_ν and valence protons N_π, and the leading term is the product $N_\nu N_\pi$. According to this relation, a rapid change in nuclear shape is expected compared to the neighboring isotopic chains around the proton shell closure at $Z = 82$ for valence neutron numbers around midshell. For the case of $_{78}$Pt the neighboring isotopic chains are $_{76}$Os and $_{80}$Hg. The ^{176,178,180}Os isotopes are known candidates [5] for the critical point symmetry X(5) [6] proposed by Iachello. On the other hand the shapes of the neutron-deficient Hg isotopes [7] are determined by the excitation of intruder states, which cause a significant prolate deformation [8] coexisting with oblate ground states.

The purpose of the present work was to deduce $E2$ transition strengths via lifetime measurements in the ground-state band of ^{180}Pt in order to extend the set of experimental

*cmgater@ikp.uni-koeln.de

observables and clarify the situation between contradicting previous lifetime experiments [9,10] for the 4_1^+ state. Furthermore, the spectroscopic properties like the level scheme as well as the transition probabilities are compared to theoretical models to characterize the nuclei in more detail. Especially if one needs multiparticle-multihole excitations to understand the observables in the isotopic chain of platinum is a long-lasting question [11]. In this work the approach of McCutchan *et al.* [11] was used again to reproduce the spectroscopic properties without intruder states, including the transition strengths which were not known at this time or were incorrect. For this purpose two collective models were used: The interacting boson model (IBM-1) [12] within the extended consistent Q-formalism (ECQF) [13] and the general collective model (GCM) [14].

II. EXPERIMENTAL DETAILS

A. Recoil distance Doppler-shift experiment

To populate excited states in ^{180}Pt, the ^{98}Mo(^{86}Kr,4n) reaction was used. The beam with an energy of 380 MeV was provided by the K-130 cyclotron of the University of Jyväskylä. The target consisted of 0.9 mg/cm^2 isotopically enriched ^{98}Mo. After a fusion-evaporation reaction, the resulting nuclei were stopped in a 15 mg/cm^2 gold foil, after a flight in vacuum with a mean velocity of about 4.4% of the velocity of light. Both the target and the stopper foils were mounted in the DPUNS plunger [15] (differential plunger for unbound nuclear states), which follows the design of the Cologne coincidence plunger [16]. The target-to-stopper distance was monitored by measuring the capacitance, and beam-induced drifts were compensated with a piezoelectric device. The plunger device was coupled to the JUROGAM II Ge-detector array, which consisted of two rings of EUROGAM (European gamma-ray microscope) clover detectors [17] around 90° and two rings
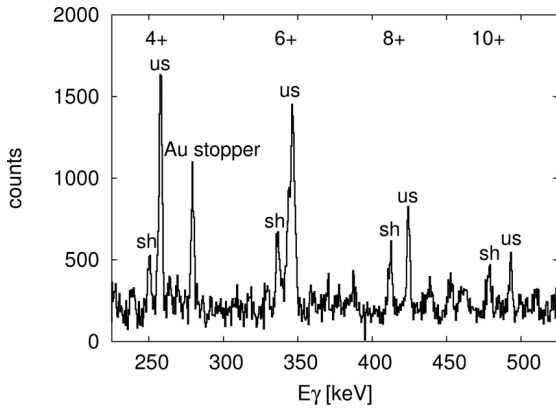
FIG. 1. γ-ray energy spectrum measured with the detectors in the ring at $133°$ (10 detectors). This is the sum over all distances with a gate on both components of the $2_1^+ \to 0_1^+$ transition (including the clover detectors around $90°$). Despite one random coincidence with the strong Coulomb excitation of ^{197}Au the spectrum is very clean. The initial states with their depopulating shifted and unshifted components are marked with "sh" and "us", respectively.

with tapered EUROGAM Phase I [18] or GASP (gamma-ray spectrometer) type [19] germanium detectors at $133°$ and $157°$ with respect to the beam direction. All detectors were Compton suppressed. Data were taken for 18 target-to-stopper distances ranging from electrical contact to 12 mm. The cross section was only around 0.5 mb resulting in a low count rate for the reaction to ^{180}Pt, where only the JUROGAM II detectors at $133°$ and $157°$ can be used for the recoil distance Doppler-shift (RDDS) experiment. Nevertheless, it was possible to analyze the data by gating on the Doppler-shifted component of each direct feeding transition of the respective level of interest. Using the differential decay curve method (DDCM) [20], one is independent of any unobserved side-feeding effects. The normalization between the distances was done via Coulomb excitation of ^{197}Au in the gold stopper. The target was changed once during the experiment. Thus a constant correction factor had to be introduced to the two groups of distances with different targets.

Figure 1 shows the total statistics of the experiment in the ring at $133°$ consisting of 10 detectors. It is summed up over all distances with a gate on both components of the $2_1^+ \to 0_1^+$ transition. This shows not only the quality of the spectra but also the low γ-ray intensities resulting from the low reaction cross section to ^{180}Pt.

B. Electronic timing experiment

Since it was not possible to deduce the lifetime of the rather long-lived 2_1^+ state within the RDDS experiment, a second experiment on ^{180}Pt was performed at the FN tandem accelerator of the University of Cologne using the fast electronic timing technique. This method is sensitive to lifetimes starting around 10 ps up to several ns, whereas the RDDS method can be used to determine lifetimes between hundreds of fs up to hundreds of ps. The Horus (high efficiency observatory for γ-ray unique spectroscopy) cube spectrometer [21] was
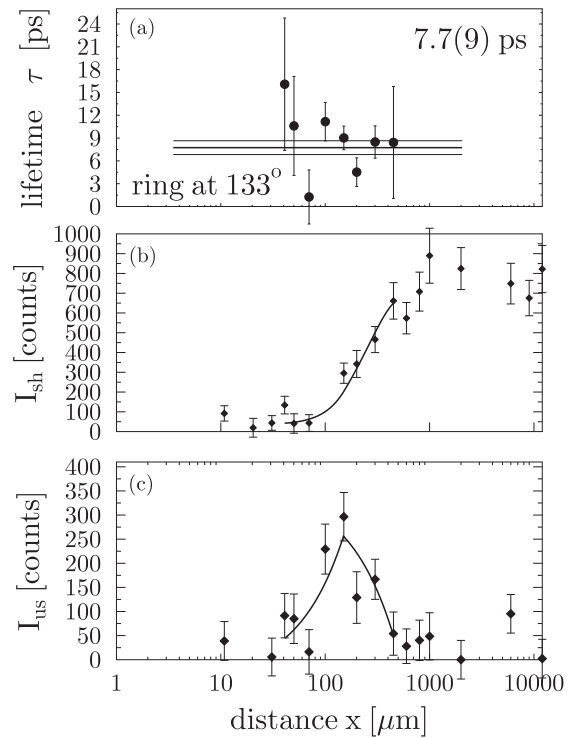

FIG. 2. τ-curve (a) of the 6_1^+ state in ^{180}Pt using the detector ring at $133°$ with a gate on the feeding 8_1^+ state in all backward angle detectors. In addition, the intensities of the shifted (b) and unshifted (c) components are shown.

equipped with eight LaBr$_3$(Ce) scintillation detectors (LaBr), six of which were equipped with anti-Compton shields, two detectors in a Pb shield were fixed inside the spectrometer as additional detectors and in intermediate positions. The remaining eight positions were used with standard single-crystal high-purity germanium (HPGe) detectors. The ^{168}Yb(^{16}O,$4n$)^{180}Pt reaction at a beam energy of 88 MeV was chosen for the triple γ coincidence measurement with a gate applied to the HPGe detectors to clean the LaBr spectrum from other reaction channels. The target was 1 mg/cm^2 ^{168}Yb enriched to 35.2% on a 2 mg/cm^2 Au backing.

III. LIFETIME ANALYSIS

A. DDCM

At each distance x, the lifetime is calculated according to the formalism of the DDCM in "coincidence mode" presented in detail in Ref. [20]. The lifetime is obtained from

$$\tau(x) = \frac{I_{us}(x)}{\frac{d}{dx}I_{sh}(x)} \frac{1}{v}, \tag{1}$$

where x is the target to stopper distance, I_{us} and I_{sh} are the areas of the unshifted and shifted peaks of the transition of interest, respectively, and v is the mean velocity of the recoiling nuclei. Equation (1) yields a set of lifetime values (the τ curve), one for each distance x, which should be independent of x. Since $\gamma\gamma$ coincidences were measured with a direct gate on the Doppler-shifted component of a feeding

TABLE I. Experimental values of the lifetimes using different methods. The adopted values are marked with *. In the theoretical calculations a lifetime of 2.2(3) ps for the 8_1^+ was employed, since no other result for the lifetime existed.

State	E_γ (keV)	τ (ps)
2_1^+	153.2	420(20)[a] *
		420(30)[b]
		540(50)[d]
4_1^+	257.6	37(2)[c] *
		36(6)[b]
		75(14)[d]
		33(4)[e]
		53(5)[f]
6_1^+	346.5	7.7(9)[c] *
		8.8(10)[g]
		13(3)[f]
8_1^+	424.3	2.2(3)[c]
		3.1(1)[g] *
		3.6(12)[f]

[a]This work using the convolution method.
[b]This work using the GCD method.
[c]This work using the RDDS method.
[d]de Voigt *et al.* [9].
[e]Williams *et al.* [10].
[f]Chen *et al.* [24].
[g]von Spee [25] using the RDDS method.

transition, no feeding has to be taken into account. Only a normalization between the distances was performed using the γ-ray lines from the Coulomb excitation of ^{197}Au. Since the target was changed once during the experiment, a constant factor of 0.65 was introduced to correct the normalization for different targets. The application of Eq. (1) for the lifetime determination of the 6_1^+ state in ^{180}Pt is shown in Fig. 2. The lifetimes using this analysis are $\tau(4_1^+) = 37(2)$ ps, $\tau(6_1^+) = 7.7(9)$ ps, and $\tau(8_1^+) = 2.2(3)$ ps and are summarized together with the lifetimes obtained in other experiments in Table I. The
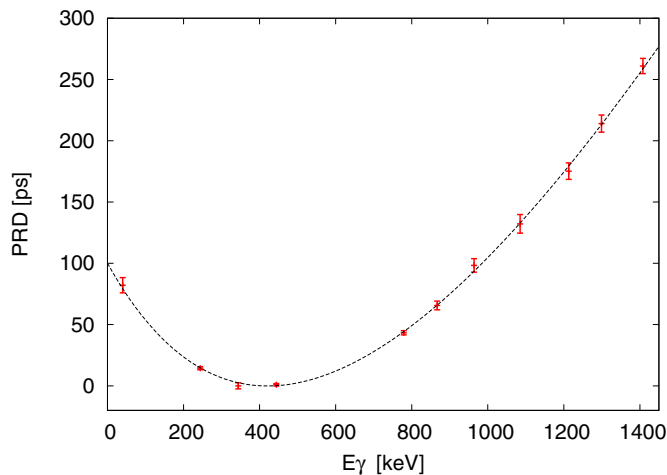

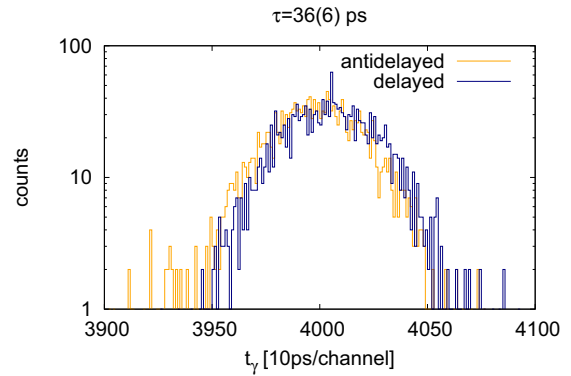FIG. 3. PRD curve of the electronics using a ^{152}Eu source.

FIG. 4. Time-difference spectra of the 4_1^+ state. The difference of the centroids between the delayed and antidelayed spectra corresponds, after correction for the PRD, to twice the lifetime of the state.

10^+ state in ^{180}Pt could not be analyzed due to contamination of a γ-ray line from ^{182}Pt with almost the same energy and the gate would have been in the tail of an intense ^{197}Au γ ray in addition to the decreasing statistics for higher lying states.

B. Electronic timing

By applying two energy gates on the LaBr detectors a feeder-decay cascade corresponding to a given state of interest can be selected. For every combination of LaBr detectors the setup provides two independent time difference spectra, the delayed and the antidelayed, measured as the time difference between a start and a stop detector. The delayed spectrum is produced when the feeding transition provides the start signal and the decay transition the stop signal. The antidelayed spectrum is incremented when the decay transition provides the start signal and the feeding transition the stop signal. To clean up the spectrum, an additional gate on a coincident γ-ray transition observed with a HPGe detector was applied, so triple coincidences were used for the lifetime analysis. Two lifetimes using two different methods were extracted, namely, the generalized centroid difference (GCD) [22] method for the 4_1^+ state and both the convolution method and the GCD method
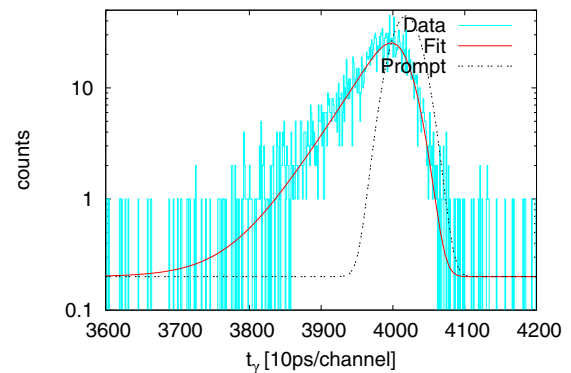

FIG. 5. Fit of the convolution of a prompt peak with the lifetime of the 2_1^+ state. Also the corresponding prompt peak (dotted) is plotted to show the low statistics in the tail.
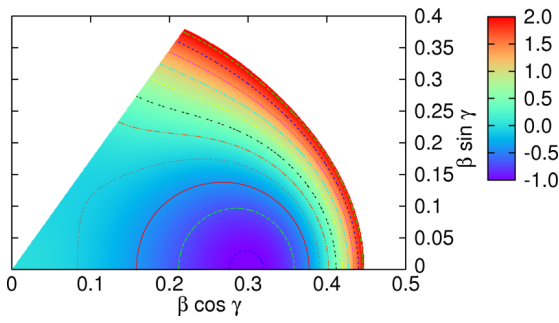
FIG. 6. Potential energy surface extracted from the GCM calculation.

for the 2_1^+ state. Details of the GCD method are presented in Ref. [22]. Since the displacement of the centroids of the delayed and antidelayed time distributions is equal to (twice) the mean lifetime of the state τ and an energy-dependent γ-γ time walk of the system, known as the prompt response difference (PRD) [23], a PRD calibration with a ^{152}Eu source was determined and is shown in Fig. 3. The function to describe the form of the PRD is

$$\text{PRD}(E_\gamma) = \frac{a}{\sqrt{E_\gamma + b}} + c E_\gamma + d. \qquad (2)$$

The analysis of the lifetime of the 4_1^+ state is then straightforward since there is no background below the peak in the LaBr spectra. The time difference spectra are shown in Fig. 4. The result is in agreement with the lifetime using DDCM. Regarding the 2_1^+ state, there is still some background below the peak at 153 keV. One can correct for the timing behavior of the background events originating from Compton-scattered photons of higher energy with the formula [22]

$$\Delta C_{\text{FEP}} = \Delta C + \frac{\Delta C - \Delta C_{\text{BG}}}{\Pi}. \qquad (3)$$

Here ΔC is a centroid difference, where BG and FEP stand for background and full energy peak, respectively, and Π is the peak-to-background ratio. In fact the centroid difference for background events is the mean value of the combinations for background in the feeder (decay) coincident with an event in the decay (feeder) respectively. The result of 420(30) ps for the lifetime is reasonable, but due to the large peak-to-background ratio a second method was applied, the so-called convolution
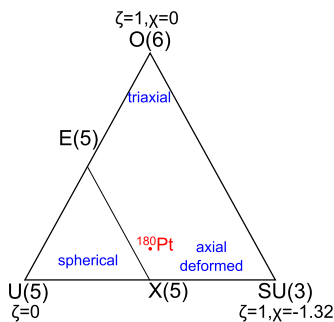

FIG. 7. Placement of ^{180}Pt in the Casten triangle.

method. Here one fits a complete convolution of a prompt peak and a decay function using the lifetime as a fit parameter to the time spectra, given by the function

$$F(t) = \frac{N_0}{\tau} e^{-\frac{t-t_0}{\tau}} \left[1 - \text{erf}\left(\frac{\sigma}{\sqrt{2}\tau} - \frac{t-t_0}{\sqrt{2}\sigma} \right) \right] \qquad (4)$$

(erf is the error function). For longer lifetimes, it is possible to restrict the fit to the tail of the time distribution in order to avoid the prompt peak. In this case, the lifetime is too short for the slope method as the statistics away from the prompt peak are too weak, resulting in a large error. The fit of the convolution is shown in Fig. 5, resulting in a lifetime of the 2_1^+ state of 420(20) ps and supporting the result of the GCD method. The deconvoluted prompt peak has the same width as prompt events in this energy regime, which is an indicator for a correct convolution, and it shows how many counts would remain for a slope fit. Using this method no correction of background events is taken into account, but the background events should correspond mostly to Compton-scattered γ rays of higher lying transitions with shorter lifetimes. Under this assumption these counts are in the timing spectrum close to the prompt peak and do not affect the measured lifetime significantly. In fact the lifetime information is in the tail and the centroid difference between the expected Compton events and a prompt peak is less than 10 ps. This worst case scenario would most probably correspond to a Compton-scattered γ ray of the decaying 6_1^+ state, because the reaction channel is selected with the HPGe gate on the 8_1^+ decay.

IV. DISCUSSION OF RESULTS

The lifetime of the first excited state in ^{180}Pt was remeasured and the value of de Voigt *et al.* [9] is longer than the value obtained in this work. This holds also for the 4_1^+ lifetime, where the data shown here are in good agreement with the lifetime of Williams *et al.* [10]. Especially it has to be noted that two independent methods within two experiments were used and the derived values agree with each other. At the time the experiment was performed the lifetimes of the 6_1^+ and 8_1^+ states were unknown, but recently Chen *et al.* [24] also published lifetimes for these states. All their results for lifetimes of the lowest yrast states are significantly longer. The results in this work were then again confirmed by another RDDS experiment on ^{180}Pt aiming for the commissioning of the GALILEO plunger [26] using the ^{154}Sm(^{32}S,6*n*) reaction. This measurement was sensitive to the lifetimes of the 6_1^+ and 8_1^+ states (also shown in Table I) [25]. For the 8_1^+ state the GALILEO plunger commissioning run has a lot more statistics than the previous experiment, therefore this lifetime is given as an adopted value which is within the errorbars consistent with Chen *et al.* The error of the RDDS experiment is purely statistical and may be underestimated. Regarding the 6_1^+ state the lifetime result is confirmed again. The fact that the results for the lifetimes of the 4_1^+ and 6_1^+ states of Chen *et al.* are both longer hints at a systematic error of these data.
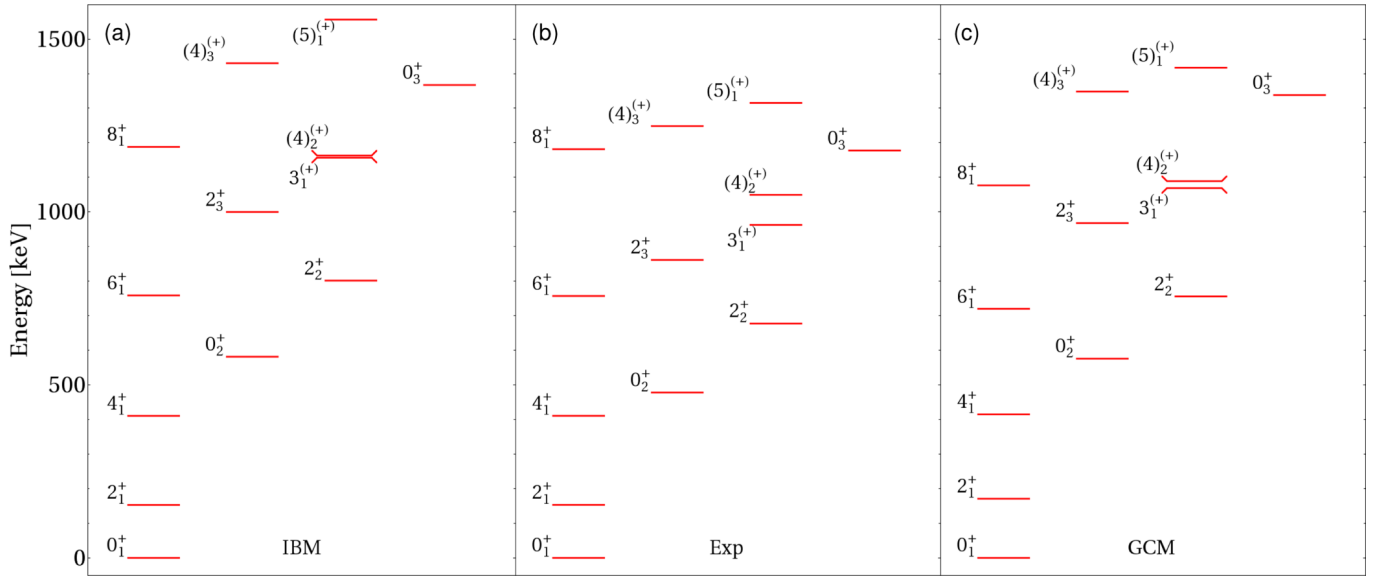
FIG. 8. Comparison of the IBM calculation (a), the experimental values (b), and the GCM calculation (c). Shown are the level energies for the ground state, β and γ bands, and the third 0^+ state. The $B(E2)$ values are summarized in Table I.

V. INTERPRETATION

Two collective models were used to reproduce the level energies and $B(E2)$ values of ^{180}Pt. The first one is the IBM-1 [12] with the Hamiltonian in the extended consistent Q formalism (ECQF) [13]

$$H(\zeta, \chi) = c\left[(1-\zeta)\hat{n}_d - \frac{\zeta}{4N_B}\hat{Q}^\chi \hat{Q}^\chi\right],$$

$$\hat{n}_d = d^\dagger \tilde{d}, \quad \hat{Q}^\chi = [s^\dagger \tilde{d} + d^\dagger s]^{(2)} + \chi[d^\dagger \tilde{d}]^{(2)}, \quad (5)$$

$$\hat{T}(E2) = e_B \hat{Q}^\chi,$$

with N_B being the boson number, $\hat{n}_d$ the d-boson number operator, $\hat{Q}^\chi$ the quadrupole operator, $s^\dagger$, s, $d^\dagger$, and $\tilde{d}$ the creation and annihilation operators for s and d bosons, c a scaling parameter for the energies, $\hat{T}(E2)$ the $E2$ transition operator, e_B the effective boson charge, and ζ, χ the fitting parameters which can directly be used for classification within the Casten triangle [27]. $\zeta = 0.57$, $\chi = -1.00$, $c = 1.25$, and $e_B = 0.18\,e$ b were deduced for ^{180}Pt to reproduce the level scheme and $B(E2)$ values. The uncertainty of these parameters corresponds to ± 1 in the last digit given.

The second model used is the general collective model [14], which approximates the Bohr-Hamiltonian with the sum of kinetic energy $\hat{T}$ and collective potential $V(\beta, \gamma)$ expanded in a series of the quadrupole variables $\alpha_{2\mu}$. The kinetic energy is

$$\hat{T} = \frac{1}{2B_2}[\hat{\pi} \times \hat{\pi}]^{[0]} + \frac{P_3}{3}\{[[\hat{\pi} \times \alpha]^{[2]} \times \hat{\pi}]^{[0]}\}, \quad (6)$$

where $\{...\}$ means the sum over all even permutations of α and the conjugated momenta $\hat{\pi}$, while B_2 is the common mass parameter and P_3 accounts for the deformation-dependent

inertial functions. The potential energy is

$$V(\beta, \gamma) = C_2 \frac{1}{\sqrt{5}}\beta^2 - C_3 \sqrt{\frac{2}{35}}\beta^3 \cos 3\gamma$$

$$+ C_4 \frac{1}{5}\beta^4 - C_5 \sqrt{\frac{2}{175}}\beta^5 \cos 3\gamma$$

$$+ D_6 \frac{1}{5\sqrt{5}}\beta^6 + C_6 \frac{2}{35}\beta^6 \cos^2 3\gamma, \quad (7)$$

with the two intrinsic vibrational variables β and γ, which are related to the quadrupole variables via the polar transformation $\alpha_{20}^{\text{intr}} = \beta \cos \gamma$ and $\alpha_{22}^{\text{intr}} = \beta \sin \gamma / \sqrt{2}$. Using the fit parameters $C_2 = -24.98$, $C_3 = 195.60$, $C_4 = 312.60$, $C_5 = -2135.80$, $C_6 = -613.70$, and $D_6 = 3051.20$ one can obtain directly the potential energy surface (PES) shown in Fig. 6. For completeness the mass parameters are $B_2 = 61.14$ and $P_3 = 0.0594$. One can summarize for both models that all level energies in the ground-state band are reproduced very well, in addition to the corresponding $B(E2)$ values within the error bars. Also the β and γ bands together with the third 0^+ state are reproduced in the correct order with most relative transition strengths from known branching ratios [28] within the error bars. Given the parameters ζ and χ from the IBM-1 calculation one can locate ^{180}Pt in the space spanned by them: the Casten triangle (Fig. 7). In addition to the three limits U(5), SU(3), and O(6), which can be geometrically interpreted as a spherical vibrator, a prolate rotor, and a γ-soft rotor, the location of the critical point symmetries E(5) [29] and X(5) [6] are marked. One sees that ^{180}Pt is, as expected, close to the X(5) symmetry, but on the axially deformed rotor side. It has to be emphasized that in contrast to the Hg nuclei no mixing with proton 2p-2h intruder excitation was introduced or needed to reproduce the spectroscopic properties with a high quality. García-Ramos et al. [30] published a series of model calculations for the platinum isotopic chain using these intruders and compared it

to the simpler ECQ calculations by McCutchan *et al.* [11]. The values given in there are consistent with the parameters of the ECQ Hamiltonian used in this work. This means the parameters found to describe ^{180}Pt in a detailed way are consistent with parameters used to describe a larger series of nuclei. Also the PES from the GCM calculation shows a prolate deformation with some γ softness for the ground state. The experimental and theoretical values from the models for the level energies and transition strengths are summarized in Fig. 8 and Table II.

In Fig. 9 experimental results of transition quadrupole moments Q_t for the $N = 102$ isotones are shown. Also given are the expectations for rotor, vibrator, and X(5)-like nuclei with increasing spin. It has been shown that multiparticle-hole excitations cause a large deformation in the neutron-deficient lead and mercury isotopes [1]. This effect is also observed in the yrast band of ^{182}Hg. One can see an abrupt increase in Q_t values of yrast transitions above the 2_1^+ state. Whereas ^{180}Pt, ^{178}Os, and ^{176}W show a rather constant behavior. Observed variations are small and can be explained by different collective structures: For ^{180}Pt, Q_t values are constant and follow the rotor expectations; the same holds for ^{176}W (unfortunately here
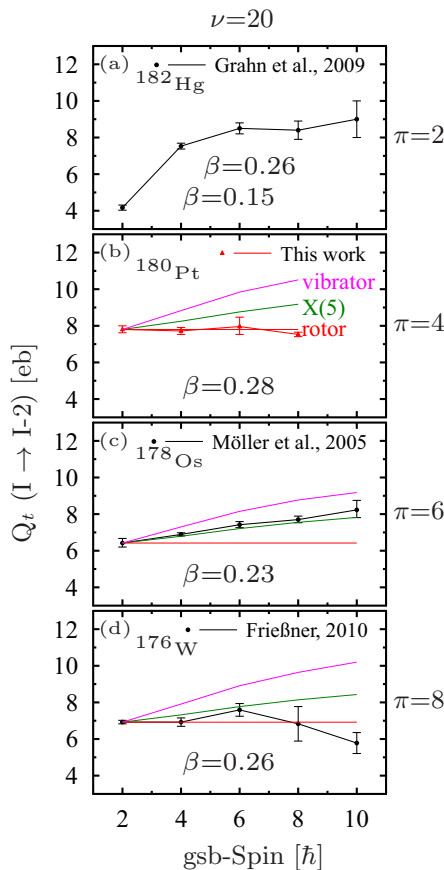

FIG. 9. Transition quadrupole moments for the $N = 102$ isotone around Pt. π and ν are the valence proton and neutron number, respectively. Experimental values taken from [7,32,33]. The indicated deformations are calculated from the lowest quadrupole moment neglecting variations described by the collective models; just for the case of ^{182}Hg the near constant deformation for the excited states is given as well.

TABLE II. Derived absolute $B(E2)$ values from the experiments for the yrast band transitions in e^2 b^2 as well as relative $B(E2)$ values from known branching ratios [28] for the states in the β and γ bands and the third 0^+ state. For each state the level energy is given in keV. The experimental data of ^{180}Pt are compared to the predictions of the IBM and GCM calculations.

J_i^π	J_f^π	E_{level} [keV]			$B(E2)$ [e^2 b^2]		
		IBM	Expt.	GCM	IBM	Expt.	GCM
2_1^+		153.1	153.3	171			
	$\rightarrow 0_1^+$				1.13	1.20(6)	1.09
4_1^+		410.6	410.7	415			
	$\rightarrow 2_1^+$				1.78	1.70(8)	1.89
6_1^+		758.8	757.1	720			
	$\rightarrow 4_1^+$				2.1	1.9(2)	2.4
8_1^+		1188.1	1181.5	1077			
	$\rightarrow 6_1^+$				2.2	2.6(4)	2.8
0_2^+		581.4	478.1	576			
2_3^+		988.7	861.4	968			
	$\rightarrow 2_2^+$				324.36	400(300)	158.23
	$\rightarrow 0_2^+$				100	100	100
	$\rightarrow 4_1^+$				56.7	61(7)	60.99
	$\rightarrow 2_1^+$				3.18	5.3(7)	1.35
	$\rightarrow 0_1^+$				9.72	12.4(9)	7.34
$(4)_3^{(+)}$		1415.9	1248.2	1348			
	$\rightarrow 2_3^+$				100	100	100
	$\rightarrow 2_2^+$				1.24	4(?)	1.43
	$\rightarrow 4_1^+$				1.34	0.9(7)	1.19
	$\rightarrow 2_1^+$				1.11	0.6(1)	1.83
2_2^+		801.5	677.5	756			
	$\rightarrow 0_2^+$				214.95	200(200)	98.41
	$\rightarrow 4_1^+$				40.33	30(20)	22.5
	$\rightarrow 2_1^+$				100	100	100
	$\rightarrow 0_1^+$				4.41	10.0(8)	9.38
$3_1^{(+)}$		1156.9	962.7	1069			
	$\rightarrow 2_2^+$				100	100	100
	$\rightarrow 4_1^+$				18.29	15(2)	20.61
	$\rightarrow 2_1^+$				11.62	17.1(7)	16.44
$(4)_2^{(+)}$		1163.2	1049.3	1089			
	$\rightarrow 2_2^+$				100	100	100
	$\rightarrow 4_1^+$				17.90	45(6)	31.84
	$\rightarrow 2_1^+$				0.04	1.4(7)	0.85
$(5)_1^{(+)}$		1556.1	1315.2	1417			
	$\rightarrow 3_1^{(+)}$				100	100	100
	$\rightarrow 4_1^+$				3.15	4.7(4)	8.02
0_3^+		1367.0	1177.7	1338			
	$\rightarrow 2_2^+$				100	100	100
	$\rightarrow 2_1^+$				0.83	22(2)	0.01

the experimental errors are larger, especially for the 6_1^+, 8_1^+ states). ^{178}Os follows very nicely the X(5) prediction. Looking to the absolute $Q_t(2_1^+ \to 0_1^+)$ values, the corresponding β deformation is given also in Fig. 9. For ^{182}Hg the β deformation of the excited states caused by the intruder configuration is given as well. The deformation decreases approaching the shell closure from ^{176}W to ^{182}Hg with one exception: ^{180}Pt. The deformation found for ^{180}Pt is comparable to the deformation of the excited states in ^{182}Hg. This strongly suggests that the large deformation in ^{180}Pt is caused by the intruder configuration becoming the ground state. This is supported by García-Ramos et al. [31] with a mean-field approach as well as an IBM calculation with 2p-2h configuration mixing. However, the authors also admit that the configuration mixing is somehow "hidden" and does not show up explicitly as it does in the isotopic chains of mercury or lead.

different from the isotopic chain of mercury and others where such excitations are needed to explain the nuclear properties [2,8]. A second note can be made that ^{180}Pt is clearly not following the expected trend for transition quadrupole moments in X(5) nuclei. The rather large quadrupole deformation in the neighboring ^{182}Pt (seen by Gladnishki et al. [34]) indicates that this is a general effect, which points to a weakening of the shell closure at $Z = 82$. In the future one should investigate also the transition quadrupole moments for the lighter ^{176,178}Pt isotopes and compare them to the calculations by García-Ramos et al. [31]. It is suggested that the weakening of the shell closure is apparent only down to ^{178}Pt and the deformation should decrease for the lower masses. So far the lifetime information on these nuclei is too sparse, but reachable with standard fusion-evaporation reactions and stable beams; they would serve as a perfect testing ground.

VI. CONCLUSION

Four lifetimes in the yrast band of ^{180}Pt were measured using three experiments to determine yrast $B(E2)$ values. IBM-1 and GCM calculations were performed to describe the nuclear structures. They indicate both an axially deformed shape with some γ softness and reproduce the level scheme and the $B(E2)$ values quite well. Except for the large Q_t values we have no indication of multiparticle-hole excitations. This is

[1] T. Grahn, A. Dewald, O. Möller, R. Julin, C. W. Beausang, S. Christen, I. G. Darby, S. Eeckhaudt, P. T. Greenlees, A. Görgen, K. Helariutta, J. Jolie, P. Jones, S. Juutinen, H. Kettunen, T. Kröll, R. Krücken, Y. Le Coz, M. Leino, A.-P. Leppänen, P. Maierbeck, D. A. Meyer, B. Melon, P. Nieminen, M. Nyman, R. D. Page, J. Pakarinen, P. Petkov, P. Rahkila, B. Saha, M. Sandzelius, J. Sarén, C. Scholey, J. Uusitalo, M. Bender, and P.-H. Heenen, Nucl. Phys. A **801**, 83 (2008).

[2] K. Heyde and J. L. Wood, Rev. Mod. Phys. **83**, 1467 (2011).

[3] P. Cejnar, J. Jolie, and R. F. Casten, Rev. Mod. Phys. **82**, 2155 (2010).

[4] R. F. Casten, Nucl. Phys. A **443**, 1 (1985).

[5] A. Dewald, O. Möller, B. Saha, K. Jessen, A. Fitzler, B. Melon, T. Pissulla, S. Heinze, J. Jolie, K. O. Zell, P. von Brentano, P. Petkov, S. Harissopulos, G. De Angelis, T. Martinez, D. R. Napoli, N. Marginean, M. Axiotis, C. Rusu, D. Tonev, A. Gadea, Y. H. Zhang, D. Bazzacco, S. Lunardi, C. A. Ur, R. Menegazzo, and E. Farnea, J. Phys. G: Nucl. Part. Phys. **31**, S1427 (2005).

[6] F. Iachello, Phys. Rev. Lett. **87**, 052502 (2001).

[7] T. Grahn, A. Petts, M. Scheck, P. A. Butler, A. Dewald, M. B. Gomez Hornillos, P. T. Greenlees, A. Görgen, K. Helariutta, J. Jolie, P. Jones, R. Julin, S. Juutinen, S. Ketelhut, R. Krücken, T. Kröll, M. Leino, J. Ljungvall, P. Maierbeck, B. Melon, M. Nyman, R. D. Page, T. Pissulla, P. Rahkila, J. Sarén, C. Scholey, A. Semchenkov, J. Sorri, J. Uusitalo, R. Wadsworth, and M. Zielinska, Phys. Rev. C **80**, 014324 (2009).

[8] J. E. García-Ramos and K. Heyde, Phys. Rev. C **89**, 014306 (2014).

[9] M. De Voigt, R. Kaczarowski, H. Riezebos, R. F. Noorman, J. Bacelar, M. Deleplanque, R. Diamond, F. Stephens, J. Sauvage, and B. Roussière, Nucl. Phys. A **507**, 472 (1990).

[10] E. Williams, C. Plettner, E. A. McCutchan, H. Levine, N. V. Zamfir, R. B. Cakirli, R. F. Casten, H. Ai, C. W. Beausang, G. Gürdal, A. Heinz, J. Qian, D. A. Meyer, N. Pietralla, and V. Werner, Phys. Rev. C **74**, 024302 (2006).

[11] E. A. McCutchan, R. F. Casten, and N. V. Zamfir, Phys. Rev. C **71**, 061301(R) (2005).

[12] A. Arima and F. Iachello, Phys. Rev. Lett. **35**, 1069 (1975).

[13] D. D. Warner and R. F. Casten, Phys. Rev. C **28**, 1798 (1983).

[14] G. Gneuss and W. Greiner, Nucl. Phys. A **171**, 449 (1971).

[15] M. J. Taylor, D. M. Cullen, A. J. Smith, A. McFarlane, V. Twist, G. A. Alharshan, M. G. Procter, T. Braunroth, A. Dewald, E. Ellinger, C. Fransen, P. A. Butler, M. Scheck, D. T. Joss, B. Saygi, C. G. McPeake, T. Grahn, P. T. Greenlees, U. Jakobsson, P. Jones, R. Julin, S. Juutinen, S. Ketelhut, M. Leino, P. Nieminen, J. Pakarinen, P. Peura, P. Rahkila, P. Ruotsalainen, M. Sandzelius, J. Sarén, C. Scholey, J. Sorri, S. Stolze, and J. Uusitalo, Nucl. Instrum. Methods A **707**, 143 (2013).

[16] A. Dewald, O. Möller, and P. Petkov, Prog. Part. Nucl. Phys. **67**, 786 (2012).

[17] G. Duchêne, F. A. Beck, P. J. Twin, G. de France, D. Curien, L. Han, C. W. Beausang, M. A. Bentley, P. J. Nolan, and J. Simpson, Nucl. Instrum. Methods A **432**, 90 (1999).

[18] C. W. Beausang, S. A. Forbes, P. Fallon, P. J. Nolan, P. J. Twin, J. N. Mo, J. C. Lisle, M. A. Bentley, J. Simpson, F. A. Beck, D. Curien, G. de France, G. Duchêne, and D. Popescu, Nucl. Instrum. Methods A **313**, 37 (1992).

[19] C. R. Alvarez, Nucl. Phys. News **3**, 10 (1993).

[20] A. Dewald, S. Harissopulos, and P. von Brentano, Z. Phys. A Atomic Nuclei **334**, 163 (1989).

[21] A. Linnemann, Ph.D thesis, Universität zu Köln, 2006.

[22] J.-M. Régis, G. S. Simpson, A. Blanc, G. de France, M. Jentschel, U. Köster, P. Mutti, V. Paziy, N. Saed-Samii, T. Soldner, C. A. Ur, W. Urban, A. M. Bruce, F. Drouet, L. M. Fraile, S. Ilieva, J. Jolie, W. Korten, T. Kröll, S. Lalkovski, H. Mach, N. Mărginean, G. Pascovici, Z. Podolyak, P. H. Regan, O. J. Roberts, J. F. Smith, C. Townsley, A. Vancraeyenest, and N. Warr, Nucl. Instrum. Methods A **763**, 210 (2014).

[23] J.-M. Régis, M. Rudigier, J. Jolie, A. Blazhev, C. Fransen, G. Pascovici, and N. Warr, Nucl. Instrum. Methods A **684**, 36 (2012).

[24] Q. M. Chen, X. G. Wu, Y. S. Chen, C. B. Li, Z. C. Gao, G. S. Li, F. Q. Chen, C. Y. He, Y. Zheng, S. P. Hu, J. Zhong, Y. H. Wu, H. W. Li, and P. W. Luo, Phys. Rev. C **93**, 044310 (2016).

[25] F. von Spee, Bachelor thesis, Universität zu Köln, 2016.

[26] A. Goasduff, C. Fransen, A. Dewald, S. Thiel, T. Braunroth, C. Müller-Gatermann, D. Bazzacco, P. Cocconi, A. Gozzelino, K. Hadyńska-Klęk, G. Jaworski, P. R. John, D. Mengoni, F. Recchia, M. Siciliano, D. Testov, J. J. Valiente-Dobón, and F. von Spee, in LNL Annual Report 2015, INFN, Laboratori Nazionali di Legnaro, 2016, pp. 91–92 (unpublished).

[27] R. F. Casten, *Nuclear Structure from a Simple Perspective*, 2nd ed. (Oxford University, Oxford, 2000).

[28] E. A. McCutchan, Nucl. Data Sheets **126**, 151 (2015).

[29] F. Iachello, Phys. Rev. Lett. **85**, 3580 (2000).

[30] J. E. García-Ramos and K. Heyde, Nucl. Phys. A **825**, 39 (2009).

[31] J. E. García-Ramos, K. Heyde, L. M. Robledo, and R. Rodríguez-Guzmán, Phys. Rev. C **89**, 034313 (2014).

[32] O. Möller, Ph.D. thesis, Universität zu Köln, 2005.

[33] G. Frießner, Diploma thesis, Universität zu Köln, 2010.

[34] K. A. Gladnishki, P. Petkov, A. Dewald, C. Fransen, M. Hackstein, J. Jolie, T. Pissulla, W. Rother, and K. Zell, Nucl. Phys. A **877**, 19 (2012).

Publication II:
A new dedicated plunger device for the GALILEO γ-ray detector array

A new dedicated plunger device for the GALILEO γ-ray detector array

C. Müller-Gatermann [a,*], F. von Spee [a], A. Goasduff [b,c], D. Bazzacco [c], M. Beckers [a],
T. Braunroth [a], A. Boso [b], P. Cocconi [d], G. de Angelis [d], A. Dewald [a], C. Fransen [a], A. Goldkuhle [a],
A. Gottardo [d], A. Gozzelino [d], K. Hadyńska-Klęk [d], G. Jawroski [d], P.R. John [b], J. Jolie [a],
S.M. Lenzi [b], J. Litzinger [a], R. Menegazzo [d], D. Mengoni [b,c], D.R. Napoli [d], F. Recchia [b],
M. Siciliano [d], D. Testov [b,c], S. Thiel [a], J.J. Valiente-Dobón [d], K.O. Zell [a]

[a] Institut für Kernphysik der Universität zu Köln, Zülpicher Straß,e 77, D-50937 Köln, Germany
[b] Dipartimento di Fisica e Astronomia dell'Università di Padova, Padova, Italy
[c] INFN, Sezione di Padova, Padova, Italy
[d] INFN, Laboratori Nazionali di Legnaro, Legnaro (Padova), Italy

ARTICLE INFO

ABSTRACT

A new device, the GALILEO plunger, has been developed for lifetime measurement studies using the GALILEO γ-ray detector array at the Laboratori Nazionali di Legnaro (LNL) in Legnaro, Italy. This plunger device holds two stretched metal foils in the beam path for the use of the recoil distance Doppler-shift technique in order to measure lifetimes of nuclear excited states in the range of 1 ps to 1 ns. The compact design allows one to combine different auxiliary detectors with the plunger device inside the target chamber and takes care of high γ-ray transparency. The design and control of the device are presented in this paper, together with lifetimes of excited states in ^{180}Pt measured within the first in-beam commissioning run.

1. Introduction

Since 1992 the GAmma-ray SPectrometer (GASP) [1] was located at the Instituto Nazionale di Fisica Nucleare (INFN) Laboratori Nazionali di Legnaro (LNL) and several hundred experiments were successfully conducted. This spectrometer could be coupled to the Cologne coincidence plunger [2] to measure lifetimes of excited nuclear states employing the recoil distance Doppler-shift (RDDS) method. Over the years some disadvantages arose, mainly the small available space for ancillary devices/detectors together with a nonflexible holding structure. These problems ought to be overcome by the successing GALILEO γ-ray spectrometer [3,4], which consists in phase I of a backward hemisphere and a detector ring around 90°. The backward hemisphere holds fifteen GASP germanium detectors distributed equally in three rings at 152°, 129° and 119° with respect to the beam direction. Around 90° another ten detectors are mounted. A divisible forward hemisphere is symmetric to the backward hemisphere and will be added later, but the inner holding structure for the ring around 21° or the complete hemisphere can be removed to gain space for ancillary detectors like a Recoil Filter Detector [5]. In its final stage the backward hemisphere will be replaced to hold ten new developed triple cluster HPGe detectors (GTC) in two rings at 152° and 118° recovering crystals from EUROBALL [6]. All detectors are Compton-suppressed using the existing GASP BGO-shields,

for the GTCs the anti-Compton shield of the EUROBALL detector will be rearranged. The electronics are changed to new preamplifiers and digitizers taking advantage of the work deployed already in the setup of AGATA [7], which shall not be discussed here further. As described before the GALILEO spectrometer [3,4] can be opened to the front and back, i.e. along the beam axis which is a major change to the GASP spectrometer opening sideways. This is the main reason for the development of a new plunger device dedicated to this spectrometer, as the formerly used Cologne coincidence plunger [2] would circumvent the opening of at least the backward hemisphere once mounted. Taking benefit of the occasion a very compact design was chosen, which fits inside the existing target chamber and should guarantee the compatibility to ancillary detectors, e.g. EUCLIDES [8] which was not given before.

2. Mechanical design

Several constrains have to be overcome in the design of the plunger device. First of all as little material as possible has to be used to get the maximum transparency for γ-rays as well as particles, still ensuring the needed stability to measure and maintain the target to degrader distance with high precision in the sub-micrometer regime. Several ancillary detectors for charged particles are existing (e.g. EUCLIDES), which should fit together with the plunger in the target chamber. At

---

* Corresponding author.
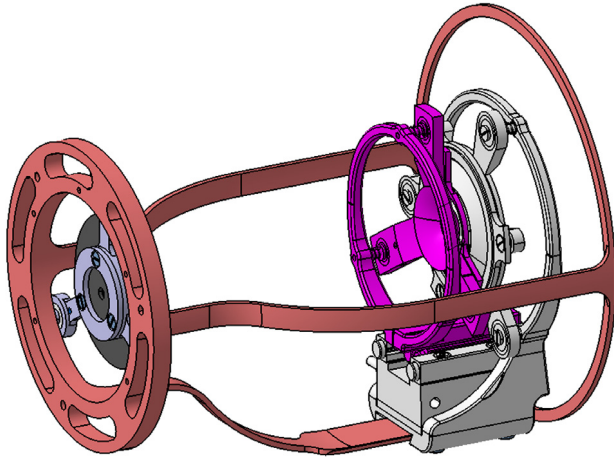 E-mail address: cmgater@ikp.uni-koeln.de (C. Müller-Gatermann).

Fig. 1. (Color online) The holding structure which is fixed to the beam entrance of the GALILEO target chamber is shown in red (intermediate gray) with the 4 mm entrance collimator on the left. At the right end of this structure the holder of the degrader is fixed, this is shown in light gray as well as the bottom part of the motor. The movable upper part of the motor is connected to the target holder and shown in violet (dark gray).
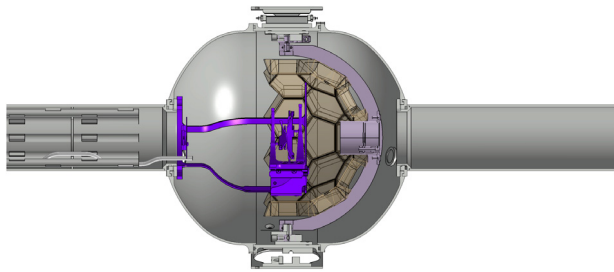

Fig. 2. (Color online) The plunger in dark purple (dark gray) together with the forward hemisphere of the EUCLIDES detector array in beige (light gray) in the target chamber. The beam is coming from the left.

least one collimator has to be installed close to the focus point on the target to enable focussing of the beam. Since the space is very limited even without ancillary detectors, the parallel alignment of the stretched metal foils has to be done outside of the target chamber assuring reproducibility for the reinstallation. Of course all features of a plunger device like an active feedback system to compensate for beam induced changes of the target to degrader distance shall be given as well. A visualization of the GALILEO plunger device with its holding structure is shown in Fig. 1 and together with EUCLIDES [8] in the target chamber in Fig. 2.

The design idea is the following:

- A compact motor allows the movement of the target with respect to the fixed degrader and also the operation of the feedback system.
- The target is attached to the motor via a small holding structure that bears the target cone required for stretching.
- The fixed degrader with its cone is directly attached to a holder, which also carries the motor
- The complete unit is mounted on a support inside the chamber

The mechanical support is realized by attaching it to the beam-entrance of the GALILEO target chamber. An entrance collimator with a diameter of 4 mm is fixed to the support. The holding structure of the degrader can be screwed on the lower arm of the support in a fixed position to have the degrader foil in the center of the spectrometer. Target and degrader cones are compatible to the Cologne coincidence plunger [2]. The degrader cone is fixed with spacers to its holder. The target cone is attached with adjustable springs to the respective holder on the
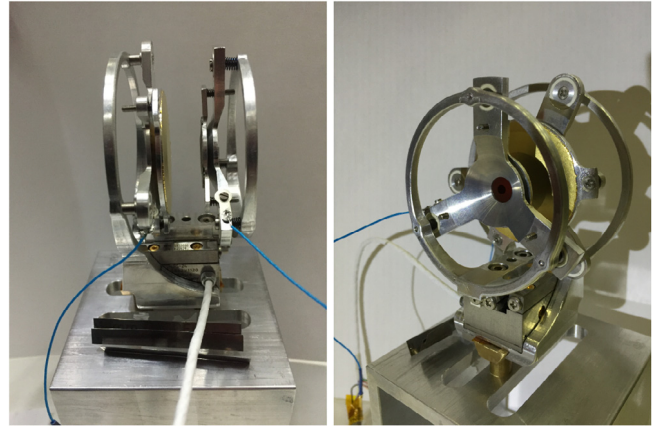

Fig. 3. (Color online) Pictures of the plunger unit outside of the target chamber being fully operational on the support block. The parallel alignment of the foils can be done with the springs between the target cone and the holding structure. The PI LPS-24 motor serves as the connection between the two holding structures of the target and stopper.

motor, via these springs the foils can be aligned parallel. The motor with the assembly for target and degrader can be attached to another support block, which eases the alignment procedure outside of the target chamber. The motor is a compact linear table with piezodrive capable of use in vacuum from Physik Instrumente (PI), the model number is LPS-24 [9]. It was chosen due to its small dimensions of 24 mm × 33 mm × 20 mm shadowing only detectors around 90° according to its position below the foils. These detectors cannot be used in Doppler-shift experiments, because the Doppler effect is zero at 90° with respect to a moving source. The distance range of the motor is 15 mm which is large enough to cover the foil separations of interest. Larger separations may also make it necessary to correct the intensity of the γ-rays emitted shortly after the target since the opening angle between the target and the Compton-suppressed detectors gets smaller. The resolution of the position sensor in the motor is 20 nm and thus precise enough that there is no need for a second measurement of the relative distance between the foils. This is typically done in the Cologne $\gamma\gamma$-coincidence plunger devices [2] with inductive transducers (e.g. from Tesa technology [10]) reducing the transparency with additional material. Also an additional piezostack to correct the beam induced distance fluctuations is not needed, because the target can be moved with the LPS-24 motor with a precision of around 40 nm. That the precision of a piezo motor is sufficient for the feedback control is already shown with other plunger devices, e.g. the Orsay Universal Plunger System (OUPS) [11]. In Fig. 3 the plunger on the support block is shown.

3. Feedback control

The Plunger Feedback Control software for Linux (PFCL) was initially developed to control the Cologne coincidence plunger [2]. The programs were also adopted to work with other plunger devices with different motors or other Multi Channel Analyser (MCA) cards used for distance measurements between the foils from the capacitance signal, i.e. the induced voltage in a foil from a pulse generator signal applied to the other foil. There exists an automatic feedback control to keep a distance constant during the experiment with a precision in the sub-micrometer range as well as individual programs to control or examine the plunger signals manually, e.g. to drive the motor or check the MCA readout. The software package is written in LABVIEW 8.6 [12] working with openSUSE 11.2 [13] and was translated recently to work with Microsoft Windows operating systems [14] as well. The new system is tested with Microsoft Windows 10 [14] and LABVIEW 2017 [12], but it should work also with operating systems starting from Microsoft Windows 7 [14]. This is needed due to the dismissed Linux driver support of National

Instruments (NI) [12] for future hardware components. A calibration of relative foil separations can be done using the position information of the motor encoder in advance of the experiment. The induced voltage is then used during the experiment to maintain the separation adjusting the motor in the feedback system running on the control computer. The MCA card used is a NI PCIe-6251 [12] which gets a trigger from the pulser through a NIM Logic Shaper and Delay module at the same time as the signal arrives from a NIM Linear Gate and Stretcher module after the amplifier. The motor controller E861 also from PI [9] is connected via USB to the control computer, which is located in the experimental hall II near the GALILEO spectrometer. During the experiment, the operator moves and checks the plunger position from a PC installed in the experimental box, using the laboratory network. The plunger is also monitored in the readout graphics user interface as a channel in the data acquisition system with a fixed rate of 500 Hz.

4. Plunger commissioning

The plunger was first commissioned in Cologne using the ^{12}C and ^{32}S beams impinging on a Cd target. This was done to check the stability of the fragile construction under real experimental conditions, e.g. with vacuum pumps nearby inducing oscillations since fast vibrations or similar cannot be corrected by the feedback system. After the first test the plunger was transported and mounted inside the GALILEO reaction chamber to validate the mechanical construction. 15 ΔE-E telescopes from the EUCLIDES array [8] were mounted downstream of the target together with the plunger to check the compatibility of the devices. All tests were completed successfully and finally an in-beam test to reproduce known lifetimes was performed, which is described in the following.

4.1. RDDS experiment on ^{180}Pt

The ^{154}Sm(^{32}S,6n)^{180}Pt fusion evaporation reaction has been chosen to measure lifetimes of the 6_1^+ and 8_1^+ states in ^{180}Pt using the RDDS technique in $\gamma\gamma$-coincidence. The beam was delivered by the XTU tandem accelerator with an energy of 183 MeV. GALILEO was fully equipped with HPGe detectors in the backward hemisphere and around 90°, downstream of the target the setup consisted of the Neutron Wall [15] but it was not used in this experiment. The target was 1 mg/cm^2 ^{154}Sm (enrichment $\geq$ 98%) on a 2.2 mg/cm^2 Ta backing, 9.4 mg/cm^2 Au was used as a stopper foil for the recoiling nuclei after the reaction. Data were taken for 10 distances ranging from 5 μm to 150 μm between target and stopper foils approximately 8 h for each distance and a beam current of 3 pnA. This led to sufficient statistics to perform the lifetime analysis applying the Differential Decay Curve Method (DDCM) [16] with coincidences. A spectrum to illustrate the quality of the data is shown in Fig. 4.

4.2. Analysis and results

The recoil velocity was extracted by the Doppler-shifts in energy of the $8_1^+ \rightarrow 6_1^+$, $6_1^+ \rightarrow 4_1^+$ and $4_1^+ \rightarrow 2_1^+$ transitions in ^{180}Pt in each ring of the backward hemisphere. A mean value of 1.53(5) % of the speed of light was calculated for the reaction of interest. A normalization of the distances was applied by gating on the decay of the 2_1^+-, 4_1^+- and 6_1^+-state and integrating the intensity of all populating yrast transitions up the 8_1^+-state. Also a peakwidth calibration was performed for shifted and unshifted component individually with respect to the γ-ray energy. In the subsequent fitting process these widths as well as the peak positions were fixed parameters. The lifetime analysis was done applying a gate on the feeding transition of each respective excited state for a lifetime determination excluding unknown delayed feeding. According to the DDCM [16] the lifetimes were calculated via Eq. (1):

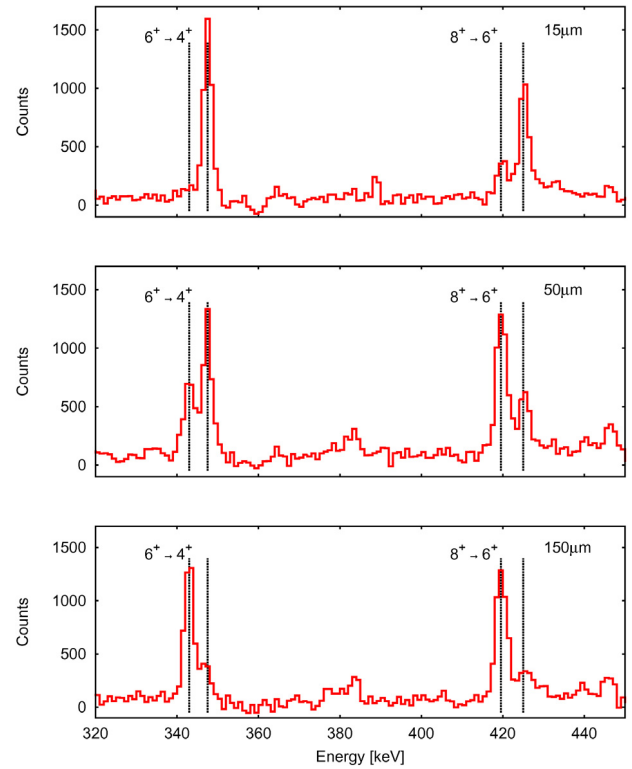$$\tau = \frac{\{B_s, A_u\}}{v \frac{d}{dx}\{B_s, A_s\}}$$ (1)

Fig. 4. (Color online) γ-ray spectrum of the experiment on ^{180}Pt gated on the $10_1^+ \rightarrow 8_1^+$ transition. The evolution with the distance of the $8_1^+ \rightarrow 6_1^+$ and the $6_1^+ \rightarrow 4_1^+$ is shown for three distances. The shifted and unshifted component of the transitions corresponding to the detector ring at 152° are marked with dashed lines.

where $B(A)$ is a populating (depopulating) transition of the state of interest, $s(u)$ stands for shifted (unshifted) component of the respective transition, v is the recoil velocity and the brackets denote a coincidence between the transitions B and A selected with a gate on the first one. In this analysis, the quantities $\{B_s, A_u\}$ and $\{B_s, A_s\}$ were not directly obtained by gating onto the shifted component of transition B, but using a gate on the full transition B and subtracting the contribution of the unshifted component. This method eases the fitting procedure together with less free parameters for a reliable description of the spectra and prevents wrong intensities at large distances where only shifted components would remain in coincidence. In terms of the upper notation this corresponds to:

$$\{B_s, A_u\} = \{B, A_u\} - \{A, B_u\}$$

$$\{B_s, A_s\} = \{B, A_s\}$$

The chosen distances were in the sensitive region to the lifetimes of the 6_1^+ and 8_1^+ state. The sensitive region is defined via the normalized intensities of the shifted component with respect to the distance, the limits are those distances where the slope of the curve is at the half of the maximum value. The analysis was done using direct gates on the $8_1^+ \rightarrow 6_1^+$ and $10_1^+ \rightarrow 8_1^+$ transitions while the latter was also used as a indirect gate for the 6_1^+ state. All detector rings in the backward hemisphere were used for the analysis and a mean value from the independently extracted lifetimes was calculated. The variance of the values for the 6_1^+ state was larger than expected and is reflected in the given error, though no systematics can be seen with respect to the gate or detector angle. The results (mean values) from the lifetime analysis are:

$$\tau(6_1^+) = 8.8(10) \text{ ps and } \tau(8_1^+) = 3.1(1) \text{ ps}$$

In Fig. 5 a τ-curve of the 8_1^+ state in ^{180}Pt using the detector ring at 129° with a gate on the feeding $10_1^+ \rightarrow 8_1^+$ transition in all backward
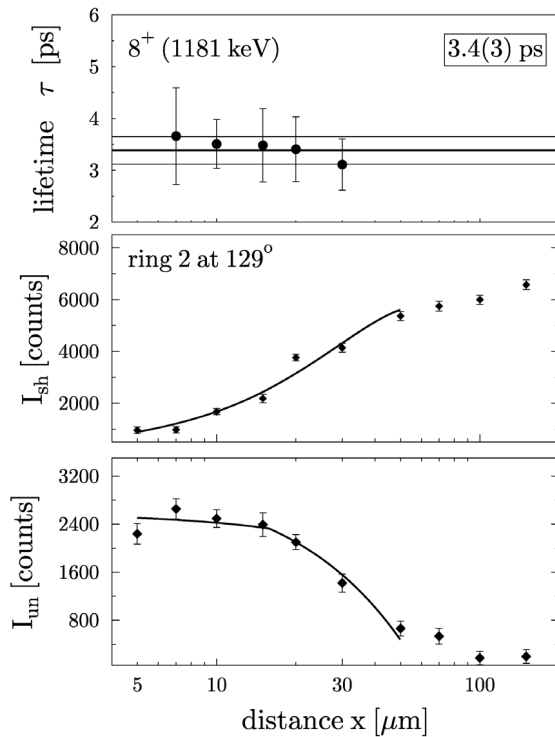
Fig. 5. τ-curve (upper) of the 8^+_1 state in ^{180}Pt using the detector ring at 129° with a gate on the feeding 10^+_1 state in all backward angle detectors. In addition, the intensities of the shifted (middle) and unshifted (lower) components are shown.

Fig. 6. τ-curve (upper) of the 6^+_1 state in ^{180}Pt using the detector ring at 152° with a gate on the feeding 8^+_1 state in all backward angle detectors. In addition, the intensities of the shifted (middle) and unshifted (lower) components are shown.
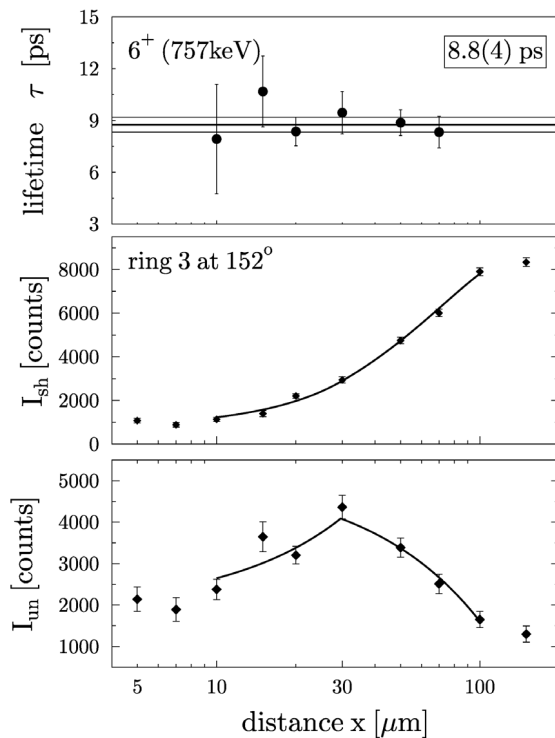
angle detectors is shown. In addition, the intensities of the shifted and unshifted components are depicted. A similar picture is given in Fig. 6 for the 6^+_1 state. The lifetime fits were done with the software

napatau [17]. The results are in agreement with the adopted lifetime of the 6^+_1 state ($\tau(6^+_1) = 7.7(9)$ ps) published in Ref. [18]. For the 8^+_1 state it is stated in Ref. [18] that the purely statistical error may be underestimated and the value from this experiment is recommended as adopted value. The main goal of reproducing the lifetime of the 6^+_1 state within a commissioning run is achieved and a reliable lifetime of the 8^+_1 state with a small error was measured. No additional lifetimes could be analyzed using the chosen distances.

5. Conclusion

A new plunger device for the GALILEO γ-ray detector array [3,4] was build. It is compatible to ancillary detectors especially the EUCLIDES [8] charged particle Si detector array being as transparent as possible for charged particles and photons. The feedback system maintaining the target-to-degrader separation uses a piezo motor only. The performance was shown in several tests and finally in an in-beam commissioning run, which was analyzed with standard methods confirming lifetimes of yrast states in ^{180}Pt. The GALILEO plunger is therewith utilizable by the community to determine electromagnetic transition strengths in both stable (Tandem-ALPI) and future radioactive (SPES [19]) beam experiments.

References

[1] C. Alvarez, The GASP array, Nucl. Phys. News 3 (1993) 10–13, http://dx.doi.org/10.1080/10506899308221154, URL https://www.tandfonline.com/doi/abs/10.1080/10506899308221154.

[2] A. Dewald, O. Möller, P. Petkov, Developing the Recoil Distance Doppler-Shift technique towards a versatile tool for lifetime measurements of excited nuclear states, Prog. Part. Nucl. Phys. 67 (2012) 786–839, http://dx.doi.org/10.1016/j.ppnp.2012.03.003, URL http://www.sciencedirect.com/science/article/pii/S0146641012000713.

[3] J. Valiente-Dobón, D. Mengoni, F. Recchia, G. de Angelis, et al., Status of the Gamma-Ray Spectrometer GALILEO, in: LNL Annual Report 2014, INFN, Laboratori Nazionali di Legnaro, 2014, pp. 95–96, URL http://www.lnl.infn.it/~annrep/read_ar/2014/contributions/pdfs/095_C_79_C074.pdf.

[4] A. Goasduff, D. Bazzacco, R. Menegazzo, D. Mengoni, et al., Possible geometries of GALILEO phase II, in: LNL Annual Report 2016, INFN, Laboratori Nazionali di Legnaro, 2016, pp. 86–87, URL http://www.lnl.infn.it/~annrep/read_ar/2016/contributions/pdfs/086_C_118_C113.pdf.

[5] W. Męczyński, P. Bednarczyk, J. Grębosz, J. Heese, et al., A detector for filtering γ-ray spectra from weak fusionevaporation reactions out of strong background and for Doppler correction: The recoil filter detector, RFD, Nucl. Instrum. Methods A 580 (2007) 1310–1326, http://dx.doi.org/10.1016/j.nima.2007.07.132, URL http://www.sciencedirect.com/science/article/pii/S0168900207014684.

[6] F. Beck, EUROBALL: Large gamma ray spectrometers through european collaborations, Prog. Part. Nucl. Phys. 28 (1992) 443–461, http://dx.doi.org/10.1016/0146-6410(92)90047-6, URL https://www.sciencedirect.com/science/article/pii/0146641092900476.

[7] S. Akkoyun, A. Algora, B. Alikhani, F. Ameil, et al., AGATA advanced gamma tracking array, Nucl. Instrum. Methods A 668 (2012) 26–58, http://dx.doi.org/10.1016/j.nima.2011.11.081, URL http://www.sciencedirect.com/science/article/pii/S0168900211021516.

[8] D. Testov, D. Mengoni, C. Boiano, P. Cocconi, et al., The first physical campaign of the EUCLIDES Si-ball detector coupled to GALILEO gamma-ray spectrometer, in: LNL Annual Report 2015, INFN, Laboratori Nazionali di Legnaro, 2015, pp. 105–106, URL https://www.lnl.infn.it/~annrep/read_ar/2015/contributions/pdfs/105_C_95_C090.pdf.

[9] Physik Instrumente, (July 2018). URL https://www.physikinstrumente.com/en/.

[10] TESA Technology (July 2018). URL http://www.tesatechnology.com.

[11] J. Ljungvall, G. Georgiev, S. Cabaret, et al., The orsay universal plunger system, Nucl. Instrum. Methods A 679 (2012) 61–66, http://dx.doi.org/10.1016/j.nima.2012.03.041, URL https://www.sciencedirect.com/science/article/pii/S0168900212003427.

[12] National Instruments (July 2018). URL http://www.ni.com.

[13] openSUSE (July 2018). URL http://www.opensuse.org.

[14] Microsoft Windows (July 2018). URL https://www.microsoft.com/en-us/windows.

[15] O. Skeppstedt, H. Roth, L. Lindström, R. Wadsworth, et al., The EUROBALL neutron wall design and performance tests of neutron detectors, Nucl. Instrum. Methods A 421 (1999) 531–541, http://dx.doi.org/10.1016/S0168-9002(98)01208-X, URL http://www.sciencedirect.com/science/article/pii/S016890029801208X.

[16] A. Dewald, S. Harissopulos, P. von Brentano, The differential plunger and the differential decay curve method for the analysis of recoil distance Doppler-shift data, Z. Phys. A 334 (1989) 163–175, http://dx.doi.org/10.1007/BF01294217, URL http://link.springer.com/article/10.1007/BF01294217.

[17] B. Saha, Bestimmung der Lebensdauern kollektiver Kernanregungen in ^{124}Xe und Entwicklung von entsprechender Analysesoftware (Ph.D. thesis), Universität zu Köln, 2004, URL https://kups.ub.uni-koeln.de/1246/.

[18] C. Müller-Gatermann, A. Dewald, C. Fransen, T. Braunroth, et al., Low-lying electromagnetic transition strengths in ^{180}Pt, Phys. Rev. C 97 (2018) 024336, http://dx.doi.org/10.1103/PhysRevC.97.024336, URL https://journals.aps.org/prc/abstract/10.1103/PhysRevC.97.024336.

[19] G. Bisoffi, G. Prete, A. Andrighetto, V. Andreev, et al., Progress in the design and construction of SPES at INFN-LNL, Nucl. Instrum. Methods Phys. Res. B 376 (2016) 402–407, http://dx.doi.org/10.1016/j.nimb.2016.01.024, URL http://www.sciencedirect.com/science/article/pii/S0168583X16000720.

Publication III:
Shape coexistence in ^{178}Hg

Shape coexistence in ^{178}Hg

C. Müller-Gatermann,[1,*] A. Dewald,[1] C. Fransen,[1] K. Auranen,[2,†] H. Badran,[2] M. Beckers,[1] A. Blazhev,[1] T. Braunroth,[1]
D. M. Cullen,[3] G. Fruet,[4] A. Goldkuhle,[1] T. Grahn,[2] P. T. Greenlees,[2] A. Herzáň,[5,6,2] U. Jakobsson,[7,2] D. Jenkins,[8] J. Jolie,[1]
R. Julin,[2] S. Juutinen,[2] J. Konki,[2,‡] M. Leino,[2] J. Litzinger,[1] K. Nomura,[9] J. Pakarinen,[2] P. Peura,[10,2] M. G. Procter,[3]
P. Rahkila,[2] P. Ruotsalainen,[11,2] M. Sandzelius,[2] J. Sarén,[2] C. Scholey,[2] J. Sorri,[12,2] S. Stolze,[2,†] M. J. Taylor,[13,3]
J. Uusitalo,[2] and K. O. Zell[1]

[1]*Institut für Kernphysik der Universität zu Köln, Zülpicher Straße 77, D-50937 Köln, Germany*
[2]*University of Jyvaskyla, Department of Physics, P.O. Box 35, FI-40014 Jyvaskyla, Finland*
[3]*Schuster Laboratory, University of Manchester, Manchester M13 9PL, United Kingdom*
[4]*Université de Strasbourg, CNRS, IPHC UMR 7178, F-67000 Strasbourg, France*
[5]*Institute of Physics, Slovak Academy of Sciences, SK-84511 Bratislava, Slovakia*
[6]*Oliver Lodge Laboratory, University of Liverpool, Liverpool L69 7ZE, United Kingdom*
[7]*Laboratory of Radiochemistry, Department of Chemistry, P.O. Box 55, FI-00014 University of Helsinki, Finland*
[8]*Department of Physics, University of York, YO10 5DD York, United Kingdom*
[9]*Advanced Science Research Center, Japan Atomic Energy Agency, Tokai, 319-1195 Ibaraki, Japan*
[10]*Helsinki Institute of Physics, University of Helsinki, P.O. Box 64, 00014 Helsinki, Finland*
[11]*TRIUMF, Westbrook Mall, Vancouver, British Columbia V6T 2A3, Canada*
[12]*Sodankylä Geophysical Observatory, University of Oulu, FI-99600 Sodankylä, Finland*
[13]*Division of Cancer Sciences, University of Manchester, Manchester M13 9PL, United Kingdom*

Lifetime measurements of excited states in ^{178}Hg have been performed using the ^{103}Rh(^{78}Kr, $p2n$) reaction at a beam energy of 354 MeV. The recoil-decay tagging (RDT) technique was applied to select the ^{178}Hg nuclei and associate the prompt γ rays with the correlated characteristic ground-state α decay. Lifetimes of the four lowest yrast states of ^{178}Hg have been determined using the recoil distance Doppler-shift (RDDS) method. The experimental data are compared to theoretical predictions with focus on shape coexistence. The results confirm the shift of the deformed prolate structures to higher lying states but also indicate their increasing deformation with decreasing neutron number.

I. INTRODUCTION

Even-even nuclei close to shell closures have been the subject of numerous experimental and theoretical studies [1,2]. Phenomena like shape coexistence [2] and shape transitions [3] have been observed around the shell closure at $Z = 82$ near the neutron $N = 104$ midshell. The shapes of the neutron-deficient even-even Hg isotopes [4–6] are interpreted to be determined by the excitation of protons across the $Z = 82$ shell closure, forming "intruder states." The intruder states may have a significant prolate deformation [7] coexisting with less deformed oblate ground states. The level-energy systematics show a rather constant trend for the band build upon the weak oblate minimum, while a prolate deformed intruder band exhibiting a parabolic trend with respect to the neutron number shows a minimum at ^{182}Hg. The intruding band crosses the

yrast line at ^{188}Hg and around ^{176}Hg, suggesting together with the known experimental data that the interpretation holds for all midshell Hg nuclei (Fig. 1). Nevertheless, the composition of the wave function of the 2_1^+ states changes dramatically with respect to the neutron number [5,6]. The prolate band build upon an excited 0^+ state can be related to similar structures in the neighboring Pb nuclei. An overview of the spectroscopic studies in this mass region ranging from $_{80}$Hg to $_{84}$Po isotopes is given in Ref. [8]. In the odd-mass nuclei ^{183,185}Hg, a dramatic change in charge radius (compared to the neighboring even-mass Hg nuclei) was discovered in 1972 with isotope shift measurements [9]. Recently, the available data were extended to ^{177}Hg and the microscopic origin of the shape staggering effect was explained with the aid of the Monte Carlo shell model (MCSM) [10]. These larger charge radii are not observed in the more neutron-deficient isotopes with masses below 181. To date, the most neutron-deficient isotope of mercury for which transition probabilities are known is ^{180}Hg. The even-mass neighbor ^{178}Hg is predicted to be the start point of a shape transition by several theoretical models such as total Routhian surface (TRS) calculations [11], mean-field approaches, and the interacting boson model
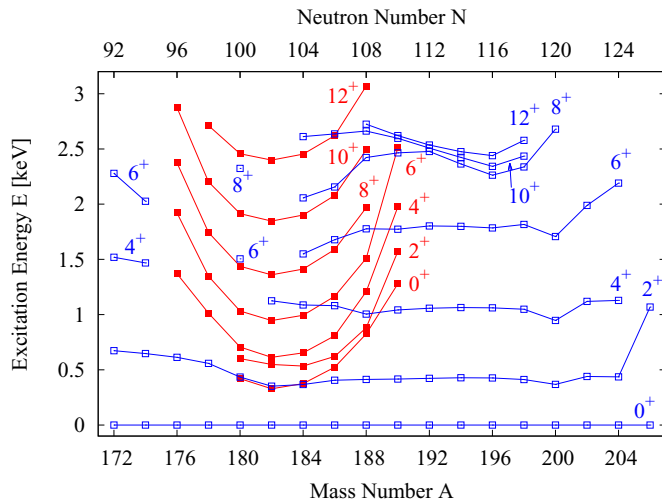
FIG. 1. Level energy systematics of the even-mass mercury isotopes. Red filled squares refer to the assumed intruder states while blue open squares refer to the assumed oblate states. The figure is adopted from Ref. [6].

FIG. 2. Spectrum of observed α-particle energies occurring within 2000 ms of an ion being implanted into the same DSSSD pixel. Assignments for the peaks are indicated. See text for details.

(IBM) with configuration mixing [12]. Therefore, to address the question of shape evolution toward even more neutron-deficient Hg isotopes, lifetime measurements of excited states in ^{178}Hg have been performed in the present work.

II. EXPERIMENTAL DETAILS

Excited states of ^{178}Hg were populated in a heavy-ion induced fusion-evaporation reaction at the Accelerator Laboratory of the University of Jyväskylä, where lifetimes of excited states were measured with the Differential Plunger for Unbound Nuclear States (DPUNS) [13]. The reaction ^{103}Rh(^{78}Kr, *p2n*)^{178}Hg with a beam energy of 354 MeV provided an initial recoil velocity of $v/c = 3.9\%$, with a target thickness of $1\,\mathrm{mg/cm^2}$. The typical beam current was of the order of 3–5 pnA, limited by heating of the stretched plunger target and degrader foils and the maximum counting rate of 30 kHz per JUROGAM II HPGe detector. The JUROGAM II Ge-detector array consisted of 24 EUROGAM (European Gamma-ray Microscope) Clover detectors [14] in two rings at 75.5° and 104.5° and two rings with tapered EUROGAM phase I [15] or GASP (Gamma-ray Spectrometer) type [16] germanium detectors at 133.6° (10 detectors) and 157.6° (5 detectors) with respect to the beam direction. All detectors were Compton-suppressed. The DPUNS was installed at the JUROGAM II target position to perform recoil distance Doppler-shift (RDDS) lifetime measurements of excited states in ^{178}Hg. A $1.6\,\mathrm{mg/cm^2}$ Mg degrader foil reduced the energy of the fusion products and allowed them to recoil into the Recoil Ion Transport Unit (RITU) [17,18] with a velocity of $v/c = 2.3\%$. RITU was filled with helium gas at a pressure of 0.6 mbar and separated the evaporation residues from the fission background and scattered beam according to their magnetic rigidity. The gas of RITU cooled the target and degrader foils, allowing the aforementioned relatively high beam intensities to be used. The recoils were transported through RITU to the Gamma Recoil Electron Alpha Tagging
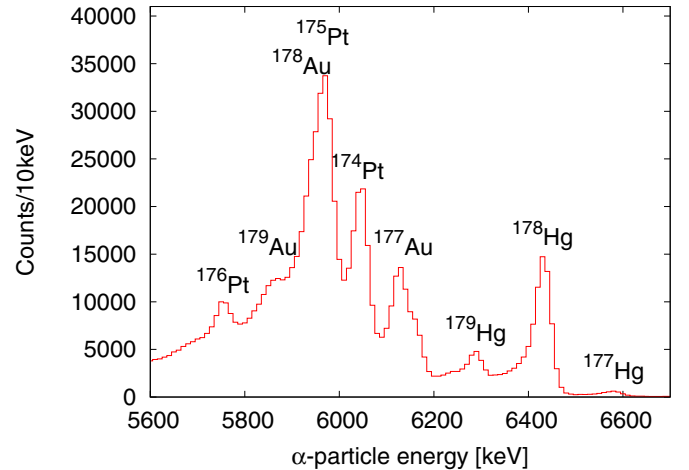
(GREAT) spectrometer [19] at the focal plane. The recoils passed through a multiwire proportional counter (MWPC) and were implanted into a pair of double-sided silicon strip detectors (DSSSDs). Discrimination between evaporation residues and scattered beam particles was achieved on the basis of energy loss in the MWPC and the time of flight between the MWPC and DSSSDs. With an anticoincidence between the MWPC and the DSSSDs, the decays in the DSSSD are distinguishable from the implantation events. For the identification of the evaporation residues, the recoil-decay tagging (RDT) technique [20] was applied, whereby an α decay is correlated with a previously implanted recoil within a specific search time. The γ rays associated with the recoil can then be extracted. To remove the random coincidences in the γ-ray spectra, stemming mainly from Coulomb excitation of the beam, the time difference spectrum between the JUROGAM II Ge detectors signals and the MWPC signal was used. The events of the pure prompt peak were selected by subtracting events of the plateau outside of the prompt peak with background using the same window sizes. For the tagging of ^{178}Hg, a search time of 2000 ms, which is about seven times the half-life, between an implantation and an α-decay event at the same position in the DSSSDs was set together with a gate on the ground state α-decay energy of 6.43 MeV and a width of 160 keV. To increase the level of statistics, recoil-α-α correlations to the daughter nucleus ^{174}Pt were also employed. If the α particle emitted by ^{178}Hg escapes, the correlated chain can still be recovered by respective cuts on time and energy. When taking this effect into account, the statistics are increased by 25%, which is expected from the geometrical escape probability and the α-decay branch of ^{174}Pt. No contamination with ^{174}Pt events is seen in the γ-ray spectra, as an earlier decay event within the time window for ^{178}Hg is required. All detector signals were passed to the triggerless Total Data Readout (TDR) data acquisition system [21]. The data were analyzed using the GRAIN [22] and TV [23] software packages. A spectrum of observed α-particle energies is presented in Fig. 2 showing the statistics for 60 h, which corresponds to
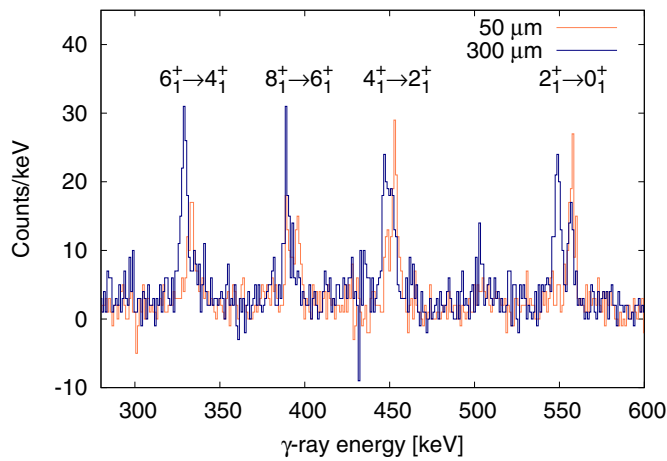
FIG. 3. Background subtracted γ-ray energy spectra measured with the JUROGAM II detectors in the ring at 157.6° (five detectors) for the shortest and longest distances. Assignments for the lowest four yrast transitions are indicated. See text for details.

one target-to-degrader distance. The region of interest around ^{178}Hg shows no contaminations. Only the decays of ^{178}Au and ^{175}Pt are not separated and in the case of ^{177}Au the peak is broader due to the decay of an excited isomeric state. In Fig. 3, the resulting γ-ray spectra for the transitions of interest are shown for the shortest and longest distances when the procedures to select ^{178}Hg described above are used. The background is low with little contamination. Only the outermost ring at 157.6° could be used to extract lifetimes due to the low Doppler shifts and an energy resolution of around 3 keV for the unshifted component (after Doppler correction). The γ-ray spectra of the Clover detectors (around 90°), having most of the efficiency and showing almost no Doppler shift, were summed up over all plunger distances and were used to determine the initial population of the individual states. In total, four different relative target-to-degrader distances were measured and analyzed, namely 50, 100, 200, and 300 μm.

III. LIFETIME ANALYSIS

Because of the very limited number of distances and the fact that only γ-ray singles spectra could be analyzed, where delayed feeding from higher states is relevant, the differential decay curve method (DDCM) [24] was not applied. The lifetime of an excited state can be determined from the decay curve, which is the intensity ratio of the degraded I_D and the sum of fast I_T and degraded peaks of γ rays depopulating the level of interest as a function of the distance d between the foils, $R(d) = I_D(d)/[I_D(d) + I_T(d)]$ [25]. In the case of a γ-ray singles analysis, all observed feeding transitions have to be taken into account. The solution of the corresponding system of differential equations (Bateman equations) is fitted to the decay curve. For such an analysis, exact absolute distance information is crucial, especially when so few target-to-degrader distances were used. The plunger device used provides relative distance information with a precision of $\approx$ 0.1 μm, but always with an offset caused by an unknown zero point which depends on the quality of the target and degrader
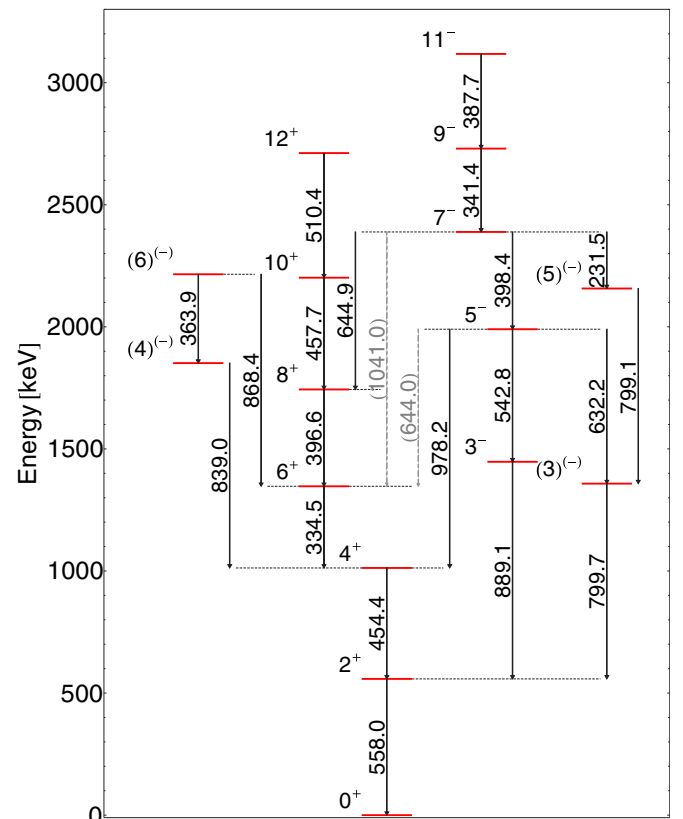

FIG. 4. Partial level scheme of ^{178}Hg up to the 11_1^- state, which is the highest lying state taken into account for feeding. γ energies, spins, and parity are taken from Ref. [27]. See text for details.

surface. An offset of 19(1) μm was determined by measuring the capacitance of the target-degrader system, as described in Refs. [25,26]. This translates to absolute time of flights between the target and the degrader of 5.52, 9.80, 18.04, and 26.27 ps for the relative target-to-degrader distances of 50, 100, 200, and 300 μm, respectively.

The effect of unobserved feeding transitions to the level of interest must be taken into account in the analysis of singles RDDS data. Therefore, the total statistics of all Clover detectors around 90° was added up for all distances. With these spectra, the efficiency-corrected initial populations were fixed for all known states up to the 11_1^- state and are in agreement with those of Ref. [27]. The efficiencies of the JUROGAM II Ge detectors were determined using a ^{152}Eu source. A partial level scheme up to the highest lying state observed in this work and taken into account in the feeding analysis is shown in Fig. 4.

The effective lifetimes of the feeding transitions were then fitted together with the state of interest, beginning with the highest lying state (8_1^+ state) for which a lifetime determination is possible. All lifetimes were then fixed and used in the following analysis of lower lying states. The uncertainty of the lifetime of the feeding transition was taken into account in the error of the decaying transition. A common assumption, that all unobserved feeding has the same time behavior as the observed feeding, i.e., the feeder with the highest intensity, was wrong in this case. Significantly longer feeding time was
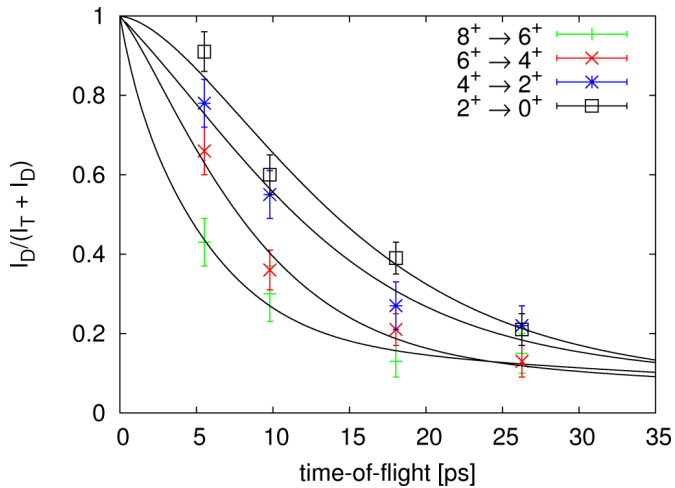
FIG. 5. Decay curves for the ground-state band up to the 8_1^+ state in ^{178}Hg constructed from the RDT singles γ-ray spectra recorded with five JUROGAM II detectors at 157.6°. The smooth lines correspond to the best fits.
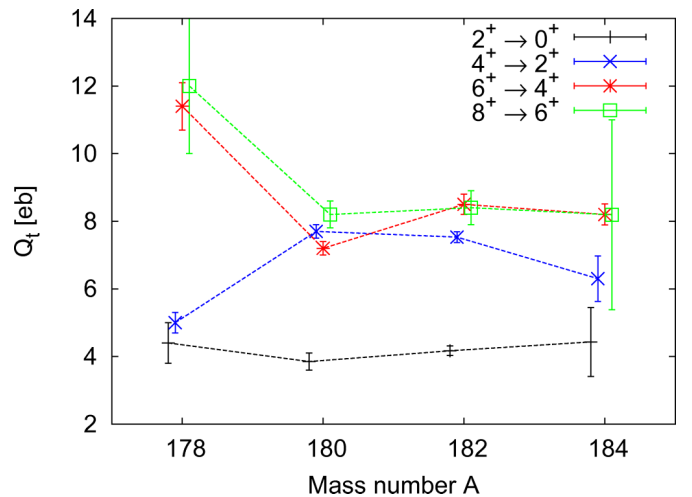

FIG. 6. Absolute values of transition quadrupole moments for the neutron-deficient Hg isotopes near midshell. See text for details.

was used, where Z is the atomic number and R_0 is the nuclear radius.

needed to reproduce the decay curves. This is ascribed to strongly populated negative-parity states, e.g., the 7_1^- state, which branch out significantly and have to be taken into account for each state with different cascades. The decay curves for the yrast states are presented in Fig. 5 and show good agreement with the experimental data. Since the feeding assumptions affect all states of interest and are based on experimentally determined initial populations and branching ratios, they seem plausible. The experimental lifetime data stems from normalized fits of the spectra in the outermost ring with fixed peak widths and positions. The Doppler shift of γ rays in the spectra from the ring of detectors at 133° was not large enough to allow an independent analysis, but they were checked for consistency.

The results of the lifetime analysis are summarized in Table I. By using the rotational model with the assumption of a rotating quadrupole deformed nucleus, the absolute values of transition quadrupole moments Q_t and deformation parameters β_2 are given in the same table together with the corresponding $B(E2)$ values. For the determination of deformation parameters,

$$\beta_2 = 0.625(-5a + \sqrt{25a^2 + 16aQ_t})/a,$$
$$a = \frac{3}{\sqrt{5\pi}ZR_0^2}, \tag{1}$$

TABLE I. Electromagnetic properties of the lowest yrast states in ^{178}Hg.

I^π [27]	E_γ [keV] [27]	τ [ps]	$B(E2)$ [W.u.]	$\lvert Q_t \rvert$ [eb]	$\lvert \beta_2 \rvert$
2_1^+	558.0	3.8(9)	$66(^{+20}_{-12})$	$4.4(^{+6}_{-5})$	$0.16(^{+2}_{-2})$
4_1^+	454.4	5.7(6)	$120(^{+14}_{-11})$	$5.0(^{+3}_{-2})$	$0.18(^{+1}_{-1})$
6_1^+	334.5	4.4(5)	$690(^{+90}_{-70})$	$11.4(^{+7}_{-6})$	$0.41(^{+3}_{-3})$
8_1^+	396.6	1.7(5)	$800(^{+300}_{-200})$	$11.9(^{+20}_{-14})$	$0.43(^{+8}_{-5})$

IV. DISCUSSION

The $B(E2)$ values shown in Table I indicate a structural change for the lowest lying states. This is known for Hg isotopes with $A \gtrsim 180$ at the 2_1^+ state [4]. The Q_t values for $^{178-184}$Hg as a function of mass number A are shown in Fig. 6. The weakly deformed oblate configuration, which forms also the ground-state mixes with the prolate deformed structure of the intruder states. The 2_1^+ state for $A \gtrsim 180$ is already strongly mixed and reduces the transition probability of the $2_1^+ \rightarrow 0_1^+$ transition. Mixing calculations for these midshell nuclei which were performed in Refs. [5] and [6] as well as Ref. [4] for ^{182}Hg reveal up to $\approx 80\%$ prolate contribution to the wave function of the 2_1^+ state. At higher spins, the Q_t values stay rather constant and a deformation of $\beta_2 \approx 0.25$ can be attributed to the rotational structure corresponding to the prolate band. The authors of Ref. [5] assume from Coulomb-excitation measurements and the two-level mixing calculations of Ref. [6] that there significant changes in the composition of the 2_1^+ states. To reproduce the $B(E2)$ values in ^{178}Hg, a two-band mixing calculation assuming interband transitions to be forbidden has been performed. The calculation suggests that the 2_1^+ state has an $\approx 80\%$ contribution of oblate deformed structure in the wave function similar to the ground state. The 4_1^+ state wave function changes to an $\approx 80\%$ portion of the prolate band and reduces the $4_1^+ \rightarrow 2_1^+$ transition strength. For the higher lying states, an unperturbed rotational band can be assumed with a deformation of $\beta_2 \approx 0.4$ due to the large Q_t values for the respective transitions. Since the ground state and the 2_1^+ state have a large overlap of the wave functions, one could extract a deformation of $\beta \approx 0.15$, which is consistent with the ground-state deformations of heavier Hg isotopes extracted from isotope shift measurements. It is not meaningful to deduce a deformation from the transition between the structures because the small overlap of the wave functions lowers the transition strength.
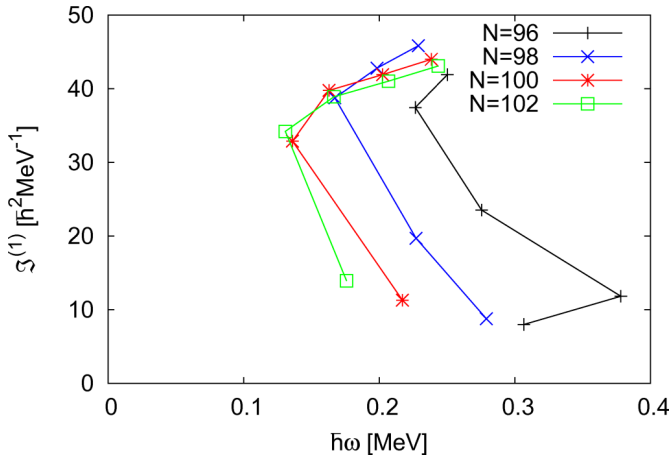
FIG. 7. Kinetic moments of inertia $\Im^{(1)}(J)$ for the Hg isotopes as a function of frequency $\omega(J \rightarrow J-2)$ for transitions along the yrast line up to the 10^+ state. The figure is adopted from Ref. [31]. See text for details.

The shape change seems to be shifted toward the 4_1^+ state, consistent with the trend seen by Bree *et al.* [5]. A larger deformation of $\beta_2 \approx 0.4$ is revealed (extracted from the pure 6_1^+, 8_1^+ states). This so-called intermediate deformation [between normal and superdeformation (SD)] is discussed in Ref. [28] and is explained by the shape-driving effect of intruder neutron orbitals. These are clearly manifested by the negative-parity band built upon a 11^- state in ^{186}Hg (band 3 in Ref. [28]) and the population of a pair of quasineutrons to configurations with involvement of the $\nu[651]\frac{1}{2}$ orbital. The occupation of these orbitals is also expected for the SD configurations of heavier Hg isotopes [29]. SD bands leading to various shape-coexisting configurations in the light Hg isotopes with $N \leqslant 98$ were predicted in Ref. [30]. The deformation is also consistent with predictions of TRS calculations presented in Ref. [11], in which the authors state that for the nuclei ^{172,174,176}Hg the near-oblate ground state evolves steadily toward a more spherical shape with decreasing N as the $N = 82$ closed shell is approached. Second, no prolate minimum is seen in the TRS calculations with $\beta_2 \approx 0.25$ for $^{172-176}$Hg, but for increasing neutron number a well-deformed minimum ($\beta_2 \approx 0.35$) starts to develop and is first observed in ^{176}Hg. The level energy systematics showing the prolate (red filled squares) as well as the oblate (blue open squares) structures are tracked throughout the Hg isotopes and depicted in Fig. 1. For the more neutron-deficient isotope ^{178}Hg, the energy of the prolate structure increases and the mixing with low-lying states decreases as described above. The structural change becomes apparent also in the kinetic moments of inertia $\Im^{(1)}$ along the yrast band. Resuming the statements of Ref. [31], there are well-established generic properties of the moments of inertia such as their increase with deformation, or that for the same value of $|\beta_2|$ the moment of inertia is larger for prolate deformations than for oblate ones. In Fig. 7, the kinetic moments of inertia are shown for the yrast bands in $^{176-182}$Hg as a function of frequency $\omega(J \rightarrow J-2)$. The first observation is that the moments of inertia for high-spin group at high absolute values can be attributed to a stable

deformation (constant moment of inertia for an idealized static rotor). The moment of inertia for $J = 2$ is significantly different from those corresponding to transitions from higher spins. This is consistent with the picture discussed earlier. Second, at $N = 98$ the moment of inertia is lowered for $J = 4$ in comparison to the heavier isotopes, and this trend is continued for $N = 96$ in this case and also for $J = 6$. Confirming the expectation from the level-energy systematics, the influence of an intruding structure is displaced to higher spins. In summary, there is a good agreement between the interpretations deduced from level energies and lifetimes.

Alternative calculations from Ref. [12] are based on Hartree-Fock-Bogoliubov (HFB) methodology using the Gogny-D1M energy density functional (EDF), which is mapped on the corresponding energy surface of the IBM with configuration mixing. In this case, the proton-neutron IBM (IBM-2) is used. For the configuration mixing, only 2p-2h proton excitations were allowed for $^{176-190}$Hg. This results in a near-spherical structure for ^{172}Hg with a slight prolate minimum evolving toward ^{176}Hg of $\beta_2 \approx 0.25$–0.3. For the heavier Hg isotopes, this minimum gets more pronounced but does not change its quadrupole deformation. This description is consistent with the experimental data for $A \geqslant 180$, and unfortunately it cannot reproduce the transition strengths given in Table I. The discrepancy is probably due to the limited model space of the configuration-mixing IBM-2 used in Ref. [12], which comprised only up to 2p-2h proton excitations, as well as the possibility that the mixing between different configurations may not have been properly accounted for in that calculation. In addition, the topology of the potential energy surface is rather sensitive to the choice of the underlying EDF. The inclusion of neutron intruder excitations, in the configuration-mixing IBM-2 framework could improve the description of the $B(E2)$ transition rates for the considered Hg nuclei.

Recently, more evidence was given supporting the importance of neutron occupation in Ref. [10]. The authors extended the experimental data on charge radii of the ground state with isotope shift measurements down to ^{177}Hg. The first observation is that the shape staggering of the odd-mass Hg nuclei with respect to their even-mass neighbor breaks down at ^{180}Hg. This means that ^{179}Hg has a near-spherical ground state, whereas the ground state of ^{181}Hg was associated with $\beta_2 = 0.313$. Second, the authors present a Monte Carlo shell model (MCSM) calculation and explain the large deformation for Hg isotopes with $A > 180$ with the strong occupation of specific proton and neutron orbitals, namely the $\pi(h_{\frac{9}{2}})$ and the $\nu(i_{\frac{13}{2}})$ orbitals. This is another hint that the deformation-driving structures move away from the ground state in ^{178}Hg and that the neutron contribution should be also taken into account. The extension of the MCSM calculation to excited states would also be an alternative starting point for interpretations of the data.

The level spacings in ^{176}Hg reveal a change in deformation shifted to the 6_1^+ state [32], continuing the trend seen in the data of this work. $B(E2)$ values of excited states in ^{176}Hg are not known so far. These would test the predictions of the TRS

calculations, especially the evolving prolate minimum with intermediate deformation. However, also independent IBM-2 calculations with configuration mixing allowing specific neutron excitations should be done now systematically with the new data available.

V. SUMMARY AND CONCLUSIONS

Excited states in the neutron-deficient nucleus ^{178}Hg were populated in heavy-ion fusion-evaporation reactions and studied using the JUROGAM II and GREAT spectrometers, coupled to the DPUNS and the gas-filled separator RITU. The RDT technique was applied to identify the ^{178}Hg nuclei and the RDDS method was used to determine lifetimes of yrast states up to the 8^+_1 state for the first time. Deformation parameters β_2 were extracted from the corresponding $B(E2)$ values. The 2^+_1 state shows a deformation comparable to the ground state and the ground states in the heavier neighboring even-even Hg isotopes. It is expected from energy systematics that the deformation-driving structures shift toward higher excitation energies. This is verified by experimental transition strengths and a mixing calculation. For the higher lying states, an intermediate deformation between normal and superdeformation has been attributed, which is a new phenomenon in the chain of the Hg isotopes. Consistency with TRS calculations

and isotope shift measurements propose ^{178}Hg to be at the point where the nuclear structure changes. This can also be seen from the 2^+ state energies in Fig. 1. It is proposed to include also specific neutron intruder excitations for systematic IBM-2 calculations including the new data. An alternative approach would be to extend the MCSM calculations to excited states. From an experimental point of view, $B(E2)$ values of excited states in the even-even neighbor ^{176}Hg would be very interesting for comparison. Using the largest available Ge-detector arrays in combination with large acceptance gas-filled recoil separators, this goal seems feasible although on the edge of the detection limit.

ACKNOWLEDGMENTS

[1] T. Grahn, A. Dewald, O. Möller, R. Julin, C. W. Beausang, S. Christen, I. G. Darby, S. Eeckhaudt, P. T. Greenlees, A. Görgen *et al.*, Nucl. Phys. A **801**, 83 (2008).

[2] K. Heyde and J. L. Wood, Rev. Mod. Phys. **83**, 1467 (2011).

[3] P. Cejnar, J. Jolie, and R. F. Casten, Rev. Mod. Phys. **82**, 2155 (2010).

[4] T. Grahn, A. Petts, M. Scheck, P. A. Butler, A. Dewald, M. B. Gomez Hornillos, P. T. Greenlees, A. Görgen, K. Helariutta, J. Jolie *et al.*, Phys. Rev. C **80**, 014324 (2009).

[5] N. Bree, K. Wrzosek-Lipska, A. Petts, A. Andreyev, B. Bastin, M. Bender, A. Blazhev, B. Bruyneel, P. Butler, J. Butterworth *et al.*, Phys. Rev. Lett. **112**, 162701 (2014).

[6] L. P. Gaffney, M. Hackstein, R. D. Page, T. Grahn, M. Scheck, P. A. Butler, P. F. Bertone, N. Bree, R. J. Carroll, M. P. Carpenter *et al.*, Phys. Rev. C **89**, 024307 (2014).

[7] J. E. García-Ramos and K. Heyde, Phys. Rev. C **89**, 014306 (2014).

[8] R. Julin, T. Grahn, J. Pakarinen, and P. Rahkila, J. Phys. G: Nucl. Part. Phys. **43**, 024004 (2016).

[9] J. Bonn, G. Huber, H.-J. Kluge, L. Kugler, and E. Otten, Phys. Lett. B **38**, 308 (1972).

[10] B. Marsh, T. Day Goodacre, S. Sels, Y. Tsunoda, B. Andel, A. Andreyev, N. Althubiti, D. Atanasov, A. Barzakh, J. Billowes *et al.*, Nat. Phys. **14**, 1163 (2018).

[11] M. Sandzelius, E. Ganioğlu, B. Cederwall, B. Hadinia, K. Andgren, T. Bäck, T. Grahn, P. Greenlees, U. Jakobsson, A. Johnson *et al.*, Phys. Rev C **79**, 064315 (2009).

[12] K. Nomura, R. Rodríguez-Guzmán, and L. M. Robledo, Phys. Rev. C **87**, 064313 (2013).

[13] M. J. Taylor, D. M. Cullen, A. J. Smith, A. McFarlane, V. Twist, G. A. Alharshan, M. G. Procter, T. Braunroth, A. Dewald, E. Ellinger *et al.*, Nucl. Instr. Meth. A **707**, 143 (2013).

[14] G. Duchêne, F. A. Beck, P. J. Twin, G. de France, D. Curien, L. Han, C. W. Beausang, M. A. Bentley, P. J. Nolan, and J. Simpson, Nucl. Instr. Meth. A **432**, 90 (1999).

[15] C. W. Beausang, S. A. Forbes, P. Fallon, P. J. Nolan, P. J. Twin, J. N. Mo, J. C. Lisle, M. A. Bentley, J. Simpson, F. A. Beck, D. Curien, G. de France, G. Duchêne, and D. Popescu, Nucl. Instr. Meth. A **313**, 37 (1992).

[16] C. R. Alvarez, Nucl. Phys. News **3**, 10 (1993).

[17] M. Leino, J. Äystö, T. Enqvist, P. Heikkinen, A. Jokinen, M. Nurmia, A. Ostrowski, W. H. Trzaska, J. Uusitalo, K. Eskola, P. Armbruster, and V. Ninov, Nucl. Instr. Meth. B **99**, 653 (1995).

[18] J. Sarén, J. Uusitalo, M. Leino, and J. Sorri, Nucl. Instr. Meth. A **654**, 508 (2011).

[19] R. D. Page, A. N. Andreyev, D. E. Appelbe, P. A. Butler, S. J. Freeman, P. T. Greenlees, R.-D. Herzberg, D. G. Jenkins, G. D. Jones, P. Jones *et al.*, Nucl. Instr. Meth. B **204**, 634 (2003).

[20] E. S. Paul, P. J. Woods, T. Davinson, R. D. Page, P. J. Sellin, C. W. Beausang, R. M. Clark, R. A. Cunningham, S. A. Forbes, D. B. Fossan *et al.*, Phys. Rev. C **51**, 78 (1995).

[21] I. Lazarus, E. Appelbe, P. Butler, P. Coleman-Smith, J. Cresswell, S. Freeman, R. Herzberg, I. Hibbert, D. Joss, S. Letts *et al.*, IEEE Trans. on Nucl. Sci. **48**, 567 (2001).

[22] P. Rahkila, Nucl. Instr. Meth. A **595**, 637 (2008).

[23] J. Theuerkauf, S. Esser, S. Krink, M. Luig, N. Nicolay, O. Stuch, and H. Wolters, Program TV, Institute for Nuclear Physics, Cologne, Germany.

[24] A. Dewald, S. Harissopulos, and P. von Brentano, Z. Phys. A **334**, 163 (1989).

[25] T. Alexander and A. Bell, Nucl. Instr. Meth. **81**, 22 (1970).

[26] A. Dewald, O. Möller, and P. Petkov, Prog. Part. Nucl. Phys. **67**, 786 (2012).

[27] E. Achterberg, O. Capurro, and G. Marti, Nuclear Data Sheets **110**, 1473 (2009).

[28] W. C. Ma, J. H. Hamilton, A. V. Ramayya, L. Chaturvedi, J. K. Deng, W. B. Gao, Y. R. Jiang, J. Kormicki, X. W. Zhao, N. R. Johnson *et al.*, Phys. Rev. C **47**, R5(R) (1993).

[29] R. Janssens and T. Khoo, Annu. Rev. Nucl. Part. Sci. **41**, 321 (1991).

[30] W. Nazarewicz, Phys. Lett. B **305**, 195 (1993).

[31] J. M. Yao, M. Bender, and P.-H. Heenen, Phys. Rev. C **87**, 034322 (2013).

[32] M. Muikku, J. F. C. Cocks, K. Helariutta, P. Jones, R. Julin, S. Juutinen, H. Kankaanpää, H. Kettunen, P. Kuusiniemi, M. Leino *et al.*, Phys. Rev. C **58**, R3033(R) (1998).

Summary and conclusions

In the first part of this thesis the question, whether the neutron-mishell platinum isotopes show remnants of the X(5) symmetry [30] or if two configurations including multiparticle-multihole excitations are needed to reproduce the B(E2) values, is investigated. The former is seen in the neighboring osmium isotopes, while the latter is needed in the mercury isotopes on the other side of platinum. Additionally an older RRDS measurement on ^{180}PT of de Voigt et al. [32] showed an unusual $B_{4/2}$ ratio below unity, which is often questionable. In a later experiment of Williams et al. [33] revisiting two cases with low $B_{4/2}$ ratio only the B(E2;$4_1^+ \rightarrow 2_1^+$) was determined with a contradicting result to de Voigt et al. In this work a RDDS experiment employing $\gamma - \gamma$ coincidences was analysed confirming the lifetime of the 4_1^+ in ^{180}Pt of Williams et al. Further on lifetimes of the 6_1^+ and 8_1^+ state were determined within this experiment. The lifetimes were also compared to a recent RDDS experiment by Chen et al. [39], which was published during the analysis. This data presents systematically longer lifetimes for all states which have been measured. In a second RDDS experiment, which was at the same time the commissioning run of a new plunger device, the lifetimes deduced in this work were confirmed again using a different reaction and independend analysis. Both plunger experiments were not dedicated to measure long lifetimes. To determine the lifetime of the longlived 2_1^+ state a separate experiment using the delayed-coincidence technique was performed. The HORUS spectrometer [40] was equipped with HPGe and LaBr detectors and triple coincidences were sorted to evaluate germanium-gated $\gamma - \gamma$ fast-timing matrices. Since the GCD method is sensitive to the lifetime of the 4_1^+ state, again a completely independend analysis was carried out. The deduced lifetime has a larger error, due to the method, but confirms the lifetime in this work, the work of Williams et al. and excludes the value of Chen et al. and de Voigt et al. The lifetime of the 2_1^+ state was measured only once by de Voigt et al., also this value was revised to a shorter lifetime. The analysis was done with the GCD method and corrected for the timing behaviour of the background. The peak-to-background ratio increases the error in this analysis, because of the large Compton background at the low γ-ray energy of the 2_1^+ state. The lifetime is with about 0.5 ns long enough to see an exponential decay curve convoluted with a prompt peak. The direct access to the lifetime by fitting only the slope outside of the prompt peak is not possible in this case. The statistics are too low to get a meaningful error with this method. Therefore the complete convolution has to be fitted and special care has to be taken of the width of the prompt peak to assure that it is consistent with the widths in this energy regime. No correction or subtraction of background is applied, which is reliable in this case because the background in the time spectrum is generated by Compton events of higher-lying transitions in ^{180}Pt. These transitions all have a short lifetime and should lie within the prompt peak. The spectrum after applying the HPGe gate was checked for other contaminations, and nothing but the higher-lying states in ^{180}Pt was observed. The function

$$F(t) = \frac{N_0}{\tau} e^{-\frac{t-t_0}{\tau}} [1 - erf(\frac{\sigma}{\sqrt{2}\tau} - \frac{t-t_0}{\sqrt{2}\sigma})] \qquad (5.1)$$

has to be fitted to the time spectrum, where erf is the errorfunction. The result is in agreement with the GCD method and even gives a slightly smaller error. In summary four lifetimes were measured for the lowest yrast states in ^{180}Pt, which are now reliable and consistent within all the different analyses. De Voigt et al. [32] determined longer lifetimes for the 4_1^+ and 2_1^+ state, which is probably related to feeding as they were using γ-ray singles. The result of Williams et al. [33] is confirmed within the statistical error. Only the recent result of Chen et al. [39] can not be explained without further ado. Since the analysis used also $\gamma - \gamma$ coincidences and DDCM there should be no feeding contribution. It is striking that the lifetime of the 4_1^+ and 6_1^+ state are systematically longer by the same factor. This could hint to a problem affecting all lifetimes, e.g. a wrong recoil velocity, but without detailed information about the analysis this can not be explained.

The corresponding transition strengths to the extracted lifetimes were calculated model independend to compare these to predictions of nuclear models. An IBM-1 calculation was performed using a minimum set of parameters and without any configuration mixing. For the calculation the code ArbModel [41] was used with the Hamiltonian

$$H(\zeta, \chi) = c\left[(1-\zeta)\hat{n}_d - \frac{\zeta}{4N_B}\hat{Q}^\chi \cdot \hat{Q}^\chi\right] \tag{5.2}$$

and only two free parameters ζ and χ. c is a scaling parameter for the energies and N_B the boson number. The reproduction of not only the level energies and B(E2) values (within the error bars) of the yrast band, but also the excitation energies and relative transition strengths of the β and γ band as well as of another 0^+ state in this energy regime is remarkably well. This shows already that no second configuration is needed for the description of midshell Pt isotopes. There existed an older IBM calculation also without configuration mixing from McCutchan et al. [34] for a chain of even-even Pt isotopes. Having in mind that less information on transition strengths was known at this time, it is in good agreement with the present calculation and shows the description on a larger scale. The parameters ζ and χ are as expected close to the X(5) symmetry in the Casten triangle, but on the axially-deformed rotor side. Approaching the shell closure with respect to the Os isotopes one would expect a trend to sphericity, if the simple $N_\pi \cdot N_\nu$ scheme is valid. A second model calculation was performed using the GCM [36], which can describe intrinsically also shape coexistence. The predictions are again in good agreement with the experimental results. The potential energy surface is extracted from the collective potential showing only one minimum with some γ softness, but clearly pointing to a prolate rotor without shape coexistence. Both models motivate that also the rigid rotor model will give a valid description. Therefore the transition quadrupole moments Q_t and the corresponding deformations β are calculated. The first observation is that the Q_t values are nearly constant following the trend for a rotor and not the expectations in X(5) nuclei. Secondly the absolute value of β is the same for the higher lying states in the even-even neighbor ^{182}Hg, which are explained via an intruder configuration [21, 22] (c.f. Fig.6). The interpretation in the present work is, that the intruder configuration becomes the ground state. In an alternative approach with configuration mixing employing mean-field and IBM aclculations [42], the authors admit that the configuration

mixing does not show up explicitly. This further supports the hypothesis of a weakening of the shell closure. This does not show up only in ^{180}Pt, but also in the neighboring even Pt isotopes. In ^{178}Pt exactly the same behaviour is seen [43]. The case of ^{182}Pt is so far discussed favoring remnants of the X(5) symmetry [31], but the absolute value of the transition quadrupole moments would also allow an interpretation based on multiparticle-multihole excitations reaching the ground state. The main argument for the X(5) hypothesis is a slightly lowered transition strength for the two lowest states with respect to the higher-lying yrast states. This relies on a plunger experiment with very low recoil velocity and due to the also low γ-ray energies unresolved components in the spectrum. It would be worth to confirm the lifetime of the 2_1^+ and 4_1^+ state in ^{182}Pt with delayed coincidences as it was done within this work.

Another approach to increase the separation of shifted and unshifted component in a RDDS experiment on ^{182}Pt would be a reaction similar to the one used within the commissioning run of the GALILEO plunger, e.g. ^{154}Sm(^{32}S, 4n)^{182}Pt or ^{154}Sm(^{34}S, 6n)^{182}Pt. In the commissioning also the 6n channel was chosen with a ^{32}S beam impinging on a ^{154}Sm target leading to a high crosssection for ^{180}Pt in comparison to the quite symmetric reaction ^{98}Mo(^{86}Kr,4n)^{180}Pt used in the RDDS experiment described so far. The latter has the advantage of a higher Doppler shift, but suffers from higher crosssections on fusion-fission and Coulomb excitation. The asymmetric reaction worked well to reach a proof of concept for the newly build plunger device within a short time using the known lifetimes in ^{180}Pt. The goal to reproduce the lifetime of the 6_1^+ state and being sensitive to the 8_1^+ lifetime with high statistics was reached. The change of γ-ray spectrometer from GASP [44] to GALILEO [3] made it necessary to change the concept of the plunger. GASP was opened sideways, while GALILEO opens along the beam axis which circumvents the use of the Cologne coincidence plunger [45]. To maximize the transparency for γ rays and charged particles, all optional components of a plunger device (e.g. a piezo stack and an inductive transducer) were not included. The device consists of a support structure attached to the chamber, which guarantees the mechanical stability with a minimum of material and the plunger itself. The plunger is composed of a piezo motor with high precision, that is operationable in high vaccuum as well as of two holders for target and degrader. This design allows to install additional charged particle detectors, e.g. EUCLIDES [46] inside the target chamber. The plunger part can be taken off the support structure and assembled outside of the chamber on a mounting stand. This enables an easier mounting and alignment of the two foils and could be done in principle also in a glovebox with inert gas or vaccuum if the target is very sensitive to oxygen. Within the test run the mechanical compatibility with EUCLIDES was shown and also the precision of the motor is high enough that a piezo stack is dispensable. Since this first proof of principle the plunger device was used many times proving longterm stability and also in conjunction with EUCLIDES in beam. The design idea is expendable to a plunger device with three foils for special cases and could also have advantages for experiments at other accelerator facilities, because it can be taken out of the chamber with good reproducabilty. An optical distance measurement could be used to align the two foils and would also enable the measurement of absolute distances between the foils. Since the degrader foil is fixed and the target is aligned, this must be done from the side of the target where

there is usually no space. Finally also the analysis of the data resulted in lifetimes consistent with the first experiment. The evaluation differed slightly from a standard procedure in a way, that gates were set on both components of a feeding transition and depopulating transition. The coincident events between the two unshifted components were subtracted from unshifted components of the decay afterwards. This eases the fitting procedure and more importantly does not select a part of the velocity distribution while taking into account all events coincident to a shifted feeding transition.

In the last part of this thesis the trend of shape coexistence in the mercury isotopes is investigated towards even more neutron-deficient ^{178}Hg. The experiment was conducted in Jyväskylä (Finland) as a RDDS measurement making use of RDT [7]. The crosssection of around 20 µb allowed a γ-singles analysis only. To maximize the statistics for the nucleus of interest and minimize the background events, the sortcode had to be adopted. Two methods were implemented in the code for GRAIN [13]. The first one makes a random event subtraction using the timestamps of events from the γ spectrometer JUROGAM II and the MWPC. The second one takes also consecutive α-decay events in the focal plane into account just in the case that the first α particle escapes from the DSSSD detector. The latter one increased the statistics by 25 % as expected from geometrical escape probability and α-branching ratio. The former one was essentially to suppress the random Coulomb-excitation events of the beam ^{78}Kr. Otherwise the analysis would not have been feasible, because of similar γ-ray energies in ^{78}Kr and ^{178}Hg. The lifetime analysis was performed with only five HPGe detectors at most extreme backward angles, while the whole JUROGAM II spectrometer was utilized to measure the initial population of levels. A script for Mathematica [6] was written to print out the Bateman equations in explicit form for any given feeding scenario. The function was then fitted to the decay curve of the state of interest. Since only four target-to-degrader distances were measured and delayed feeding with partially complicated branching has to be taken into account, the DDCM was not used. A common assumption, that unobserved and observed feeding has the same time behaviour was proven to be wrong in this case. Whereas the initial population was consistent with publications of similar experiments [47], the lifetimes of the four lowest yrast states in ^{178}Hg were measured for the first time. In comparison to the next heavier even Hg isotopes the trend of E2 transition strengths with respect to the initial spin is completely different. Putting the transition quadrupole moment against the initial spin in a diagram, a constant value hints for a rotational band with unchanged deformation. The same holds for the kinetic moment of inertia $\mathfrak{J}^{(1)}$ as a function of frequency $\omega(J \rightarrow J-2)$. Both indicate a structural change at the 4_1^+ state in ^{178}Hg. A mixing calculation was performed, similar to the ones for the heavier midshell Hg isotopes [25–27]. The conclusion is that in all cases the contribution in the wavefunction from states of a different structure is small but the structural change in ^{178}Hg is shifted to higher energies. More precisely the 2_1^+ state belongs to the weakly oblate deformed ground-state band whereas the rotational band with larger deformation becomes yrast at the 4_1^+ state. The small overlap of the wavefunctions reduces therefore the B(E2;$4_1^+ \rightarrow 2_1^+$), which by chance resembles the $2_1^+ \rightarrow 0_1^+$ transition in terms of transition quadrupole moment. In the heavier Hg isotopes already the 2_1^+ state belongs to the intruder structure reducing the B(E2) and Q_t value of the $2_1^+ \rightarrow 0_1^+$ transition. The difference is evident in the deformation of the higher-lying rotational band, ^{178}Hg manifests a

much larger deformation of $\beta \approx 0.4$. This is an intermediate value between a normal deformation and superdeformation (SD), which is also known and explained for a negative parity band in ^{186}Hg build upon a 11^- state [48]. The deformation of the low-lying structure is fully consistent with the measurement of charge radii via isotope shifts and changes only very little and smoothly with respect to the mass [24]. The isotope shift measurements also show a significant staggering of charge radii between even and odd Hg isotopes just around midshell. The ground state of the odd nucleus has a larger charge radius compared to the even neighbor, which breaks down at ^{179}Hg. It confirms again that the deformation driving structure ist shifted to higher excitation energy for neutron-deficient Hg isotopes. Further the authors explain the observed deformation with the occupation of the $\pi(h_{\frac{9}{2}})$ and $\nu(i_{\frac{13}{2}})$ orbitals within a Monte Carlo shell model (MCSM) calculation. Ma et al. [48] claim also neutron excitations involving the $\nu[651]\frac{1}{2}$ orbital at large deformations to explain the intermediate deformation in ^{186}Hg. In contrast, all existing model calculations for ^{178}Hg take only into account proton intruder structures. Particularly Hartree-Fock-Bogoliubov calculations using the Gogny-D1M energy density functional and mappings to the PES of the IBM are available [49]. The IBM version is extended to configuration mixing of 2p-2h proton excitations (up to ^{190}Hg) and distinguishes between protons and neutrons (IBM-2). Nevertheless the model predicts a trend towards near-spherical shapes with a vanishing prolate minimum of normal deformation $\beta \approx 0.25 - 0.3$ for $A \leq 178$. In the recent publications only total routhian surface (TRS) calculations existing for $^{172-176}$Hg [50] predict a well-deformed ($\beta \approx 0.35$) minimum evolving in the PES with increasing neutron number. Earlier W. Nazarewicz prognosticated SD bands leading to various shape-coexisting configurations for Hg isotopes with $N \leq 98$ [28]. Unfortunately the experimental data was rather sparse at this time for proton-rich nuclei and many questions remained open. Though many predictions were correct, e.g. the oblate 0_2^+ state in ^{186}Pb [51], the picture stays rather qualitative. No MCSM calculation exists for excited states, except isomeric states. From a theoretical point of view new calculations are needed not excluding possible neutron-intruder structures, which is not yet implemented in IBM codes so far. Alternatively MCSM calculations would be of high interest for the whole chain of Hg isotopes. Experimentally again the neighboring Pt isotopes become interesting, as ^{174,176}Pt seem to be feasible for a $\gamma - \gamma$ coincidence RDDS experiment in contrast to ^{176}Hg. The intermediate deformation may be also seen there to further test the models and understand the dominating structure as it was the case for the normal deformed intruder structure at midshell. In the case of ^{176}Pt there exists older γ-singles data, but no clear conclusion can be drawn taking into account excitation energies and transition strengths, where the influence of delayed feeding is possibly underestimated. The transition quadrupole moments shown in Fig. 6 look rather similar to ^{178,180}Pt, just with slightly lower absolute values and consistent with the expected trend for a rotor. However the level scheme hints for a vibrational excitation at low spins, i.e. the $R_{4/2}$ ratio in ^{176}Pt is 2.14 and close to the expectation value of 2 for a vibrator. In ^{174}Pt no transition strengths are known. To illustrate the changes of the level scheme for the platinum isotopes the kinetic moments of inertia are again calculated and shown in Fig. 5 as it was done within the publication on ^{178}Hg. One notices the constant trend for ^{178,180}Pt with respect to the frequency (as expected for a rotor) and the similarity of the kinetic moments of inertia for the isotones ^{174}Pt and ^{176}Hg (c.f. Fig. 7 in publication III). The kinetic moments of

inertia in ^{176}Pt indicate the beginning of a structural change, but lifetimes to determine the transition strengths should be checked.

Fig. 6 summarizes what has been achieved in this work, the spin-dependent transition quadrupole moments are presented for the even-even neutron-deficient Hg and Pt nuclei. It shows the similarities between midshell Pt and Hg nuclei, where the more deformed structure reaches the ground state in platinum while lying at higher spins in mercury. If one neglects small variations, then the absolute values of transition quadrupole moments are for ^{180}Pt and ^{182}Hg both Q_t=8 eb. On the other hand leaving midshell towards more proton-rich Hg isotopes the change in absolute value of deformation is visible as well as the shift to higher spins.
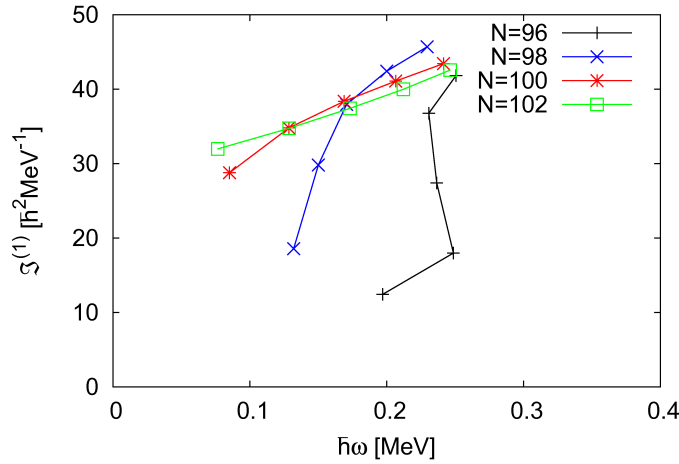
Figure 5: Kinetic moments of inertia $\mathfrak{I}^{(1)}(J)$ for the Pt isotopes as a function of frequency $\omega(J{\to}J\text{-}2)$ for transitions along the yrast line up to the 10^+ state.
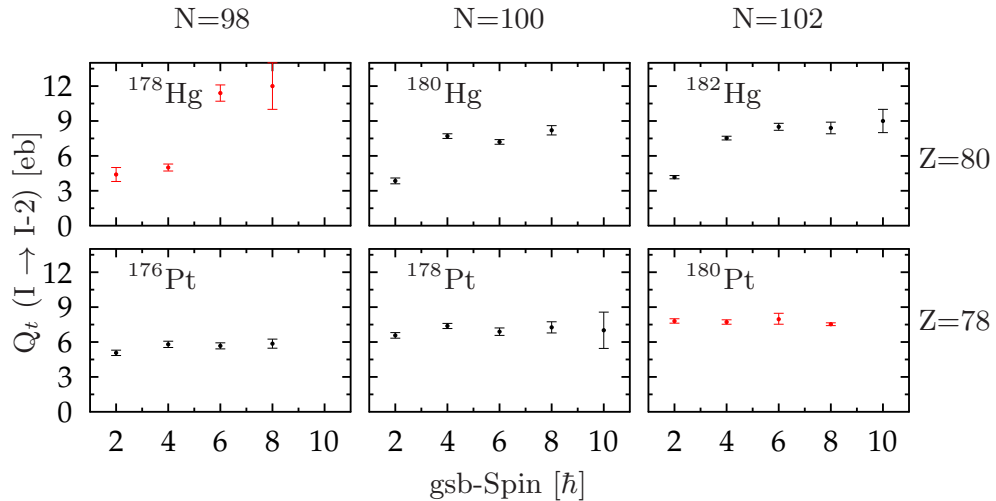

Figure 6: Transition quadrupole moments between the lowest yrast states in ^{178}Hg, ^{180}Hg [25], ^{182}Hg [25], ^{176}Pt, ^{178}Pt [43] and ^{180}Pt, Z and N are the proton and neutron number respectively.

Bibliography

[1]   H. Morinaga and T. Yamazaki. In-beam Gamma-ray spectroscopy. 1st ed. North-Holland publishing company, 1976 (cit. on p. 7).

[2]   R. Casten. Nuclear Structure from a Simple Perspective. 2nd ed. Oxford University Press Inc., 2000 (cit. on pp. 7, 12, 15–17).

[3]   J. Valiente-Dobón, D. Mengoni, F. Recchia, G. de Angelis and et al. "Status of the Gamma-Ray Spectrometer GALILEO." *LNL Annual Report 2014*. INFN, Laboratori Nazionali di Legnaro, 2014, pp. 95–96 (cit. on pp. 7, 49).

[4]   A. Goasduff, D. Bazzacco, R. Menegazzo, D. Mengoni and et al. "Possible geometries of GALILEO phase II." *LNL Annual Report 2016*. INFN, Laboratori Nazionali di Legnaro, 2016, pp. 86–87 (cit. on p. 7).

[5]   H. Bateman. "Solution of a system of differential equations occuring in the theory of radioactive transformations." *Proc. Cambridge Philos. Soc.* 15 (1910), pp. 423–427 (cit. on p. 8).

[6]   W. R. Inc. Mathematica, Version 8. Champaign, IL, 2019 (cit. on pp. 8, 50).

[7]   E. Paul, P. Woods, T. Davinson, R. Page and et al. "In-beam γ-ray spectroscopy above ^{100}Sn using the new technique of recoil decay tagging." *Phys. Rev. C* 51 (1 1995), pp. 78–87 (cit. on pp. 9, 50).

[8]   T. Alexander and A. Bell. "A target chamber for recoil-distance lifetime measurements." *Nucl. Inst. Meth.* 81 (1970), pp. 22–26 (cit. on p. 9).

[9]   A. Dewald, S. Harissopulos and P. von Brentano. "The differential plunger and the differential decay curve method for the analysis of recoil distance Doppler-shift data." *Z. Phys. A* 334 (1989), pp. 163–175 (cit. on p. 9).

[10]   M. Leino, J. Äystö, T. Enqvist, P. Heikkinen and et al. "Gas-filled recoil separator for studies of heavy elements." *Nucl. Instr. Meth. B* 99 (1995), pp. 653–656 (cit. on p. 9).

[11]   J. Sarén, J. Uusitalo, M. Leino and J. Sorri. "Absolute transmission and separation properties of the gas-filled recoil separator RITU." *Nucl. Instr. Meth. A* 654 (2011), pp. 508–521 (cit. on p. 9).

[12]   R. Page, A. Andreyev, D. Appelbe, P. Butler and et al. "The GREAT spectrometer." *Nucl. Instr. Meth. B* 204 (2003), pp. 634–637 (cit. on p. 9).

[13]   P. Rahkila. "Grain—A Java data analysis system for Total Data Readout." *Nucl. Instr. Meth. A* 595 (2008), pp. 637–642 (cit. on pp. 9, 50).

[14]   E. Bell. "Beta and Gamma Ray Spectroscopy." Ed. by K. Siegbahn. Amsterdam: North-Holland Publishing Co, 1955 (cit. on p. 10).

[15]   A. Schwarzschild. "A survey of the latest developments in delayed coincidence measurements." *Nucl. Instr. Meth.* 21 (1963), pp. 1–16 (cit. on p. 10).

[16]   E. van Loef, D. P, C. van Eijk, K. Krämer and et al. "Scintillation properties of LaBr$_3$:Ce^{3+} crystals: fast, efficient and high-energy-resolution scintillators." *Nucl. Instr. Meth. A* 486 (2002), pp. 254–258 (cit. on p. 10).

[17]   J.-M. Régis, N. Saed-Samii, M. Rudigier, S. Ansari and et al. "Reduced $\gamma - \gamma$ time walk to below 50 ps using the multiplexed-start and multiplexed-stop fast-timing technique with LaBr3(Ce) detectors." *Nucl. Instr. Meth. A* 823 (2016), pp. 72–82 (cit. on p. 10).

[18]   H. Mach, R. Gill and M. Moszyński. "A method for picosecond lifetime measurements for neutron-rich nuclei: (1) Outline of the method." *Nucl. Instr. Meth. A* 280 (1989), pp. 49–72 (cit. on p. 10).

[19]   J.-M. Régis, H. Mach, G. Simpson, J. Jolie and et al. "The generalized centroid difference method for picosecond sensitive determination of lifetimes of nuclear excited states using large fast-timing arrays." *Nucl. Instr. Meth. A* 726 (2013), pp. 191–202 (cit. on p. 11).

[20]   R. Julin, K. Helariutta and M. Muikku. "Intruder states in very neutron-deficient Hg, Pb and Po nuclei." *J Phys. G: Nucl. Part. Phys.* 27.7 (2001), R109–R139 (cit. on p. 12).

[21]   K. Heyde and J. L. Wood. "Shape coexistence in atomic nuclei." *Rev. Mod. Phys.* 83 (4 2011), p. 1467 (cit. on pp. 12, 48).

[22]   J. E. García-Ramos and K. Heyde. "Nuclear shape coexistence: A study of the even-even Hg isotopes using the interacting boson model with configuration mixing." *Phys. Rev. C* 89 (1 2014), p. 014306 (cit. on pp. 12, 48).

[23]   J. Bonn, G. Huber, H.-J. Kluge, L. Kugler and et al. "Sudden change in the nuclear charge distribution of very light mercury isotopes." *Phys. Lett. B* 38.5 (1972), pp. 308–311 (cit. on p. 12).

[24]   B. Marsh, T. Day Goodacre, S. Sels, Y. Tsunoda and et al. "Characterization of the shape-staggering effect in mercury nuclei." *Nature Physics* 14 (12 2018), p. 1163 (cit. on pp. 12, 51).

[25]   T. Grahn, A. Petts, M. Scheck, P. A. Butler and et al. "Evolution of collectivity in ^{180}Hg and ^{182}Hg." *Phys. Rev. C* 80 (1 2009), p. 014324 (cit. on pp. 12, 50, 52).

[26]   N. Bree, K. Wrzosek-Lipska, A. Petts, A. Andreyev and et al. "Shape Coexistence in the Neutron-Deficient Even-Even $^{182-188}$Hg Isotopes Studied via Coulomb Excitation." *Phys. Rev. Lett.* 112 (16 2014), p. 162701 (cit. on pp. 12, 50).

[27]   L. Gaffney, M. Hackstein, R. Page, T. Grahn and et al. "Shape coexistence in neutron-deficient Hg isotopes studied via lifetime measurements in ^{184,186}Hg and two-state mixing calculations." *Phys. Rev. C* 89 (2 2014), p. 024307 (cit. on pp. 12–13, 50).

[28]   W. Nazarewicz. "Variety of shapes in the mercury and lead isotopes." *Phys. Lett. B* 305 (3 1993), p. 195 (cit. on pp. 12, 51).

[29]   A. Dewald, O. Möller, B. Saha, K. Jessen and et al. "Test of the critical point symmetry X(5) in the mass A = 180 region." *J. Phys. G* 31 (10 2005), p. 1427 (cit. on p. 12).

[30]   F. Iachello. "Analytic Description of Critical Point Nuclei in a Spherical-Axially Deformed Shape Phase Transition." *Phys. Rev. Lett.* 87 (5 2001), p. 052502 (cit. on pp. 12, 47).

[31]   K. Gladnishki, P. Petkov, A. Dewald, C. Fransen and et al. "Yrast electromagnetic transition strengths and shape coexistence in ^{182}Pt." *Nucl. Phys. A* 877 (2012), pp. 19–34 (cit. on pp. 12, 49).

[32]   M. De Voigt, R. Kaczarowski, H. Riezebos, R. F. Noorman and et al. "Collective and quasiparticle excitations in ^{180}Pt." *Nucl. Phys. A* 507 (2 1990), pp. 472–496 (cit. on pp. 12, 47–48).

[33]   E. Williams, C. Plettner, E. A. McCutchan, H. Levine and et al. "Revisiting anomalous $B(E2; 4_1^+ \rightarrow 2_1^+)/B(E2; 2_1^+ \rightarrow 0_1^+)$ values in ^{98}Ru and ^{180}Pt." *Phys. Rev. C* 74 (2 2006), p. 024302 (cit. on pp. 12, 47–48).

[34]   E. A. McCutchan, R. F. Casten and N. V. Zamfir. "Simple interpretation of shape evolution in Pt isotopes without intruder states." *Phys. Rev. C* 71 (6 2005), 061301(R) (cit. on pp. 13, 48).

[35] A. Bohr and B. Mottelson. Nuclear Structure - volume II. 1st ed. W. A. Benjamin Inc., Advanced Book Program, 1975 (cit. on pp. 14, 16).

[36]   G. Gneuss and W. Greiner. "Collective potential energy surfaces and nuclear structure." *Nucl. Phys. A* 171 (3 1971), pp. 449–479 (cit. on pp. 14, 48).

[37]   A. Arima and F. Iachello. "Collective Nuclear States as Representations of a SU(6) Group." *Phys. Rev. Lett.* 35 (16 1975), p. 1069 (cit. on pp. 15–16).

[38]   D. D. Warner and R. F. Casten. "Predictions of the interacting boson approximation in a consistent Q framework." *Phys. Rev. C* 28 (4 1983), p. 1798 (cit. on p. 15).

[39]   Q. Chen, X. Wu, Y. Chen, C. Li and et al. "Lifetime measurements in ^{180}Pt." *Phys. Rev. C* 93 (4 2016), p. 044310 (cit. on pp. 47–48).

[40] A. Linnemann. "Das HORUS-Würfelspektrometer und Multiphononanregungen in 106Cd." PhD thesis. Universität zu Köln, 2006 (cit. on p. 47).

[41] S. Heinze. "Eine Methode zur Lösung beliebiger bosonischer und fermionischer Vielteilchen-systeme." PhD thesis. Universität zu Köln, 2008 (cit. on p. 48).

[42]   J. E. García-Ramos and K. Heyde. "The Pt isotopes: Comparing the Interacting Boson Model with configuration mixing and the extended consistent-Q formalism." *Nucl. Phys. A* 825 (1-2 2009), pp. 39–70 (cit. on p. 48).

[43]   C. Fransen, F. Mammes, R. Bark, T. Braunroth and et al. "Structural investigation of neutron-deficient Pt isotopes: the case of 178Pt." *EPJ Web Conf.* 223 (2019), p. 01016 (cit. on pp. 49, 52).

[44]   C. Alvarez. "The GASP array." *Nucl. Phys. News* 3 (3 1993), pp. 10–13 (cit. on p. 49).

[45]   A. Dewald, O. Möller and P. Petkov. "Developing the Recoil Distance Doppler-Shift technique towards a versatile tool for lifetime measurements of excited nuclear states." *Prog. Part. Nucl. Phys.* 67 (3 2012), pp. 786–839 (cit. on p. 49).

[46]   D. Testov, D. Mengoni, A. Goasduff, A. Gadea and et al. "The 4π highly-efficient light-charged-particle detector EUCLIDES, installed at the GALILEO array for in-beam γ-ray spectroscopy." *Eur. Phys. J. A* 55.4 (2019), p. 47 (cit. on p. 49).

[47]   E. Achterberg, O. Capurro and G. Marti. "Nuclear Data Sheets for A = 178." *Nuclear Data Sheets* 110 (7 2009), pp. 1473–1688 (cit. on p. 50).

[48]   W. Ma, J. Hamilton, A. Ramayya, L. Chaturvedi and et al. "First evidence for states in Hg nuclei with deformations between normal and super deformation." *Phys. Rev. C* 47 (1 1993), R5–R8 (cit. on p. 51).

[49]   K. Nomura, R. Rodríguez-Guzmán and L. Robledo. "Shape evolution and the role of intruder configurations in Hg isotopes within the interacting boson model based on a Gogny energy density functional." *Phys. Rev. C* 87 (6 2013), p. 064313 (cit. on p. 51).

[50]   M. Sandzelius, E. Ganioğlu, B. Cederwall, B. Hadinia and et al. "First observation of excited states in ^{172}Hg." *Phys. Rev C* 79 (6 2009), p. 064315 (cit. on p. 51).

[51]   A. Andreyev, M. Huyse, P. Van Duppen, L. Weissman and et al. "A triplet of differently shaped spin-zero states in the atomic nucleus 186Pb." *Nature Physics* 405 (2000), p. 430 (cit. on p. 51).

List of publications

Publications in refereed journals

[1]   L. Netterdon, V. Derya, J. Endres, C. Fransen, A. Hennig, J. Mayer, C. Müller-Gatermann, A. Sauerwein, P. Scholz, M. Spieker and A. Zilges.
The γ-ray spectrometer HORUS and its applications for nuclear astrophysics.
Nuclear Instruments and Methods in Physics Research, Section A: Accelerators, Spectrometers, Detectors and Associated Equipment 754 (2014), pp. 94–100 .

[2]   D. Kocheva, G. Rainovski, J. Jolie, N. Pietralla, C. Stahl, P. Petkov, A. Blazhev, A. Hennig, A. Astier, T. Braunroth, M. Cortés, A. Dewald, M. Djongolov, C. Fransen, K. Gladnishki, V. Karayonchev, J. Litzinger, C. Müller-Gatermann, M. Scheck, P. Scholz, R. Stegmann, P. Thöle, V. Werner, W. Witt, D. Wölk and P. Van Isacker.
Low-lying isovector 2^+ valence-shell excitations of Po 212.
Physical Review C 93.1 (2016) .

[3]   J.-M. Régis, M. Dannhoff, J. Jolie, C. Müller-Gatermann and N. Saed-Samii.
On the time response of background obtained in γ-ray spectroscopy experiments using LaBr3(Ce) detectors with different shielding.
Nuclear Instruments and Methods in Physics Research, Section A: Accelerators, Spectrometers, Detectors and Associated Equipment 811 (2016), pp. 42–48 .

[4]   J.-M. Régis, N. Saed-Samii, M. Rudigier, S. Ansari, M. Dannhoff, A. Esmaylzadeh, C. Fransen, R.-B. Gerst, J. Jolie, V. Karayonchev, C. Müller-Gatermann and S. Stegemann.
Reduced γ-γ Time walk to below 50 ps using the multiplexed-start and multiplexed-stop fast-timing technique with LaBr3(Ce) detectors.
Nuclear Instruments and Methods in Physics Research, Section A: Accelerators, Spectrometers, Detectors and Associated Equipment 823 (2016), pp. 72–82 .

[5]   A. Vogt, B. Birkenbach, P. Reiter, A. Blazhev, M. Siciliano, K. Hadyńska-Klęk, J. Valiente-Dobón, C. Wheldon, E. Teruya, N. Yoshinaga, K. Arnswald, D. Bazzacco, M. Bowry, A. Bracco, B. Bruyneel, R. Chakrawarthy, R. Chapman, D. Cline, L. Corradi, F. Crespi, M. Cromaz, G. De Angelis, J. Eberth, P. Fallon, E. Farnea, E. Fioretto, S. Freeman, B. Fu, A. Gadea, K. Geibel, W. Gelletly, A. Gengelbach, A. Giaz, A. Görgen, A. Gottardo, A. Hayes, H. Hess, R. Hirsch, H. Hua, P. John, J. Jolie, A. Jungclaus, L. Kaya, W. Korten, I. Lee, S. Leoni, L. Lewandowski, X. Liang, S. Lunardi, A. Macchiavelli, R. Menegazzo, D. Mengoni, C. Michelagnoli, T. Mijatović, G. Montagnoli, D. Montanari, C. Müller-Gatermann, D. Napoli, C. Pearson, L. Pellegri, Z. Podolyák, G. Pollarolo, A. Pullia, M. Queiser, F. Radeck, F. Recchia, P. Regan, D. Rosiak, N. Saed-Samii, E. Şahin, F. Scarlassara, D. Schneiders, M. Seidlitz, B. Siebeck, G. Sletten, J. Smith, P.-A. Söderström, A. Stefanini, T. Steinbach, O. Stezowski, S. Szilner, B. Szpak, R. Teng, C. Ur, V. Vandone, D. Warner, A. Wiens, C. Wu and K. Zell.
Isomers and high-spin structures in the N=81 isotones Xe 135 and Ba 137.
Physical Review C 95.2 (2017) .

[6]   V. Karayonchev, J.-M. Régis, J. Jolie, A. Blazhev, R. Altenkirch, S. Ansari, M. Dannhoff, F. Diel, A. Esmaylzadeh, C. Fransen, R.-B. Gerst, K. Moschner, C. Müller-Gatermann, N. Saed-Samii, S. Stegemann, N. Warr and K. Zell.
Evolution of collectivity in the N=100 isotones near Yb 170.
Physical Review C 95.3 (2017) .

[7]   D. Ralet, G. Georgiev, A. Stuchbery, E. Clément, A. Lemasson, C. Michelagnoli, M. Rejmund, L. Atanasova, D. Balabanski, G. Bocchi, R. Carroll, A. Dewald, J. Dudouet, B. Fornal, G. France, S. Franchoo, C. Fransen, C. Müller-Gatermann, A. Goasduff, A. Gadea, B. Jacquot, P. John, D. Kocheva, T. Konstantinopoulos, A. Korichi, A. Kusoglu, S. Lenzi, S. Leoni, J. Ljungvall, R. Lozeva, A. Maj, A. Navin, R. Perez, N. Pietralla, C. Shand, O. Stezowski and D. Yordanov.
Toward lifetime and g factor measurements of short-lived states in the vicinity of 208 Pb.
Physica Scripta 92.5 (2017)   .

[8]   A. Vogt, M. Siciliano, B. Birkenbach, P. Reiter, K. Hadyńska-Klęk, C. Wheldon, J. Valiente-Dobón, E. Teruya, N. Yoshinaga, K. Arnswald, D. Bazzacco, A. Blazhev, A. Bracco, B. Bruyneel, R. Chakrawarthy, R. Chapman, D. Cline, L. Corradi, F. Crespi, M. Cromaz, G. De Angelis, J. Eberth, P. Fallon, E. Farnea, E. Fioretto, C. Fransen, S. Freeman, B. Fu, A. Gadea, W. Gelletly, A. Giaz, A. Görgen, A. Gottardo, A. Hayes, H. Hess, R. Hetzenegger, R. Hirsch, H. Hua, P. John, J. Jolie, A. Jungclaus, V. Karayonchev, L. Kaya, W. Korten, I. Lee, S. Leoni, X. Liang, S. Lunardi, A. MacChiavelli, R. Menegazzo, D. Mengoni, C. Michelagnoli, T. Mijatović, G. Montagnoli, D. Montanari, C. Müller-Gatermann, D. Napoli, C. Pearson, Z. Podolyák, G. Pollarolo, A. Pullia, M. Queiser, F. Recchia, P. Regan, J.-M. Régis, N. Saed-Samii, E. Şahin, F. Scarlassara, M. Seidlitz, B. Siebeck, G. Sletten, J. Smith, P.-A. Söderström, A. Stefanini, O. Stezowski, S. Szilner, B. Szpak, R. Teng, C. Ur, D. Warner, K. Wolf, C. Wu and K. Zell.
High-spin structures in Xe 132 and Xe 133 and evidence for isomers along the N=79 isotones.
Physical Review C 96.2 (2017)   .

[9]   M. Schiffer, R. Altenkirch, C. Feuerstein, C. Müller-Gatermann, G. Hackenberg, S. Herb, P. Bhandari, S. Heinze, A. Stolz and A. Dewald.
A dedicated AMS setup for medium mass isotopes at the Cologne FN tandem accelerator.

Nuclear Instruments and Methods in Physics Research, Section B: Beam Interactions with Materials and Atoms 406 (2017), pp. 287–291 .

[10]   A. Stolz, A. Dewald, R. Altenkirch, S. Herb, S. Heinze, M. Schiffer, C. Feuerstein, C. Müller-Gatermann, A. Wotte, J. Rethemeyer and T. Dunai.
Radiocarbon measurements of small gaseous samples at CologneAMS.
Nuclear Instruments and Methods in Physics Research, Section B: Beam Interactions with Materials and Atoms 406 (2017), pp. 283–286 .

[11]   D. Kocheva, G. Rainovski, J. Jolie, N. Pietralla, A. Blazhev, A. Astier, R. Altenkirch, S. Ansari, T. Braunroth, M. Cortés, A. Dewald, F. Diel, M. Djongolov, C. Fransen, K. Gladnishki, A. Hennig, V. Karayonchev, J. Keatings, E. Kluge, J. Litzinger, C. Müller-Gatermann, P. Petkov, M. Rudigier, M. Scheck, P. Scholz, P. Spagnoletti, M. Spieker, C. Stahl, R. Stegmann, M. Stoyanova, P. Thöle, N. Warr, V. Werner, W. Witt, D. Wölk, K. Zell, P. Van Isacker and V. Ponomarev.
A revised B(E2;$2_1^+ \to 0_1^+$) value in the semi-magic nucleus 210 Po.
European Physical Journal A 53.9 (2017)   .

[12]   K. Arnswald, T. Braunroth, M. Seidlitz, L. Coraggio, P. Reiter, B. Birkenbach, A. Blazhev, A. Dewald, C. Fransen, B. Fu, A. Gargano, H. Hess, R. Hirsch, N. Itaco, S. Lenzi, L. Lewandowski, J. Litzinger, C. Müller-Gatermann, M. Queiser, D. Rosiak, D. Schneiders, B. Siebeck, T. Steinbach, A. Vogt, K. Wolf and K. Zell.
Enhanced collectivity along the N = Z line: Lifetime measurements in 44Ti, 48Cr, and 52Fe.

Physics Letters, Section B: Nuclear, Elementary Particle and High-Energy Physics 772 (2017), pp. 599–606 .

[13]   P. Petkov, C. Müller-Gatermann, A. Dewald, A. Blazhev, C. Fransen, J. Jolie, P. Scholz, K. Zell and A. Zilges.
Lifetime measurements with improved precision in S 30,32 and possible influence of large-scale clustering on the appearance of strongly deformed states.
Physical Review C 96.3 (2017)   .

[14]   D. Kocheva, G. Rainovski, J. Jolie, N. Pietralla, A. Blazhev, R. Altenkirch, S. Ansari, A. Astier, M. Bast, M. Beckers, T. Braunroth, M. Cappellazzo, A. Dewald, F. Diel, M. Djongolov, C. Fransen, K. Gladnishki, A. Goldkuhle, A. Hennig, V. Karayonchev, J. Keatings, E. Kluge, T. Kröll, J. Litzinger, K. Moschner, C. Müller-Gatermann, P. Petkov, M. Scheck, P. Scholz, T. Schmidt, P. Spagnoletti, C. Stahl, R. Stegmann, A. Stolz, A. Vogt, N. Warr, V. Werner, D. Wölk, J. Zamora, K. Zell, V. Ponomarev and P. Van Isacker.
Low collectivity of the 2_1^+ state of Po 212.
Physical Review C 96.4 (2017)   .

[15]   M. Queiser, A. Vogt, M. Seidlitz, P. Reiter, T. Togashi, N. Shimizu, Y. Utsuno, T. Otsuka, M. Honma, P. Petkov, K. Arnswald, R. Altenkirch, B. Birkenbach, A. Blazhev, T. Braunroth, A. Dewald, J. Eberth, C. Fransen, B. Fu, H. Hess, R. Hetzenegger, R. Hirsch, J. Jolie, V. Karayonchev, L. Kaya, L. Lewandowski, C. Müller-Gatermann, J.-M. Régis, D. Rosiak, D. Schneiders, B. Siebeck, T. Steinbach, K. Wolf and K.-O. Zell.
Cross-shell excitations from the fp shell: Lifetime measurements in Zn 61.
Physical Review C 96.4 (2017)   .

[16]   C. Müller-Gatermann, A. Dewald, C. Fransen, T. Braunroth, J. Jolie, J. Litzinger, J. Régis, F. Von Spee, N. Warr, K. Zell, T. Grahn, P. Greenlees, K. Hauschild, U. Jakobsson, R. Julin, S. Juutinen, S. Ketelhut, P. Nieminen, M. Nyman, P. Peura, P. Rahkila, P. Ruotsalainen, M. Sandzelius, J. Sarén, C. Scholey, J. Sorri, S. Stolze, J. Uusitalo and P. Petkov.
Low-lying electromagnetic transition strengths in Pt 180.
Physical Review C 97.2 (2018)   .

[17]   M. Spieker, P. Petkov, E. Litvinova, C. Müller-Gatermann, S. Pickstone, S. Prill, P. Scholz and A. Zilges.
Shape coexistence and collective low-spin states in Sn 112,114 studied with the (p,p'γ) Doppler-shift attenuation coincidence technique.
Physical Review C 97.5 (2018)   .

[18]   L. Kaya, A. Vogt, P. Reiter, M. Siciliano, B. Birkenbach, A. Blazhev, L. Coraggio, E. Teruya, N. Yoshinaga, K. Higashiyama, K. Arnswald, D. Bazzacco, A. Bracco, B. Bruyneel, L. Corradi, F. Crespi, G. De Angelis, J. Eberth, E. Farnea, E. Fioretto, C. Fransen, B. Fu, A. Gadea, A. Gargano, A. Giaz, A. Görgen, A. Gottardo, K. Hadyńska-Klęk, H. Hess, R. Hetzenegger, R. Hirsch, N. Itaco, P. John, J. Jolie, A. Jungclaus, W. Korten, S. Leoni, L. Lewandowski, S. Lunardi, R. Menegazzo, D. Mengoni, C. Michelagnoli, T. Mijatović, G. Montagnoli, D. Montanari, C. Müller-Gatermann, D. Napoli, Z. Podolyák, G. Pollarolo, A. Pullia, M. Queiser, F. Recchia, D. Rosiak, N. Saed-Samii, E. Şahin, F. Scarlassara, D. Schneiders, M. Seidlitz, B. Siebeck, J. Smith, P.-A. Söderström, A. Stefanini, T. Steinbach, O. Stezowski, S. Szilner, B. Szpak, C. Ur, J. Valiente-Dobón, K. Wolf and K. Zell.
High-spin structure in the transitional nucleus Xe 131: Competitive neutron and proton alignment in the vicinity of the N=82 shell closure.
Physical Review C 98.1 (2018)   .

[19]   A. Esmaylzadeh, L. Gerhard, V. Karayonchev, J.-M. Régis, J. Jolie, M. Bast, A. Blazhev, T. Braunroth, M. Dannhoff, F. Dunkel, C. Fransen, G. Häfner, L. Knafla, M. Ley, C. Müller-Gatermann, K. Schomacker, N. Warr and K.-O. Zell.
Lifetime determination in Hg 190,192,194,196 via γ-γ Fast-timing spectroscopy.
Physical Review C 98.1 (2018) .

[20]   P. Petkov, C. Müller-Gatermann, A. Dewald, A. Blazhev, C. Fransen, J. Jolie, P. Scholz, K. Zell and A. Zilges.
Erratum: Lifetime measurements with improved precision in S 30,32 and possible influence of large-scale clustering on the appearance of strongly deformed states (Physical Review C (2017) 96 (034326) DOI: 10.1103/PhysRevC.96.034326).
Physical Review C 98.1 (2018) .

[21]   P. Singh, W. Korten, T. Hagen, A. Görgen, L. Grente, M.-D. Salsac, F. Farget, E. Clément, G. De France, T. Braunroth, B. Bruyneel, I. Celikovic, O. Delaune, A. Dewald, A. Dijon, J.-P. Delaroche, M. Girod, M. Hackstein, B. Jacquot, J. Libert, J. Litzinger, J. Ljungvall, C. Louchart, A. Gottardo, C. Michelagnoli, C. Müller-Gatermann, D. Napoli, T. Otsuka, N. Pillet, F. Recchia, W. Rother, E. Sahin, S. Siem, B. Sulignano, T. Togashi, Y. Tsunoda, C. Theisen and J. Valiente-Dobon.
Evidence for Coexisting Shapes through Lifetime Measurements in Zr 98.
Physical Review Letters 121.19 (2018) .

[22]   L. Kaya, A. Vogt, P. Reiter, C. Müller-Gatermann, M. Siciliano, L. Coraggio, N. Itaco, A. Gargano, K. Arnswald, D. Bazzacco, B. Birkenbach, A. Blazhev, A. Bracco, B. Bruyneel, L. Corradi, F. Crespi, G. De Angelis, M. Droste, J. Eberth, E. Farnea, E. Fioretto, C. Fransen, A. Gadea, A. Giaz, A. Görgen, A. Gottardo, K. Hadyńska-Klęk, H. Hess, R. Hetzenegger, R. Hirsch, P. John, J. Jolie, A. Jungclaus, W. Korten, S. Leoni, L. Lewandowski, S. Lunardi, R. Menegazzo, D. Mengoni, C. Michelagnoli, T. Mijatović, G. Montagnoli, D. Montanari, D. Napoli, Z. Podolyák, G. Pollarolo, F. Recchia, D. Rosiak, N. Saed-Samii, E. Şahin, F. Scarlassara, M. Seidlitz, P.-A. Söderström, A. Stefanini, O. Stezowski, S. Szilner, B. Szpak, C. Ur, J. Valiente-Dobón, M. Weinert, K. Wolf and K. Zell.
Millisecond 23/2+ isomers in the N=79 isotones Xe 133 and Ba 135.
Physical Review C 98.5 (2018) .

[23]   M. Schiffer, R. Spanier, C. Müller-Gatermann, S. Herb, C. Feuerstein, G. Hackenberg, M. Marock, S. Heinze, A. Stolz, A. Dewald and S. Binnie.
The first (53Mn/55Mn) isotopic ratio measurements at the Cologne FN-Tandem Accelerator.
Nuclear Instruments and Methods in Physics Research, Section B: Beam Interactions with Materials and Atoms 437 (2018), pp. 87–92 .

[24]   R. Altenkirch, C. Feuerstein, M. Schiffer, G. Hackenberg, S. Heinze, C. Müller-Gatermann and A. Dewald.
Operating the 120° Dipol-Magnet at the CologneAMS in a gas-filled mode.
Nuclear Instruments and Methods in Physics Research, Section B: Beam Interactions with Materials and Atoms 438 (2019), pp. 184–188 .

[25]   L. Kaya, A. Vogt, P. Reiter, C. Müller-Gatermann, A. Gargano, L. Coraggio, N. Itaco, A. Blazhev, K. Arnswald, D. Bazzacco, B. Birkenbach, A. Bracco, B. Bruyneel, L. Corradi, F. Crespi, G. De Angelis, M. Droste, J. Eberth, E. Farnea, E. Fioretto, C. Fransen, A. Gadea, A. Giaz, A. Görgen, A. Gottardo, K. Hadyńska-Klęk, H. Hess, R. Hetzenegger, R. Hirsch, P. John, J. Jolie, A. Jungclaus, W. Korten, S. Leoni, L. Lewandowski, S. Lunardi, R. Menegazzo, D. Mengoni, C. Michelagnoli, T. Mijatović, G. Montagnoli, D. Montanari, D. Napoli, Z. Podolyák, G. Pollarolo, F. Recchia,

D. Rosiak, N. Saed-Samii, E. Şahin, M. Siciliano, F. Scarlassara, M. Seidlitz, P.-A. Söderström, A. Stefanini, O. Stezowski, S. Szilner, B. Szpak, C. Ur, J. Valiente-Dobón, M. Weinert, K. Wolf and K. Zell.
Identification of high-spin proton configurations in Ba 136 and Ba 137.
Physical Review C 99.1 (2019) .

[26]   A. Stolz, A. Dewald, S. Heinze, R. Altenkirch, G. Hackenberg, S. Herb, <u>C. Müller-Gatermann</u>, M. Schiffer, G. Zitzer, A. Wotte, J. Rethemeyer and T. Dunai.
Improvements in the measurement of small 14CO2 samples at CologneAMS.
Nuclear Instruments and Methods in Physics Research, Section B: Beam Interactions with Materials and Atoms 439 (2019), pp. 70–75 .

[27]   P. Petkov and <u>C. Müller-Gatermann</u>.
On the imprecisions that may be induced when applying the Blaugrund approximation for the analysis of Doppler-shift attenuation lifetime measurements.
Nuclear Instruments and Methods in Physics Research, Section A: Accelerators, Spectrometers, Detectors and Associated Equipment 915 (2019), pp. 40–46 .

[28]   V. Karayonchev, A. Blazhev, A. Esmaylzadeh, J. Jolie, M. Dannhoff, F. Diel, F. Dunkel, C. Fransen, L. Gerhard, R.-B. Gerst, L. Knafla, L. Kornwebel, <u>C. Müller-Gatermann</u>, J.-M. Régis, N. Warr, K. Zell, M. Stoyanova and P. Van Isacker.
Lifetimes in at 211 and their implications for the nuclear structure above Pb 208.
Physical Review C 99.2 (2019) .

[29]   S. Ziliani, M. Ciemała, F. Crespi, S. Leoni, B. Fornal, A. Maj, P. Bednarczyk, G. Benzoni, A. Bracco, C. Boiano, S. Bottoni, S. Brambilla, M. Bast, M. Beckers, T. Braunroth, F. Camera, N. Cieplicka-Oryńczak, E. Clément, O. Dorvaux, S. Erturk, G. De France, A. Goldkuhle, J. Grębosz, M. Harakeh, Ł. Iskra, B. Jacquot, M. Kicińska-Habior, Y. Kim, M. Kmiecik, A. Lemasson, H. Li, I. Matea, K. Mazurek, C. Michelagnoli, B. Million, <u>C. Müller-Gatermann</u>, P. Napiorkowski, V. Nanal, M. Matejska-Minda, M. Rejmund, C. Schmitt, M. Stanoiu, I. Stefan, B. Wasilewska and M. Ziębliński.
Spectroscopy of neutron-rich C, O, N and F isotopes with the Agata+Paris+Vamos setup at Ganil.
Acta Physica Polonica B 50.3 (2019), pp. 625–631 .

[30]   M. Ciemała, S. Ziliani, F. Crespi, S. Leoni, B. Fornal, A. Maj, P. Bednarczyk, G. Benzoni, A. Bracco, C. Boiano, S. Bottoni, S. Brambilla, M. Bast, M. Beckers, T. Braunroth, F. Camera, N. Cieplicka-Oryńczak, E. Clément, O. Dorvaux, S. Ertürk, G. De France, A. Goldkuhle, J. Grębosz, M. Harakeh, Ł. Iskra, B. Jacquot, A. Karpov, M. Kicińska-Habior, Y. Kim, M. Kmiecik, A. Lemasson, H. Li, I. Matea, K. Mazurek, C. Michelagnoli, B. Millon, <u>C. Müller-Gatermann</u>, P. Napiorkowski, V. Nanal, M. Matejska-Minda, M. Rejmund, B. Sowicki, C. Schmitt, M. Stanoiu, I. Stefan, B. Wasilewska, M. Zielińska and M. Ziębliński.
Determination of lifetimes of excited states in neutron-rich 20 O isotope from experiment with the Agata+Paris+Vamos setup.
Acta Physica Polonica B 50.3 (2019), pp. 615–624 .

[31]   <u>C. Müller-Gatermann</u>, F. von Spee, A. Goasduff, D. Bazzacco, M. Beckers, T. Braunroth, A. Boso, P. Cocconi, G. de Angelis, A. Dewald, C. Fransen, A. Goldkuhle, A. Gottardo, A. Gozzelino, K. Hadyńska-Klęk, G. Jawroski, P. John, J. Jolie, S. Lenzi, J. Litzinger, R. Menegazzo, D. Mengoni, D. Napoli, F. Recchia, M. Siciliano, D. Testov, S. Thiel, J. Valiente-Dobón and K. Zell.
A new dedicated plunger device for the GALILEO γ-ray detector array.

Nuclear Instruments and Methods in Physics Research, Section A: Accelerators, Spectrometers, Detectors and Associated Equipment 920 (2019), pp. 95–99 .

[32]   A. Goldkuhle, C. Fransen, A. Dewald, K. Arnswald, M. Bast, M. Beckers, A. Blazhev, T. Braunroth, G. Hackenberg, G. Häfner, J. Litzinger, J. Jolie, <u>C. Müller-Gatermann</u>, F. von Spee, N. Warr, D. Werner and K. Zell.
Lifetime measurement of excited states in 46 Ti.
European Physical Journal A 55.4 (2019)   .

[33]   M. Giles, B. Nara Singh, L. Barber, D. Cullen, M. Mallaburn, M. Beckers, A. Blazhev, T. Braunroth, A. Dewald, C. Fransen, A. Goldkuhle, J. Jolie, F. Mammes, <u>C. Müller-Gatermann</u>, D. Wölk, K. Zell, S. Lenzi and A. Poves.
Probing isospin symmetry in the (Fe 50, Mn 50, Cr 50) isobaric triplet via electromagnetic transition rates.
Physical Review C 99.4 (2019)   .

[34]   <u>C. Müller-Gatermann</u>, A. Dewald, C. Fransen, K. Auranen, H. Badran, M. Beckers, A. Blazhev, T. Braunroth, D. Cullen, G. Fruet, A. Goldkuhle, T. Grahn, P. Greenlees, A. Herzáň, U. Jakobsson, D. Jenkins, J. Jolie, R. Julin, S. Juutinen, J. Konki, M. Leino, J. Litzinger, K. Nomura, J. Pakarinen, P. Peura, M. Procter, P. Rahkila, P. Ruotsalainen, M. Sandzelius, J. Sarén, C. Scholey, J. Sorri, S. Stolze, M. Taylor, J. Uusitalo and K. Zell.
Shape coexistence in Hg 178.
Physical Review C 99.5 (2019)   .

[35]   P. Petkov, <u>C. Müller-Gatermann</u>, D. Werner, A. Dewald, A. Blazhev, C. Fransen, J. Jolie, S. Ohkubo and K. Zell.
New lifetime measurements for the lowest quadrupole states in Ne 20,22 and possible explanations of the high collectivity of the depopulating E2 transitions.
Physical Review C 100.2 (2019)   .

[36]   L. Kaya, A. Vogt, P. Reiter, M. Siciliano, N. Shimizu, Y. Utsuno, H.-K. Wang, A. Gargano, L. Coraggio, N. Itaco, K. Arnswald, D. Bazzacco, B. Birkenbach, A. Blazhev, A. Bracco, B. Bruyneel, L. Corradi, F. Crespi, G. De Angelis, M. Droste, J. Eberth, A. Esmaylzadeh, E. Farnea, E. Fioretto, C. Fransen, A. Gadea, A. Giaz, A. Görgen, A. Gottardo, H.-K. K., H. Hess, R. Hirsch, P. John, J. Jolie, A. Jungclaus, V. Karayonchev, L. Kornwebel, W. Korten, S. Leoni, L. Lewandowski, S. Lunardi, R. Menegazzo, D. Mengoni, C. Michelagnoli, T. Mijatović, G. Montagnoli, D. Montanari, <u>C. Müller-Gatermann</u>, D. Napoli, Z. Podolyák, G. Pollarolo, F. Recchia, J.-M. Régis, N. Saed-Samii, E. Şahin, F. Scarlassara, K. Schomacker, M. Seidlitz, B. Siebeck, P.-A. Söderström, A. Stefanini, O. Stezowski, S. Szilner, B. Szpak, E. Teruya, C. Ur, J. Valiente-Dobón, K. Wolf, K. Yanase, N. Yoshinaga and K. Zell.
Isomer spectroscopy in Ba 133 and high-spin structure of Ba 134.
Physical Review C 100.2 (2019)   .

[37]   D. Ralet, E. Clément, G. Georgiev, A. Stuchbery, M. Rejmund, P. Van Isacker, G. de France, A. Lemasson, J. Ljungvall, C. Michelagnoli, A. Navin, D. Balabanski, L. Atanasova, A. Blazhev, G. Bocchi, R. Carroll, J. Dudouet, E. Dupont, B. Fornal, S. Franchoo, C. Fransen, <u>C. Müller-Gatermann</u>, A. Goasduff, A. Gadea, P. John, D. Kocheva, T. Konstantinopoulos, A. Korichi, A. Kusoglu, S. Lenzi, S. Leoni, R. Lozeva, A. Maj, R. Perez, N. Pietralla, C. Shand, O. Stezowski, D. Wilmsen, D. Yordanov, D. Barrientos, P. Bednarczyk, B. Birkenbach, A. Boston, H. Boston, I. Burrows, B. Cederwall, M. Ciemala, J. Collado, F. Crespi, D. Cullen, H. Eberth, J. Goupil, L. Harkness, H. Hess, A. Jungclaus, W. Korten, M. Labiche, R. Menegazzo, D. Mengoni, B. Million, J. Nyberg, Z. Podolyák, A. Pullia, B. Quintana Arnés, F. Recchia, P. Reiter, F. Saillant, M. Salsac, E. Sanchis,

C. Theisen, J. Valiente Dobon and O. Wieland.
Evidence of octupole-phonons at high spin in 207Pb.
Physics Letters, Section B: Nuclear, Elementary Particle and High-Energy Physics 797 (2019) .

[38]   A. Goldkuhle, C. Fransen, A. Blazhev, M. Beckers, B. Birkenbach, T. Braunroth, E. Clément, A. Dewald, J. Dudouet, J. Eberth, H. Hess, B. Jacquot, J. Jolie, Y.-H. Kim, A. Lemasson, S. Lenzi, H. Li, J. Litzinger, C. Michelagnoli, C. Müller-Gatermann, B. Nara Singh, R. Pérez-Vidal, D. Ralet, P. Reiter, A. Vogt, N. Warr, K. Zell, A. Ataç, D. Barrientos, C. Barthe-Dejean, G. Benzoni, A. Boston, H. Boston, P. Bourgault, I. Burrows, J. Cacitti, B. Cederwall, M. Ciemala, D. Cullen, G. De France, C. Domingo-Pardo, J.-L. Foucher, G. Fremont, A. Gadea, P. Gangnant, V. González, J. Goupil, C. Henrich, C. Houarner, M. Jean, D. Judson, A. Korichi, W. Korten, M. Labiche, A. Lefevre, L. Legeard, F. Legruel, S. Leoni, J. Ljungvall, A. Maj, C. Maugeais, L. Ménager, N. Ménard, R. Menegazzo, D. Mengoni, B. Million, H. Munoz, D. Napoli, A. Navin, J. Nyberg, M. Ozille, Z. Podolyak, A. Pullia, B. Raine, F. Recchia, J. Ropert, F. Saillant, M. Salsac, E. Sanchis, C. Schmitt, J. Simpson, C. Spitaels, O. Stezowski, C. Theisen, M. Toulemonde, M. Tripon, J.-J. Valiente Dobón, G. Voltolini, M. Zielińska and A. Collaboration.
Lifetime measurements in Ti 52,54 to study shell evolution toward N=32.
Physical Review C 100.5 (2019) .

[39]   M. Stoyanova, G. Rainovski, J. Jolie, N. Pietralla, A. Blazhev, M. Beckers, A. Dewald, M. Djongolov, A. Esmaylzadeh, C. Fransen, L. Gerhard, K. Gladnishki, S. Herb, P. John, V. Karayonchev, J. Keatings, R. Kern, L. Knafla, D. Kocheva, L. Kornwebel, T. Kröll, M. Ley, K. Mashtakov, C. Müller-Gatermann, J.-M. Régis, M. Scheck, K. Schomacker, J. Sinclair, P. Spagnoletti, C. Sürder, N. Warr, V. Werner and J. Wiederhold.
Lifetimes of the 41+ states of Po 206 and Po 204: A study of the transition from noncollective seniority-like mode to collectivity.
Physical Review C 100.6 (2019) .

[40]   M. Schiffer, A. Stolz, D. López, R. Spanier, S. Herb, C. Müller-Gatermann, S. Heinze, S. Binnie, J. Melchert, N. Kivel, D. Schumann, J. Rethemeyer, T. Dunai and A. Dewald.
Method developments for accelerator mass spectrometry at CologneAMS, 53Mn/3He burial dating and ultra-small 14CO2 samples.
Global and Planetary Change 184 (2020) .

[41]   L. Barber, D. Cullen, M. Giles, B. Nara Singh, M. Mallaburn, M. Beckers, A. Blazhev, T. Braunroth, A. Dewald, C. Fransen, A. Goldkuhle, J. Jolie, F. Mammes, C. Müller-Gatermann, D. Wölk and K. Zell.
Performing the differential decay curve method on γ-ray transitions with unresolved Doppler-shifted components.
Nuclear Instruments and Methods in Physics Research, Section A: Accelerators, Spectrometers, Detectors and Associated Equipment 950 (2020) .

Publications in conference proceedings

[42]   G. Pascovici, A. Dewald, S. Heinze, L. Fink, C. Müller-Gatermann, M. Schiffer, C. Feuerstein, M. Pfeiffer, J. Jolie, S. Thiel, K. Zell, O. Arnopolina and F. Von Blanckenburg.
A new beam profile monitor and time of flight system for CologneAMS.
Nuclear Instruments and Methods in Physics Research, Section B: Beam Interactions with Materials and Atoms 294 (2013), pp. 410–415 .

[43]   A. Dewald, S. Heinze, C. Feuerstein, C. Müller-Gatermann, A. Stolz, M. Schiffer, G. Zitzer, T. Dunai, J. Rethemeyer, M. Melles, H. Wiesel and F. Blanckenburg.
The first year of operation of CologneAMS; Performance and developments.
EPJ Web of Conferences 63 (2013) .

[44]   D. Kocheva, R. Stegmann, G. Rainovski, J. Jolie, N. Pietralla, C. Stahl, P. Petkov, A. Blazhev, A. Hennig, C. Bauer, T. Braunroth, M. Carpenter, L. Cortes, A. Dewald, M. Djongolov, C. Fransen, K. Gladnishki, R. Janssens, V. Karayonchev, M. Lettmann, C. Lister, J. Litzinger, T. Möller, C. Müller-Gatermann, M. Scheck, P. Scholz, C. Schramm, P. Thöle, V. Werner, D. Wölk, S. Zhu and P. Van Isacker.
Search formixed-symmetry states of nuclei in the vicinity of the double-magic nucleus 208 Pb.
EPJ Web of Conferences 107 (2016) .

[45]   D. Kocheva, G. Rainovski, J. Jolie, N. Pietralla, C. Stahl, P. Petkov, A. Blazhev, A. Hennig, A. Astier, T. Braunroth, L. Cortes, A. Dewald, M. Djongolov, C. Fransen, K. Gladnishki, V. Karayonchev, J. Litzinger, C. Müller-Gatermann, M. Scheck, P. Scholz, C. Schramm, P. Tölle, V. Werner, W. Witt, D. Wölk and P. Van Isacker.
Search for mixed-symmetry states in 212 Po.
Journal of Physics: Conference Series 724.1 (2016) .

[46]   M. Siciliano, J. Valiente-Dobón, A. Goasduff, D. Bazzacco, N. Alahari, G. Benzoni, T. Braunroth, N. Cieplicka, F. Crespi, E. Clement, G. De France, M. Doncel, S. Ertürk, C. Fransen, A. Gadea, G. Georgiev, A. Goldkuhle, U. Jakobsson, G. Jaworski, P. John, I. Kuti, A. Lemasson, A. Lopez-Martens, H. Li, S. Lunardi, T. Marchi, D. Mengoni, C. Michelagnoli, T. Mijatovic, C. Müller-Gatermann, D. Napoli, J. Nyberg, M. Palacz, R. Pérez-Vidal, M. Rejmund, B. Saygi, D. Sohler, S. Szilner and D. Testov.
Study of quadrupole correlations in N = Z = 50 region via lifetime measurements.
Acta Physica Polonica B 48.3 (2017), pp. 331–336 .

[47]   K. Arnswald, P. Reiter, L. Coraggio, B. Birkenbach, A. Blazhev, T. Braunroth, A. Dewald, C. Fransen, B. Fu, A. Gargano, H. Hess, R. Hirsch, N. Itaco, S. Lenzi, L. Lewandowski, J. Litzinger, C. Müller-Gatermann, M. Queiser, D. Rosiak, D. Schneiders, M. Seidlitz, B. Siebeck, T. Steinbach, A. Vogt, K. Wolf and K. Zell.
Enhanced collectivity along the N = Z line: Lifetime measurements in 44Ti, 48Cr, and 52Fe.
Journal of Physics: Conference Series 966.1 (2018) .

[48]   D. Kocheva, G. Rainovski, J. Jolie, N. Pietralla, A. Blazhev, A. Astier, R. Altenkirch, M. Bast, M. Beckers, S. Ansari, T. Braunroth, M. Cappellazzo, M. Cortés, A. Dewald, F. Diel, M. Djongolov, C. Fransen, K. Gladnishki, A. Goldkuhle, A. Hennig, V. Karayonchev, J. Keatings, E. Kluge, T. Kröll, J. Litzinger, K. Moschner, C. Müller-Gatermann, P. Petkov, M. Rudigier, M. Scheck, P. Spagnoletti, P. Scholz, T. Schmidt, M. Spieker, C. Stahl, R. Stegmann, A. Stolz, A. Vogt, M. Stoyanova, P. Thöle, N. Warr, V. Werner, W. Witt, D. Wölk, J. Zamora, K. Zell, P. Van Isacker and V. Ponomarev.
Low collectivity of the first 2^+ states of 212,210 Po.
Journal of Physics: Conference Series 1023.1 (2018) .

[49]   M. Trichkova, M. Beckers, K. Gladnishki, A. Dewald, A. Blazhev, C. Müller-Gatermann, C. Fransen, J. Jolie, D. Kalaydjieva, G. Rainovski and K.-O. Zell.
Lifetimes and electromagnetic transition strength in 124Ba.
EPJ Web of Conferences 194 (2018) .

[50]   C. Fransen, F. Mammes, R. Bark, T. Braunroth, Z. Buthelezi, A. Dewald, T. Dinoko, S. Förtsch, M. Hackstein, J. Jolie, P. Jones, E. Lawrie, J. Litzinger, C. Müller-Gatermann, R. Newman, N. Saed-Samii, J. Sharpey-Schafer, O. Shirinda, R. Smit, N. Warr, M. Wiedeking and K.-O. Zell.
Structural investigation of neutron-deficient Pt isotopes: the case of 178Pt.
EPJ Web of Conferences 223 (2019) .

[51]   A. Goldkuhle, C. Fransen, A. Dewald, A. Navin, M. Beckers, B. Birkenbach, A. Blazhev, T. Braunroth, E. Clément, G. De France, J. Dudouet, J. Eberth, H. Hess, B. Jacquot, Y.-H. Kim, A. Lemasson, S. Lenzi, H. Li, J. Ljungvall, J. Litzinger, C. Michelagnoli, C. Müller-Gatermann, D. Napoli, B. Nara Singh, R. Pérez-Vidal, D. Ralet, P. Reiter, M. Rejmund, A. Vogt, N. Warr, K. Zell and M. Zielińska.
Preliminary results of lifetime measurements in neutron-rich 53Ti.
EPJ Web of Conferences 223 (2019) .

Publications in annual reports

[52]   M. Siciliano, A. Goasduff, V.-D. J.J., R. Pérez-Vidal, D. Bazzacco, N. Alahari, G. Benzoni, T. Braunroth, N. Cieplicka, F. Crespi, E. Clement, M. Doncel, S. Ertürk, C. Fransen, A. Gadea, G. Georgiev, A. Goldkuhle, U. Jakobsson, G. Jaworski, P. John, I. Kuti, A. Lemasson, H. Li, T. Marchi, D. Mengoni, C. Micheelagnoli, T. Mijatovic, C. Müller-Gatermann, D. Napoli, J. Nyberg, M. Palacz, M. Rejmund, B. Saygi, D. Sohler, S. Szilner and D. Testov.
Study of Quadrupole Correlations in the ^{106,108}Sn Isotopes via Lifetimes Measurements.
LNL Annual Report 2015 242 (2016), pp. 76–77.

[53]   A. Goasduff, C. Fransen, A. Dewald, S. Thiel, T. Braunroth, C. Müller-Gatermann, D. Bazzacco, P. Cocconi, A. Gozzelino, Hadyńska-Klęk, G. Jaworski, P. John, D. Mengoni, F. Recchia, M. Siciliano, D. Testov, J. Valiente-Dobón and F. von Spee.
A New Dedicated Plunger Device for the GALILEO γ-ray array.
LNL Annual Report 2015 242 (2016), pp. 91–92.

[54]   M. Siciliano, V.-D. J.J., A. Goasduff, D. Bazzacco, A. Lopez-Martens, N. Alahari, G. Benzoni, T. Braunroth, N. Cieplicka, E. Clement, F. Crespi, M. Doncel, S. Ertürk, de France G., C. Fransen, A. Gadea, G. Georgiev, A. Goldkuhle, U. Jakobsson, G. Jaworski, P. John, I. Kuti, A. Lemasson, H. Li, S. Lunardi, T. Marchi, D. Mengoni, C. Michelagnoli, T. Mijatovic, C. Müller-Gatermann, D. Napoli, J. Nyberg, M. Palacz, R. Pérez-Vidal, M. Rejmund, B. Saygi, D. Sohler, S. Szilner and T. D.
Lifetime measurement in Z=N=50 region: Optimization of OFT Parameters.
LNL Annual Report 2016 250 (2017), pp. 102–103.

[55]   M. Siciliano, V.-D. J.J., A. Goasduff, D. Bazzacco, N. Alahari, G. Benzoni, T. Braunroth, N. Cieplicka, F. Crespi, E. Clement, de France G., M. Doncel, S. Ertürk, C. Fransen, A. Gadea, G. Georgiev, A. Goldkuhle, U. Jakobsson, G. Jaworski, P. John, I. Kuti, A. Lemasson, A. Lopez-Martens, H. Li, S. Lunardi, T. Marchi, D. Mengoni, C. Michelagnoli, T. Mijatovic, C. Müller-Gatermann, D. Napoli, J. Nyberg, M. Palacz, R. Pérez-Vidal, M. Rejmund, B. Saygi, D. Sohler, S. Szilner and T. D.
Neutron-Deficient Sn Isotopes Populated via Deep-Inelastic Collisions.
LNL Annual Report 2017 251 (2018), pp. 57–58.

Contribution to the publications in this thesis

Publication I:
Low-lying electromagnetic transition strengths in ^{180}Pt

- C. Müller-Gatermann planned the fast-timing experiment
- C. Müller-Gatermann partipated in the fast-timing experiment
- C. Müller-Gatermann sorted the data of the fast-timing experiment
- C. Müller-Gatermann performed the lifetime analysis of the fast-timing and RDDS experiment
- C. Müller-Gatermann carried out the IBM calculation
- C. Müller-Gatermann carried out the GCM calculation with P. Petkov
- C. Müller-Gatermann interpreted the results
- C. Müller-Gatermann wrote the paper

Publication II:
A new dedicated plunger device for the GALILEO γ-ray detector array

- C. Müller-Gatermann planned the experiment with C. Fransen
- C. Müller-Gatermann participated in the experiment
- C. Müller-Gatermann sorted the data
- C. Müller-Gatermann performed the lifetime analysis with F. von Spee
- C. Müller-Gatermann wrote the paper

Publication III:
Shape coexistence in ^{178}Hg

- C. Müller-Gatermann produced the targets
- C. Müller-Gatermann participated in the experiment
- C. Müller-Gatermann adapted the sort code
- C. Müller-Gatermann sorted the data
- C. Müller-Gatermann performed the lifetime analysis
- C. Müller-Gatermann interpreted the results
- C. Müller-Gatermann wrote the paper

Acknowledgments

My thanks go to all who supported me during my studies and contributed to the success of this work.

In particular I want to thank

- Prof. Dr. Alfred Dewald for the opportunity to be in his group, the award of the exciting topic, the interesting work also outside of this thesis, his supervision and the free space he gives all his students to develop their personal interests,

- Prof. Dr. Peter Reiter for his willingness to be the second examiner and also the nice collaboration in many experiments,

- Prof. Dr. Rolf-Dietmar Herzberg for being the third examiner of this work, as well as a (hopefully ongoing) successful collaboration using the charge-plunger technique,

- Prof. Dr. Ralf Bulla for his time being the chairman of the examination,

- Dr. Christoph Fransen for everything starting from detectors, many successful beamtimes together, all the paperwork he does for everyone else, not to forget his time for discussions,

- Prof. Dr. Jan Jolie for his interest in my work and helpful discussions about the theory,

- Prof. Dr. Pavel Petkov for the help with the GCM calculations and many discussions not only related to the publications presented here,

- Dr. Jean-Marc Régis for the help with the fast-timing experiment including the different analysis approaches,

- Dr. Stefan Heinze for the instructions to use the ArbModel, but also for the help with many side projects during my time here,

- all the experimentalists from JYFL and LNL, without the help of local groups the experiments would not have been successful, especially Rauno Julin and Tuomas Grahn for the discussions on ^{180}Pt, Panu Ruotsalainen all his time during the experiment on ^{178}Hg and Alain Goasduff for the help with the online sortcode in LNL,

- the whole Plunger group including all the ones, who left already. Next to the help during experiments and discussions it was always fun with you,

- the whole AMS group and their former members for also all the fun together, the help in all the sideprojects and of course the helpfulness in the daily work,

- Dr. Karl-Oskar Zell and Dr. Andrey Blazhev for the wonderful targets we can always use or the help during the work in the target lab,

- the mechanical workshop for all the great stuff I got from you, and Stefan Thiel for his ideas improving the setups,

- the electronic workshop including Gheorghe Pascovici, not only for the devices but also the discussions about electronics,

- the system administrators for their work keeping our systems alive and the answers to the small questions everyone of us has,

- Dr. Nigel Warr, your help with any computer code is as appreciable as the discussions,

- the BCGS for the financial support to conferences and also the interest in the progress of the students,

- Dr. Mark Spieker for the years of friendship, you were always there to motivate me. But I did not forget all the other companions during my whole time of study, your friendship is appreciated as much,

- last but not least my family for their general support.

Erklärung zur Dissertation

Ich versichere, dass ich die von mir vorgelegte Dissertation selbständig angefertigt, die benutzten Quellen und Hilfsmittel vollständig angegeben und die Stellen der Arbeit – einschließlich Tabellen, Karten und Abbildungen –, die anderen Werken im Wortlaut oder dem Sinn nach entnommen sind, in jedem Einzelfall als Entlehnung kenntlich gemacht habe; dass diese Dissertation noch keiner anderen Fakultät oder Universität zur Prüfung vorgelegen hat; dass sie – abgesehen von unten angegebenen Teilpublikationen – noch nicht veröffentlicht worden ist, sowie, dass ich eine solche Veröffentlichung vor Abschluss des Promotionsverfahrens nicht vornehmen werde. Die Bestimmungen der Promotionsordnung sind mir bekannt. Die von mir vorgelegte Dissertation ist von Prof. Dr. Alfred Dewald betreut worden.

Teilpublikationen

- C. Müller-Gatermann *et al.* "Low-lying electromagnetic transition strengths in ^{180}Pt". *Phys. Rev. C* 97 024336 (2018)

- C. Müller-Gatermann *et al.* "A new dedicated plunger device for the GALILEO γ-ray detector array". *Nucl. Inst. Meth. A* 920 95-99 (2019)

- C. Müller-Gatermann *et al.* "Shape coexistence in ^{178}Hg". *Phys. Rev. C* 99 054325 (2019)

Köln, den 06. Januar 2020

_____

(Claus Müller-Gatermann)